NASA TECHNICAL NOTE

NASA TN D-7404

NASA TN D-7404

A MODIFIED NEWTON-RAPHSON ANALYSIS OF FLIGHT MEASUREMENTS OF THE TRAILING VORTICES OF A HEAVY JET TRANSPORT

by Lawrence W. Taylor, Jr., and Milton D. McLaughlin

Langley Research Center

Hampton, Va. 23665

NATIONAL AERONAUTICS AND SPACE ADMINISTRATION • WASHINGTON, D. C. • AUGUST 1974

1. Report No.	2. Government Accession No.	3. Recipient's Catalog No.
NASA TN D-7404		

4. Title and Subtitle	5. Report Date
A MODIFIED NEWTON-RAPHSON ANALYSIS OF FLIGHT MEASUREMENTS OF THE TRAILING VORTICES OF A HEAVY JET TRANSPORT	August 1974
	6. Performing Organization Code
7. Author(s)	8. Performing Organization Report No.
Lawrence W. Taylor, Jr., and Milton D. McLaughlin	L-8838
	10. Work Unit No.
9. Performing Organization Name and Address	766-75-02-01
NASA Langley Research Center Hampton, Va. 23665	11. Contract or Grant No.
	13. Type of Report and Period Covered
12. Sponsoring Agency Name and Address	Technical Note
National Aeronautics and Space Administration Washington, D.C. 20546	14. Sponsoring Agency Code

15. Supplementary Notes

16. Abstract

A modified Newton-Raphson method has been used to determine the parameters in equations describing the vortex flow to obtain a best match with flight measurements of the flow behind the C-5A airplane. The flight measurements were made using a specially instrumented T-33 airplane which passed as closely as possible to the centers of the trailing vortices at several distances behind the C-5A airplane. The flight measurements were transformed to flow velocity relative to an inertial frame of reference. The assumed form of the flow consisted of the superposition of two counterrotating, finite core vortices. The positions of the vortex centers, their total circulation, the effective eddy viscosity and measurement bias were the parameters adjusted. Previous analyses of the experimental data have used graphical techniques to determine vortex-flow parameters. The modified Newton-Raphson method of analysis eliminates considerable manual labor and yields more consistent vortex-flow parameters.

The assumed form of vortex flow fit well the measured velocities for the numerous sets of data, both flaps up and down for the C-5A airplane. The resulting values of total circulation, however, were about two-thirds that expected of a wing with an elliptical loading. A partial explanation of the less than expected circulation is a dip in the spanwise lift distribution at the airplane's center line. The distance between the trailing vortices at the smallest times encountered is somewhat less than that expected for an elliptical wing loading. As the time and the distance behind the C-5A airplane increases, the positions of the vortex centers become more irregular. Although there is considerable scatter, the radius of the vortex cores appears to grow approximately as the square root of time. The initial core radius, however, is considerably smaller than expected when compared with values predicted using methods of Spreiter and Sacks and of Betz. The value of the effective eddy viscosity which would result in the measured core sizes is higher than the values obtained by most other investigators but is consistent with past results when the Reynolds number is considered.

17. Key Words (Suggested by Author(s))	18. Distribution Statement
Trailing vortices Modified Newton-Raphson method Wake turbulence	Unclassified – Unlimited STAR Category 12

19. Security Classif. (of this report)	20. Security Classif. (of this page)	21. No. of Pages	22. Price*
Unclassified	Unclassified	72	$3.75

*For sale by the National Technical Information Service, Springfield, Virginia 22151

A MODIFIED NEWTON-RAPHSON ANALYSIS OF FLIGHT MEASUREMENTS OF THE TRAILING VORTICES OF A HEAVY JET TRANSPORT

By Lawrence W. Taylor, Jr., and Milton D. McLaughlin
Langley Research Center

SUMMARY

A modified Newton-Raphson method has been used to determine the parameters in equations describing the vortex flow to obtain a best match with flight measurements of the flow behind the C-5A airplane. The flight measurements were made using a specially instrumented T-33 airplane which passed as closely as possible to the centers of the trailing vortices at several distances behind the C-5A airplane. The flight measurements were transformed to flow velocity relative to an inertial frame of reference. The assumed form of the flow consisted of the superposition of two counterrotating, finite core vortices. The positions of the vortex centers, their total circulation, the effective eddy viscosity and measurement bias were the parameters adjusted. Previous analyses of the experimental data have used graphical techniques to determine vortex-flow parameters. The modified Newton-Raphson method of analysis eliminates considerable manual labor and yields more consistent vortex-flow parameters.

The assumed form of vortex flow fit well the measured velocities for the numerous sets of data, both flaps up and down for the C-5A airplane. The resulting values of total circulation, however, were about two-thirds that expected of a wing with an elliptical loading. A partial explanation of the less than expected circulation is a dip in the spanwise lift distribution at the airplane's center line. The distance between the trailing vortices at the smallest times encountered is somewhat less than that expected for an elliptical wing loading. As the time and the distance behind the C-5A airplane increases, the positions of the vortex centers become more irregular. Although there is considerable scatter, the radius of the vortex cores appears to grow approximately as the square root of time. The initial core radius, however, is considerably smaller than expected when compared with values predicted using methods of Spreiter and Sacks and of Betz. The value of the effective eddy viscosity which would result in the measured core sizes is higher than the values obtained by most other investigators but is consistent with past results when the Reynolds number is considered.

INTRODUCTION

The hazard of flying in the wake of another airplane, particularly the wake of a large airplane, has long been recognized. Usually the problem is avoided by maintaining large distances between airplanes. In formation flight and during landing and taking off at busy airports, however, the distances between airplanes are short so that the vortex flow in their wakes can cause dangerous upsets. Unfortunately, efficient use of an airport requires airplanes to land and take-off at frequent intervals, the result being that the disturbing influence of the trailing vortices of airplanes has considerable effect on the safety and economic operation of these airplanes, particularly in the terminal area. Consequently, there is considerable interest in establishing a better understanding of the vortex flow in the wake of an airplane so that its disturbing influence can be reduced. For this reason the inflight measurements of the vortex flow in the wake of a C-5A heavy transport were made (ref. 1) and are being analyzed in this paper.

Considerable work has been performed in developing mathematical models of vortex flow. For example, in reference 2 a finite system of "horseshoe vortices" was used to approximate a particular wing loading, which in turn enabled the calculation of the "potential flow" at any point. By allowing the trailing vortex filaments to move with the induced flow, a "roll-up" of the vortex sheet into two dominant vortices is obtained (ref. 3) similar to that observed experimentally. There is, however, some question as to the validity of this lumped parameter model as far as the roll up is concerned since, as Jordan (ref. 4) has recently pointed out, an elliptical wing loading represented by a distributed system of vortices does not roll up at all without a disturbance. Also, since the viscosity of the air is neglected in these potential flow models, these vortices do not decay with age and one must resort to other formulations.

Lamb, in reference 5, gives a solution for a two dimensional, symmetrical, vortex having incompressible, laminar viscous flow. From initial conditions of infinitesimal core radius and infinite tangential velocity the solution shows that as time increases, the core radius increases, maximum tangential velocity decreases, and total circulation remains constant. Time behind the vortex generating airplane can, of course, be expressed in terms of distance. While the solution of reference 5 contains certain limitations imposed by the boundary conditions which do not allow interaction between layers of air at different distances behind the generating airplane, Lamb's solution remains a useful description of the decay of the vortex flow, particularly at large distances. Superposition may be assumed to obtain the total flow for both trailing vortices. Also, it is not necessary to use the same initial condition as that used by Lamb since a finite core radius and tangential velocity can be used by simply shifting the time reference. A rationale is needed, however, for the initial core size. Spreiter and Sacks suggest in reference 6 a way of determining a minimum core radius by equating the kinetic energy of the trailing

vortices to that created by the induced drag of the airplane. It is also possible to use the work of Betz in reference 7 to predict the initial core radius. But both methods predict an initial core radius considerably larger than that observed.

Because the actual vortex flow of an airplane may be turbulent, the assumption of laminar flow in Lamb's solution would not hold. It is common practice to use an empirical parameter, the effective eddy viscosity. Values of effective eddy viscosity which have been observed experimentally (refs. 8 to 12) range from 7 to 2000 times that of the kinematic viscosity for air. Some investigators (refs. 8 and 13) have suggested that the effective eddy viscosity is related to Reynolds number, and the experimental results of several investigations (refs. 14 to 18) support this view. It is difficult to obtain accurate values of the effective eddy viscosity in wind tunnels, especially at Reynolds numbers approaching flight values, because the test-section size restrictions prevent measurements from being made at the proper distances downstream of the model.

It was because of the hazard of trailing vortices and the limited understanding of them that a specially instrumented T-33 airplane was used to repeatedly probe the trailing vortices of a C-5A airplane. A simplified, graphical analysis of these test results have been reported in reference 1. In the present paper the same data is subjected to a more sophisticated numerical analysis to determine the characteristics of the vortex flow more accurately and to compare these results with analytical models of vortex flow. It is intended that an understanding of the phenomenon would be enhanced.

The basis of the analysis of the vortex flow in this paper involves the automatic adjustment of the parameters in a flow equation so that the calculated flow match the measured flow. Because of the nonlinear nature of the flow equation, a modified Newton-Raphson method (ref. 14) was employed to minimize the mean-square difference between the measured and theoretical flow velocities. Having applied this iterative procedure, the resulting experimental values, location of vortex center, circulation, tangential velocity, core radius, and eddy viscosity could be compared with theory.

SYMBOLS

a acceleration, m/sec^2

b bias in acceleration measurements, m/sec^2; wing span, m (see fig. 1)

b' distance between vortex centers, m

c unknown parameter vector; wing chord (see fig. 49), m

$\bar{c}$ mean aerodynamic chord (see fig. 1), m

c_l	local lift coefficient
g	acceleration due to gravity, m/sec^2
J	mean-square error
k	iteration index
p	roll rate, deg/sec
q	pitch rate, deg/sec
R	position vector, m
R_N	Reynolds number, Γ_0/ν
r	yaw rate, deg/sec; radial distance, m (see fig. 3)
r_c	radius of vortex core, m (see fig. 3)
S	wing area, m^2
T	translation matrix
t	time behind C-5A airplane, sec
V	flow velocity relative to inertial axes, m/sec
V_g	velocity of vortex-generating C-5A airplane, m/sec
V_m	measured flow velocity relative to inertial axes, m/sec
$V_{m,o}$	initial measured flow velocity, m/sec
V_p	velocity of probing T-33 airplane, m/sec
V_v	measured flow velocity relative to probing aircraft, m/sec
V_x,V_y,V_z	components of flow velocity, m/sec

$V_{y,o}, V_{z,o}$ initial values of V_y and V_z, m/sec

$\frac{dV_{y,o}}{dy}, \frac{dV_{z,o}}{dy}$ drift in V_y and V_z, 1/sec

V_θ tangential flow velocity, m/sec

$V_{\theta,max}$ maximum tangential flow velocity at core boundary, m/sec (see fig. 3)

x,y,z distance components, m

α angle of attack, deg

β angle of sideslip, deg

Γ circulation, m^2/sec

Γ_0 theoretical circulation, m^2/sec

θ pitch angle, deg

ν kinematic viscosity, m^2/sec

ν_t effective eddy viscosity, m^2/sec

ρ density, kg/m^3

ϕ bank angle, deg

ψ heading angle, deg

Superscript T denotes the transpose; subscripts 1 and 2 denote corresponding vortex.

DESCRIPTION OF FLIGHT TEST

Airplane Description

The airplane generating the trailing vortices analyzed in this study was the C-5A, a very large transport. A three-view drawing of the C-5A is given in figure 1 and the more pertinent dimensions are listed. The mass of the airplane ranged from 173 700 kilograms to 261 500 kilograms for the subject flight tests. The vortices were visible because of entrained engine smoke.

Flight Measurements

The vortex flow behind a C-5A airplane was probed using a specially instrumented T-33 airplane which measured linear accelerations, angular rates, flow vane deflections, Euler angles, and airspeed. The manner in which the probes were made is shown in figure 2. Passes of two types were used, those that were perpendicular to the flight path of the C-5A airplane and those that crossed at a shallow angle relative to the flight path of the C-5A airplane.

The raw data obtained from the instruments on board the T-33 airplane were recorded using oscillograph flight recorders. The data were processed to obtain measurements of the vortex-flow velocities relative to an inertial reference frame using the equation

$$V_m = T\left(V_v + \omega \times R\right) + \int_0^t \left\{T(a - b) + g\right\} dt - V_{m,o}$$

where V_m is measured flow velocity and

$$V_v = \begin{pmatrix} -V_p \cos \alpha \cos \beta \\ -V_p \sin \beta \\ -V_p \sin \alpha \end{pmatrix}$$

$$\omega = \begin{Bmatrix} p \\ q \\ r \end{Bmatrix}$$

R	vector distance from accelerometer location to vane location
a	acceleration vector at accelerator location
g	gravity vector
$V_{m,o}$	vector chosen to make $V_m = 0$ at $T = 0$
b	bias vector chosen to make $V_m = 0$ at end of run

$$T = \begin{bmatrix} \cos\theta\cos\psi & \sin\phi\sin\theta\cos\psi - \cos\phi\sin\psi & \cos\phi\sin\theta\cos\psi + \sin\phi\sin\psi \\ \cos\theta\sin\psi & \sin\phi\sin\theta\sin\psi + \cos\phi\cos\psi & \cos\phi\sin\theta\sin\psi - \sin\phi\cos\psi \\ -\sin\theta & \sin\phi\cos\theta & \cos\phi\cos\theta \end{bmatrix}$$

The exact alinement and location of the origin of these inertial axes was different for each run or pass of the probing airplane. As figure 2 indicates, the initial position attitude and direction of flight of the probing airplane establish the inertial axes used for each set of data analyzed. For further details see reference 1.

Although considerable care was given to insure accurate T-33 instrumentation, it was necessary to employ a special filter during data processing to partially compensate for the second-order dynamics of the flow vanes and airspeed system. The raw data were faired manually to suppress boom bending effects in the vane deflections.

One additional difficulty is a slight but occasionally important time shift that existed between the measured quantities due to differences in the response characteristics of the instruments. Although an adjustment was made in the manual analysis of reference 1, the adjustment was not made in the analysis using the modified Newton-Raphson method.

ANALYSIS

Vortex Flow Equations

The vortex-flow equation used to fit the flight measurements is based on that given by Lamb in reference 5 for two-dimensional, laminar, viscous flow. The tangential velocity for a single, isolated vortex is given by

$$V_\theta = \frac{\Gamma_0}{2\pi r}\left(1 - \exp\frac{-r^2}{4\nu t}\right)$$

The total flow velocity is assumed to be the superposition of two dominant trailing vortices with centers at y_1,z_1 and y_2,z_2. The three components of the calculated flow velocity are given by

$$V = \begin{Bmatrix} V_x \\ V_y \\ V_z \end{Bmatrix} = \frac{\Gamma\left(1 - \exp\frac{-r_1^2}{4\nu_t t}\right)}{2\pi r_1^2}\begin{pmatrix} 0 \\ -(z - z_1) \\ y - y_1 \end{pmatrix} - \frac{\Gamma\left(1 - \exp\frac{-r_2^2}{4\nu_t t}\right)}{2\pi r_2^2}\begin{pmatrix} 0 \\ -(z - z_2) \\ y - y_2 \end{pmatrix} + \begin{Bmatrix} 0 \\ V_{y,o} \\ V_{z,o} \end{Bmatrix} + \begin{pmatrix} 0 \\ \frac{dV_{y,o}}{dy} \\ \frac{dV_{z,o}}{dy} \end{pmatrix} y$$

where

$$r_1 = \sqrt{(y - y_1)^2 + (z - z_1)^2}$$

$$r_2 = \sqrt{(y - y_2)^2 + (z - z_2)^2}$$

The terms $V_{y,o}$, $V_{z,o}$, $\frac{dV_{y,o}}{dy}$, and $\frac{dV_{z,o}}{dy}$ are called bias terms and are added to account for uncertainties of the inertial reference frame.

There are, of course, many conditions which pertain to Lamb's solution which are not met. If the flow were actually symmetrical and laminar, then the value of the kinematic viscosity ν would simply be that for air. Unfortunately, the vortex flow in the wake of an airplane may be turbulent, and the initial roll-up process which forms a pair of almost symmetrical vortices may not be complete. Consequently, a value of ν that is many times that for air is often required to match the observed radius of the vortex core (ref. 11). This empirical value of ν is termed the effective eddy viscosity ν_t. The assumption of two-dimensional flow ignores the effect of shear between layers of air at different distances from the vortex-generating airplane and does not account for the axial flow V_x. Superposition is assumed to be valid for the flow of the two vortices although it is known that the Navier-Stokes equations are nonlinear.

McCormick in reference 16 has advanced an alternate form of flow equation which has been motivated by the empirical models of turbulent boundary layers and is compared with Lamb's solution and Spreiter-Sacks approximation in figure 3. It is clear that McCormick's formulation does not behave properly as the radius approaches zero. The limited information available, however, precludes a clear decision as to which flow equation might be most accurate. Lamb's solution was chosen simply because of its wide use and its analytical rather than empirical basis.

Modified Newton-Raphson Method

The purpose of the analysis is to determine the parameters Γ and ν_t in the flow equation so that the calculated flow is as close as possible to that measured. It is necessary also to determine the location of the centers of the two vortices and four bias terms to account for uncertainties in the reference frame, making a total of 10 unknown parameters:

$$c^T = y_1, y_2, z_1, z_2, \nu_t, \Gamma, V_{y,o}, \frac{dV_{y,o}}{dy}, V_{z,o}, \frac{dV_{z,o}}{dy}$$

It is apparent from the nonlinear form of the flow equation that an iterative procedure is required. A modified Newton-Raphson method (ref. 19) was selected because of its successful application in system identification problems. The criterion used in fitting the calculated flow to that measured is the mean-square error:

$$J = \sum_{n=1}^{N} \left[V_m(t_n) - V(t_n)\right]^T \left[V_m(t_n) - V(t_n)\right]$$

Estimates of the unknown parameters which form the vector $\hat{c}$ can be found by solving for the vector c which minimizes J. Since this condition is met when the gradient of J with respect to the unknown parameter vector c is zero, then $\hat{c}$ will be a root of the equation

$$\nabla_c J = 0$$

If the gradient is taken to be equal to

$$\nabla_c J_{k+1} = \nabla_c J_k + \nabla_c{}^2 J_k \left(c_{k+1} - c_k\right) = 0$$

then solving for c_{k+1} gives

$$c_{k+1} = c_k - \left[\nabla_c{}^2 J_k\right]^{-1} \nabla_c J_k$$

This is an application of the Newton-Raphson method.

For the problem considered, the first gradient is

$$\nabla_c J = -2 \sum_{n=1}^{N} \nabla_c V^T \left(V_m - V\right)$$

and the second gradient is

$$\nabla_c{}^2 J = -2 \sum_{n=1}^{N} \nabla_c V^T \nabla_c V - 2 \sum_{n=1}^{N} \nabla_c{}^2 V \left(V_m - V\right)$$

where the second term is negligible. In the interest of computational efficiency and programing simplicity, the second term in the expression for the second gradient is neglected. The recursive formula that is consequently used is

$$c_{k+1} = c_k - \left[\sum_{n=1}^{N} \left(\nabla_c V_n\right)^T \left(\nabla_c V_n\right)\right]^{-1} \sum_{n=1}^{N} \left(\nabla_c V_n\right)^T \left(V_{m,n} - V_n\right)$$

DISCUSSION OF RESULTS

Comparison of Methods of Analysis

An example result of applying the Newton-Raphson method to obtain estimates of the unknown parameters y_1, y_2, z_1, z_2, $\frac{\nu_t}{\nu}$, $\frac{\Gamma}{\Gamma_0}$, $V_{y,o}$, $\frac{dV_{y,o}}{dy}$, $V_{z,o}$, and $\frac{dV_{z,o}}{dy}$ is shown in figure 4. Shown are the mean-square error (dashed) and the 10 unknown parameters as a function of the iteration index. It is interesting that for the example shown, the mean-square error would appear to converge after seven iterations but the bias term $V_{y,o}$ required 20 iterations to settle completely. In general, the closer the probing airplane passes to the center of the vortices, the greater the reliability of the estimates and the fewer the number of iterations required. It is reasonable to expect this because of the insensitivity of the mean-square error to changes in the unknown parameters that occur at the large distances from the vortex centers. Consequently only runs which reached the edge of the core were used to determine the parameter ν_t.

An example comparison of the measured and theoretical vortex flow that results from applying the Newton-Raphson method is shown in figure 5. The data are for a perpendicular probe of the wake of a C-5A airplane with flaps up and a vortex age of about 24 sec. The theoretical values match those measured fairly well, considering both components must be matched simultaneously. By noting the sign of the lateral velocity at the points at which the vertical velocity is zero, it can be seen that the probing airplane passed above the center of the first vortex and below the center of the second vortex. Because the probing airplane happened to pass almost as close to the center of the second vortex as the first, the velocity functions are almost symmetrical.

At the bottom of figure 5 is a plot of nondimensional tangential velocity against nondimensional distance. The distance from the core has been divided by $\sqrt{4\nu_t t}$ and tangential velocity by $\Gamma_0 \Big/ \left(2\pi\sqrt{4\nu_t t}\right)$. The curve without symbols represents the calculated velocity; the curve with symbols, the measured. Both curves start on the right side, cross the origin as the probing airplane passes over or under the center of the first vortex center,

then double back over the origin as the second vortex is passed. The plot is useful in assessing whether a core penetration has been achieved by noting the minimum distance achieved.

Convergence is not always achieved in applying the Newton-Raphson method to a problem that is very nonlinear in the unknown parameters. If the starting values of the parameter differ greatly from those which minimize the mean-square error J, the iterative process will not converge. Preliminary work that is reported in reference 20 indicates the starting values of the vortex center positions need to be within 7 m of the final values. Convergence has not been difficult, however, to achieve in practice. One interesting feature of this particular problem is that the gradient of J approaches zero not only as convergence is obtained but also if the iterative process diverges. This is because of the insensitivity of the mean-square error to parameter changes at large distances from the centers of the vortices. One is assured of a legitimate solution however, if the cost subsides, if parameter values stabilize, and if the gradient of this cost continues to approach zero.

A graphical method, which was employed in reference 1 and is illustrated by figure 6, can be used to determine vortex centers. Lines are drawn perpendicular to the resultant flow. In the case of an isolated symmetrical vortex, these lines should pass through the center of the vortex. Errors in the flow measurements and the presence of at least two vortices limit, however, the accuracy with which the vortex centers can be determined. The motivation for applying the modified Newton-Raphson method to analyzing vortex-flow measurements was to eliminate the manual operations involved in the graphical approach and to improve the accuracy of the resulting estimates of core radii and effective eddy viscosity.

The flow velocities which result from applying the two methods of analysis are compared with that measured in figures 7(a) and 7(b). In the case of the graphical method, the values of core radius and tangential velocity given in reference 1 were used with Lamb's equation to compute the velocities shown. The calculated plots of the flow velocities for the modified Newton-Raphson technique are a best fit of the flight measurements. The positions of the vortex centers, eddy viscosity, circulation, and bias terms on the measured flow velocities were adjusted by the algorithm to minimize the mean-square error. As expected, the fit of the measured flow velocities is better in the case of the modified Newton-Raphson method, simply because that is the purpose of its use. In the case of figure 7(a) the difference is small, whereas in figure 7(b) the fit produced by the Newton-Raphson method is significantly better. Disagreement between the calculated and measured functions can be due to the limitations of using Lamb's solution as well as measurement errors.

Comparison of Calculated and Measured Flow

Figures 8 to 44 show the calculated vortex flow using a modified Newton-Raphson method compared with measured flow. Figures 8 to 22 are for the flaps up on the C-5A airplane, figures 23 to 44 are for flaps down. The figures are in order of increasing time behind the C-5A airplane. Table I contains a list of the vortex and generating airplane parameters that correspond to the figures.

The comparison between the calculated and measured flow is good in most cases, especially considering that both the lateral and vertical velocity components are fit simultaneously. Since the data for each run were taken for less than 1 sec, adequate instrumentation was a concern. A periodiclike error seen in many of the cases is attributed to nose boom bending. This error can be noted in figure 9, for example.

Some of the cases for flaps down indicate additional peaks in the flow velocity so that instead of two dominant trailing vortices there are four. This is most evident in figure 44. Unfortunately, the boom bending causes peaks at about the same period so that only speculation can be made. In the Newton-Raphson analysis, however, no provision for boom bending was made and only two vortices were assumed; as a result, the fit of the measured data was poor.

VORTEX CORE RADIUS AND EFFECTIVE EDDY VISCOSITY

It is usually assumed that the rollup of a vortex sheet behind a wing is essentially complete after several seconds. Further changes in the radius of the core of the pair of trailing vortices have then been attributed to viscosity of the air. For two-dimensional, symmetrical, viscous flow, Lamb shows the core radius r_c to be directly related to the kinematic viscosity by the expression

$$r_c = 2.24\sqrt{\nu t}$$

Unfortunately, the core radii calculated using this expression have not agreed with observations of vortex flow. Because of this, the practice has been to replace the kinematic viscosity with an empirical parameter, the effective eddy viscosity, and to adjust its value until the calculated core radius agrees with that observed. If this practice is applied to the results of the analysis presented herein, the comparisons shown in figures 45 to 50 can be obtained.

Since core radius, circulation, and maximum velocity are interrelated, it was necessary to consider the fairings of figures 45, 48, and 50 simultaneously to ensure the consistency of the faired results. In fairing the core-radius results of figure 45, it was

assumed that the rate of growth given by Lamb's solution would hold but that a finite, rather than an infinitesimal, core radius would exist at the time zero. It seemed reasonable to use the same value of effective eddy viscosity but not the same initial core radius for both the flaps-up and flaps-down cases. The equation of the fairings are given in figures 45(a) and 45(b).

Attempts were made to calculate the initial core radii using both the methods of Spreiter and Sacks of reference 6 and the radius of gyration of the vortex system discussed by Betz in reference 7. Both methods indicated the radius to be about 7 m to 8 m, about three times as large as that observed at points closest to the C-5A airplane. Because of this discrepancy an empirical value was used which best fit the observations.

The overall value of effective eddy viscosity which corresponds to the fairings shown on figures 45(a) and 45(b) is 634 times the kinematic viscosity ν of air. Figure 46 shows that this ratio of ν_t/ν is considerably greater than the corresponding experimental values taken from references 8, 9, 10, and 12 but is comparable to that observed by Rose and Dee in reference 11. Squire in reference 13 has suggested that the ratio of ν_t/ν should be proportional to a form of Reynolds number, $R_N = \Gamma_0/\nu$, while Owen argues ν_t/ν should vary proportional to the square root of R_N. Figure 46 shows the results of several investigations on a plot of ν_t/ν versus R_N and indicates a definite trend with Reynolds number. It would appear that ν_t/ν being proportional to the square root of R_N, as suggested by Owen, is the better description of the trend shown. A line with slope one-half has been drawn through the value of ν_t/ν obtained in the subject work. As R_N is decreased, it would be expected that the slope will become zero and ν_t/ν will approach one.

It is questionable that the entire growth of the vortex core can be attributed to viscous effects, even though it is common practice. It is disturbing that a ratio of ν_t/ν on the order of 600 is needed to match the observed core size; it is also disturbing that the core does not quite obtain the size expected from potential flow considerations. It is suspected that at least part of the observed growth in the core radius is due to the original rollup of the vortex sheet and is not entirely due to viscosity. Unfortunately, the information available is insufficient to resolve this question.

Distance Between Vortex Centers

The distance separating the trailing vortex centers as determined from the Newton-Raphson analysis is shown in figure 47. The value calculated using an elliptical spanwise lift distribution, which is $\pi/4$ times the span, is somewhat greater than that observed. As the distance and time behind the C-5A airplane is increased, a dispersion occurs which caused considerable variance in the distances measured. This is thought to be due to disturbances in the atmosphere and due to inherent instabilities of the pair of trailing vortices.

Parks (ref. 21) and many others have modeled and analyzed such phenomena and have shown that the trailing vortices snake in planes at 45^{o} to the vertical, with a wave length of 7.18 times the distance initially separating the vortices. Parks also gives a rate of divergence of the snaking. Asymptotes have been drawn on figure 47 to show the rate at which the snaking motion would grow from the same initial amplitude. It is interesting that the divergence envelopes resemble the growth of the dispersion of the distance between vortex centers. In smooth air the snaking results in the formation of "doughnuts" or ring vortices. If the wavelength of the snaking is taken as the half of the circumference of a circular ring, the maximum distance could reach 3.6 times the span. It can be seen in figure 47 that this distance is considerably greater than the largest distance measured.

Total Circulation

Another of the results of the analysis was a measure of the total circulation for each of the trailing vortices. The values obtained have been normalized using the value expected for an elliptical wing loading and are plotted in figure 48 for both flaps up and flaps down. Note that the total circulation obtained is generally less than that expected for an elliptical wing loading. Similar results have been obtained by many other investigators. It is believed that one reason lies with the fact that the spanwise lift distributions involved are not elliptical but have a dip at the plane of symmetry. Since the total circulation depends only on the center-line local lift coefficient by the relationship

$$\Gamma_0 = \frac{c_l c}{\bar{c}} \rho V_g$$

a dip in the wing loading distribution at the center line would produce less circulation than for an elliptical distribution. In the case of the C-5A flight results, a dip is known to occur for the wing and is expected to be amplified by the fuselage and tail. Figure 49 shows the wing spanwise lift distributions furnished by the Lockheed-Georgia Company. The value of the local lift coefficient at the plane of symmetry that would be necessary to agree with measured circulation is indicated by a circle for comparison. Because of interference of the sting mount used in the tunnel tests by Lockheed-Georgia, it was not possible to get complete data at the plane of symmetry.

The peak flow velocities divided by the circulation of an elliptical wing loading is presented for the C-5A airplane in figure 50. Vertical leaders on the points indicate the measured maximum values while the solid symbols give the maximum calculated velocity for each run. The open symbols are also the maximum calculated velocities; but since core penetration was not achieved, there is less confidence in their values. Except for a few points having considerable discrepancy the data is quite consistent. The fairings used

observed the direct relationship between the circulation of figure 48 and the core radius of figure 45.

CONCLUDING REMARKS

A modified Newton-Raphson method has been used successfully to determine estimates of the total circulation, effective eddy viscosity, and the locations of the centers of the trailing vortices of the C-5A airplane based on flight measurements. Lamb's solution has been used to model the vortex flow, and the comparison between the calculated flow and measured flow is good. The convergence properties when applying the modified Newton-Raphson method to such a nonlinear problem were good but required up to 20 iterations.

The vortex-core-radius values that were obtained using the analysis had considerable scatter but appear to grow in a manner similar to Lamb's solution but with a finite core radius initially. The initial core size obtained using the method of Spreiter and Sacks is considerably larger than that measured. If the growth in core size is attributed solely to viscous effects, the value of effective eddy viscosity obtained is greater than the results of most other investigations but follows a trend indicating effective eddy viscosity to be proportional to the square root of Reynolds number. The distance separating the vortices at the smallest times encountered is somewhat less than that predicted for an elliptical wing loading. At greater distances behind the C-5A airplane, dispersion exists. It is suggested that the dispersion is due in part to the unstable snaking action modeled by Parks and others. The total circulation obtained is less than that expected for an elliptical spanwise lift distribution and decreases with time and distance behind the C-5A airplane.

Previous analyses of the experimental data have used graphical techniques to determine vortex flow parameters. The modified Newton-Raphson analysis reduces considerably the manual effort of graphical techniques and is believed to give more accurate results.

Langley Research Center,
National Aeronautics and Space Administration,
Hampton, Va., July 3, 1974.

APPENDIX

GRADIENT EXPRESSIONS

The formulation used for the gradient of the flow velocity V with respect to the unknown parameter vector c is as follows:

$$\nabla_c{}^T V = \begin{bmatrix} \frac{\partial V_x}{\partial y_1} & \frac{\partial V_y}{\partial y_1} & \frac{\partial V_z}{\partial y_1} \\ \frac{\partial V_x}{\partial y_2} & \frac{\partial V_y}{\partial y_2} & \frac{\partial V_z}{\partial y_2} \\ \frac{\partial V_x}{\partial z_1} & \frac{\partial V_y}{\partial z_1} & \frac{\partial V_z}{\partial z_1} \\ \frac{\partial V_x}{\partial z_2} & \frac{\partial V_y}{\partial z_2} & \frac{\partial V_z}{\partial z_2} \\ \frac{\partial V_x}{\partial \nu_t} & \frac{\partial V_y}{\partial \nu_t} & \frac{\partial V_z}{\partial \nu_t} \\ \frac{\partial V_x}{\partial \Gamma} & \frac{\partial V_y}{\partial \Gamma} & \frac{\partial V_z}{\partial \Gamma} \\ \frac{\partial V_x}{\partial V_{y,o}} & \frac{\partial V_y}{\partial V_{y,o}} & \frac{\partial V_z}{\partial V_{y,o}} \\ \frac{\partial V_x}{\partial \frac{dV_{y,o}}{dy}} & \frac{\partial V_y}{\partial \frac{dV_{y,o}}{dy}} & \frac{\partial V_z}{\partial \frac{dV_{y,o}}{dy}} \\ \frac{\partial V_x}{\partial V_{z,o}} & \frac{\partial V_y}{\partial V_{z,o}} & \frac{\partial V_z}{\partial V_{z,o}} \\ \frac{\partial V_x}{\partial \frac{dV_{z,o}}{dy}} & \frac{\partial V_y}{\partial \frac{dV_{z,o}}{dy}} & \frac{\partial V_z}{\partial \frac{dV_{z,o}}{dy}} \end{bmatrix}$$

where

$$\frac{\partial V_x}{\partial c} = 0$$

$$\frac{\partial V_y}{\partial y_1} = V_{\theta,1} \frac{\partial \sin \theta_1}{\partial r_1} \frac{\partial r_1}{\partial y_1} + \sin \theta_1 \frac{\partial V_{\theta,1}}{\partial r_1} \frac{\partial r_1}{\partial y_1}$$

$$\frac{\partial V_z}{\partial y_1} = V_{\theta,1} \left(\frac{\partial \cos \theta_1}{\partial r_1} \frac{\partial r_1}{\partial y_1} - \frac{1}{r_1} \right) + \cos \theta_1 \frac{\partial V_{\theta,1}}{\partial r_1} \frac{\partial r_1}{\partial y_1}$$

$$\frac{\partial V_y}{\partial y_2} = -V_{\theta,2} \frac{\partial \sin \theta_2}{\partial r_2} \frac{\partial y_2}{\partial y_2} - \sin \theta_2 \frac{\partial V_{\theta,2}}{\partial r_2} \frac{\partial r_2}{\partial y_2}$$

$$\frac{\partial V_z}{\partial y_2} = -V_{\theta,2} \left(\frac{\partial \cos \theta_2}{\partial r_2} \frac{\partial r_2}{\partial y_2} - \frac{1}{r_2} \right) - \cos \theta_2 \frac{\partial V_{\theta,2}}{\partial r_2} \frac{\partial r_2}{\partial y_2}$$

$$\frac{\partial V_y}{\partial z_1} = V_{\theta,1} \left(\frac{\partial \sin \theta_1}{\partial r_1} \frac{\partial r_1}{\partial z_1} + \frac{1}{r_1} \right) + \sin \theta_1 \frac{\partial V_{\theta,1}}{\partial r_1} \frac{\partial r_1}{\partial z_1}$$

$$\frac{\partial V_z}{\partial z_1} = V_{\theta,1} \frac{\partial \cos \theta_1}{\partial r_1} \frac{\partial r_1}{\partial z_1} + \cos \theta_1 \frac{\partial V_{\theta,1}}{\partial r_1} \frac{\partial r_1}{\partial z_1}$$

$$\frac{\partial V_y}{\partial z_2} = -V_{\theta,2} \left(\frac{\partial \sin \theta_2}{\partial r_2} \frac{\partial r_2}{\partial z_2} + \frac{1}{r_2} \right) - \sin \theta_2 \frac{\partial V_{\theta,2}}{\partial r_2} \frac{\partial r_2}{\partial z_2}$$

$$\frac{\partial V_z}{\partial z_2} = -V_{\theta,2} \frac{\partial \cos \theta_2}{\partial r_2} \frac{\partial r_2}{\partial z_2} - \cos \theta_2 \frac{\partial V_{\theta,2}}{\partial r_2} \frac{\partial r_2}{\partial z_2}$$

$$\frac{\partial V_y}{\partial \nu_t} = -\frac{1}{4 \nu_t^2 t} \left(\sin \theta_1 \frac{\partial V_{\theta,1}}{\partial A} - \sin \theta_2 \frac{\partial V_{\theta,2}}{\partial A} \right)$$

$$\frac{\partial V_z}{\partial \nu_t} = -\frac{1}{4 \nu_t^2 t} \left(\cos \theta_1 \frac{\partial V_{\theta,1}}{\partial A} - \cos \theta_2 \frac{\partial V_{\theta,2}}{\partial A} \right)$$

$$\frac{\partial V_y}{\partial \Gamma} = \frac{V_y}{\Gamma}$$

$$\frac{\partial V_z}{\partial \Gamma} = \frac{V_z}{\Gamma}$$

$$\frac{\partial V_y}{\partial V_{y,o}} = 0$$

$$\frac{\partial V_z}{\partial V_{y,o}} = -1$$

$$\frac{\partial V_y}{\partial \dfrac{dV_y}{dy}} = 0$$

$$\frac{\partial V_z}{\partial \dfrac{dV_y}{dy}} = -y$$

$$\frac{\partial V_y}{\partial V_{z,o}} = -1$$

$$\frac{\partial V_z}{\partial V_{z,o}} = 0$$

$$\frac{\partial V_y}{\partial \dfrac{dV_z}{dy}} = -y$$

$$\frac{\partial V_z}{\partial \dfrac{dV_z}{dy}} = 0$$

$$\frac{\partial \sin \theta_1}{\partial r_1} = -\frac{\sin \theta_1}{r_1}$$

$$\frac{\partial \sin \theta_2}{\partial r_2} = -\frac{\sin \theta_2}{r_2}$$

$$\frac{\partial r_1}{\partial y_1} = -\cos \theta_1$$

$$\frac{\partial r_2}{\partial y_2} = -\cos \theta_2$$

$$\frac{\partial r_1}{\partial z_1} = \sin \theta_1$$

$$\frac{\partial r_2}{\partial z_2} = \sin \theta_2$$

$$\frac{\partial V_{\theta,1}}{\partial r_1} = -\frac{V_1}{r_1} + 2Ake^{-Ar_1^2}$$

$$\frac{\partial V_{\theta,2}}{\partial r_2} = \frac{V_2}{r_2} - 2Ake^{-Ar_2^2}$$

$$\frac{\partial \cos \theta_1}{\partial r_1} = -\frac{y - y_1}{r_1^2}$$

$$\frac{\partial \cos \theta_2}{\partial r_2} = -\frac{y - y_2}{r_2^2}$$

$$\frac{\partial V_{\theta,1}}{\partial A} = kr_1 e^{-Ar_1^2}$$

$$\frac{\partial V_{\theta,2}}{\partial A} = -kr_2 e^{-Ar_2^2}$$

$$A = \frac{1}{4\nu_t t}$$

$$\theta_1 = A \tan \frac{-(z - z_1)}{y - y_1}$$

$$\theta_2 = A \tan \frac{-(z - z_2)}{y - y_2}$$

$$k = \frac{\Gamma_0}{2\pi}$$

REFERENCES

1. Verstynen, Harry A., Jr., and Dunham, R. Earl, Jr.: A Flight Investigation of the Trailing Vortices Generated by a Jumbo Jet Transport. NASA TN D-7172, 1973.

2. Prandtl, L.: Tragflügeltheorie. I. Mitteilung. From "Vier Abhandlungen zur Hydrodynamik und Aerodynamik" by L. Prandtl and A. Betz. Kaiser Wilhelm-Instituts für Strömungsforschung (Göttingen), 1927.

3. Westwater, F. L.: Rolling up on the Surface of Discontinuity Behind an Aerofoil of Finite Span. R.&M. No. 1692, British A.R.C., 1935.

4. Jordan, Peter F.: Span Loading and Wake Formation. Sci. Rep. AFOSR 70-2873TR U.S. Air Force, Dec. 1970.

5. Lamb, Horace: Hydrodynamics. Sixth ed., Cambridge Univ. Press, 1932.

6. Spreiter, John R.; and Sacks, Alvin H.: The Rolling up of the Trailing Vortex Sheet and Its Effect on the Downwash Behind Wings. J. Aeronaut. Sci., vol. 18, no. 1, Jan. 1951, pp. 21-32, 72.

7. Betz, A.: Behavior of Vortex Systems. NACA TM 713, 1933.

8. Owen, P. R.: The Decay of a Trailing Vortex. Aeronaut. Quart., vol. XXI, pt. 1, Feb. 1970, pp. 69-78.

9. Newman, B. G.: Flow in a Viscous Trailing Vortex. Aeronaut. Quart., vol. X, pt. 2, May 1959, pp. 149-162.

10. Dosanjh, D. S.; Gasparek, E. P.; and Eskinazi, S.: Decay of a Viscous Trailing Vortex. Aeronaut. Quart., vol. XIII, pt. 2, May 1962, pp. 167-188.

11. Rose, R.; and Dee, F. W.: Aircraft Vortex Wakes and Their Effects on Aircraft. CP-795, Brit. A.R.C., Dec. 1965.

12. Mason, William Henry; and Marchman, James Franklin, III: Farfield Structure of an Aircraft Trailing Vortex, Including Effects of Mass Injection. Grant. No. NGL 47-004-067, Virginia Polytechnic Inst. & State Univ., Apr. 1972.

13. Squire, H. B.: The Growth of a Vortex in Turbulent Flow. Rep. No. FM 2053, Brit. A.R.C., Mar. 18, 1954; also published in Aeronaut. Quart., vol. XVI, pt. 3, Aug. 1965, pp. 302-306.

14. Birkhoff, Garrett; and Zarantonello, E. H.: Jets, Wakes and Cavities. Academic Press, Inc., 1957, p. 283.

15. Schaefer, John W.; and Eskinazi, Salamon: An Analysis of the Vortex Street Generated in a Viscous Fluid. J. Fluid Mech., vol. 6, pt. 2, Aug. 1959, pp. 241-260.

16. McCormick, Barnes W.; Tangler, James L.; and Sherrieb, Harold E.: Structure of Trailing Vortices. J. Aircraft, vol. 5, no. 3, May-June 1968, pp. 260-267.

17. Eisenhuth, Joseph J.; McCormick, Barnes W.; Nelson, Robert C.; and Garodz, Leo J.: Analysis of Experimental Measurements of Trailing Vortex Systems of Large Jet Transport Aircraft. 1971 Proceedings of the National Aerospace Electronics Conference, IEEE, May 1971, pp. 28-35.

18. Kerr, T. H.; and Dee, F.: A Flight Investigation Into the Persistence of Trailing Vortices Behind Large Aircraft. Tech. Note No. Aero. 2649, British R.A.E., Sept. 1959.

19. Taylor, Lawrence W., Jr.; and Iliff, Kenneth W.: Systems Identification Using a Modified Newton-Raphson Method – A FORTRAN Program. NASA TN D-6734, 1972.

20. Taylor, Lawrence W., Jr.; and McLaughlin, Milton D.: Application of a Modified Newton-Raphson Method for Estimation of Vortex Flow Parameters. 1971 IEEE Conference on Decision and Control, Inst. Elect. Electron. Eng., c.1971, pp. 40-41.

21. Parks, P. C.: A New Look at the Dynamics of Vortices With Finite Cores. Symposium on Aircraft Wake Turbulence, Doc. D1-82-0993, Flight Sci. Lab., Boeing Sci. Res. Labs., Sept. 1970, pp. 63-64. (Available from DDC as AD 712 080.)

TABLE I.- VORTEX AND GENERATING AIRPLANE PARAMETERS

Symbols used in figs. 45, 47, 48, and 50 (a)	Vortex age, sec	Distance, m	Mass, kg	Altitude, m	Velocity, m/sec	Circulation (theor.), m^2/sec	Heading angle, deg	Figure
Flaps up								
□	12	1 130	206 200	1975	98	383	76	8
▲	19	2 148	215 500	4590	113	456	75	9
◆	24	2 371	197 000	1766	96	365	-96	10
◣	29	2 759	197 000	2009	98	369	-82	11
◤	32	3 352	189 200	3658	105	390	-6	12
◙	34	3 945	187 800	4578	116	387	-87	13
▼	42	4 093	191 000	1972	97	360	[b]-9	14
⬟	46	4 463	191 000	1981	98	357	12	15
⬟	60	6 889	239 000	4578	115	478	83	16
◢	63	6 334	179 700	1993	98	334	84	17
◤	70	7 093	175 100	2286	101	326	94	18
◙	70	7 704	233 700	3652	110	461	84	19
●	98	10 538	261 500	3652	108	526	76	20
■	104	10 192	173 700	2295	99	331	90	21
◇	114	13 131	189 300	4578	116	390	-81	22
Flaps down								
▽	22	1 852	224 900	4572	84	635	-75	23
○	30	2 889	240 900	4572	96	600	92	24
◇	37	2 889	201 200	4572	89	537	75	25
△	40	3 537	202 300	4572	89	540	-75	26
⬠	41	3 648	207 200	4572	89	553	-85	27
◸	41	3 648	201 900	4572	89	539	86	28
□	42	3 760	201 300	4572	89	537	-80	29
⌂	44	4 167	236 700	4572	96	590	-91	30
●	59	5 260	204 600	4572	89	546	-88	31
■	60	5 389	204 400	4572	89	546	85	32
◿	60	5 037	204 600	4596	84	586	-94	33
◤	63	6 019	236 600	4572	96	589	80	34
⬠	64	5 667	206 300	4572	89	551	87	35
◁	68	7 871	184 900	4578	116	381	-77	36
◆	78	7 464	236 300	4572	96	589	-90	37
▲	82	7 815	239 600	4572	96	597	-90	38
⬠	85	7 186	222 600	4578	84	629	93	39
◣	92	7 704	204 400	4596	84	585	76	40
◇	109	9 093	197 900	4587	84	566	84	41
◇	115	11 001	235 700	4572	96	587	-85	42
◤	116	9 723	204 100	4590	84	584	-95	43
◙	133	12 668	238 700	4572	96	595	-78	44

[a]Filled symbols denote core penetration.

[b]Adjusted to be consistent with distance between vortex centers.

C-5A

S = 576 m^2

b = 66.7 m

$\bar{c}$ = 9.2 m

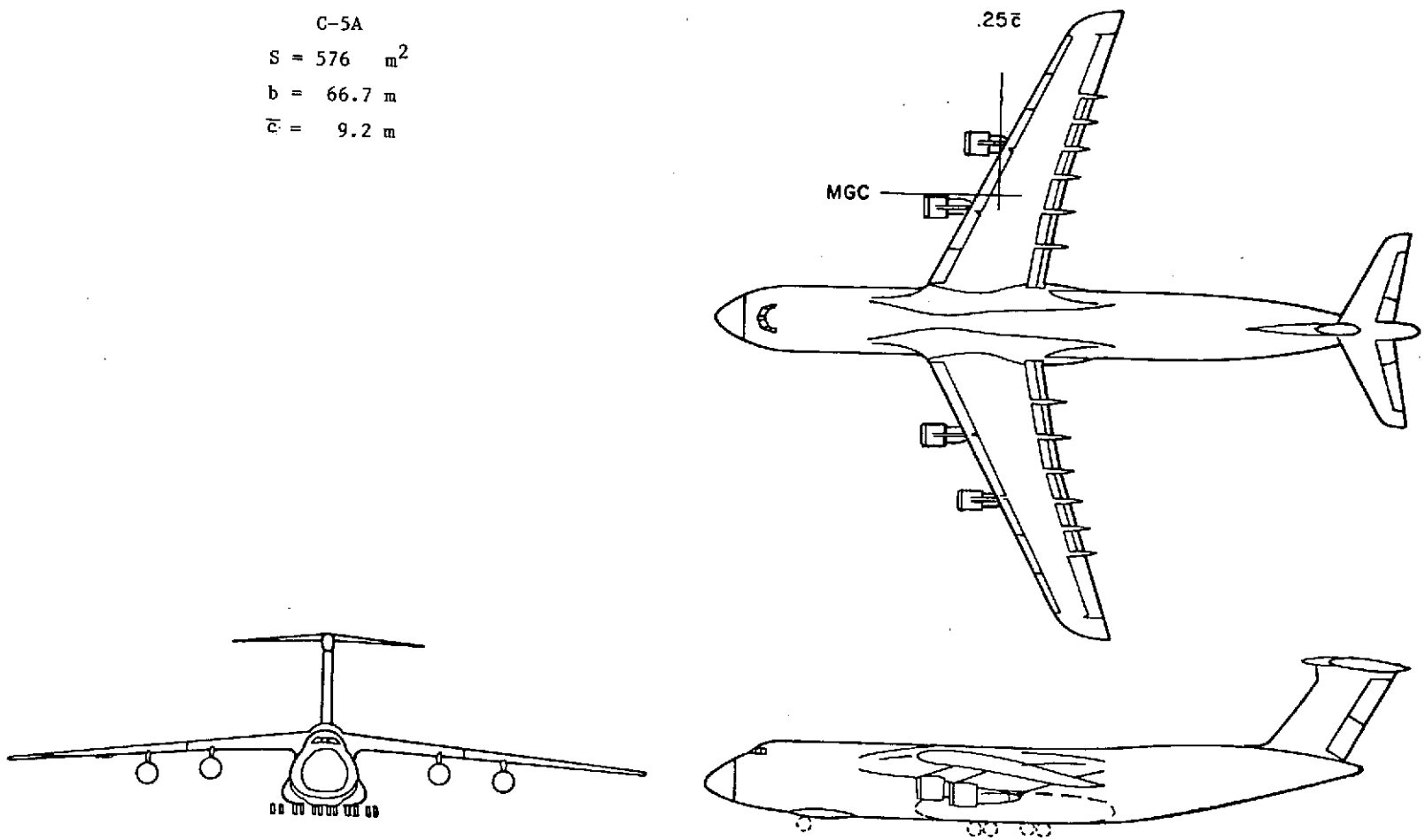

Figure 1.- Three-view drawing of the C-5A heavy jet transport.

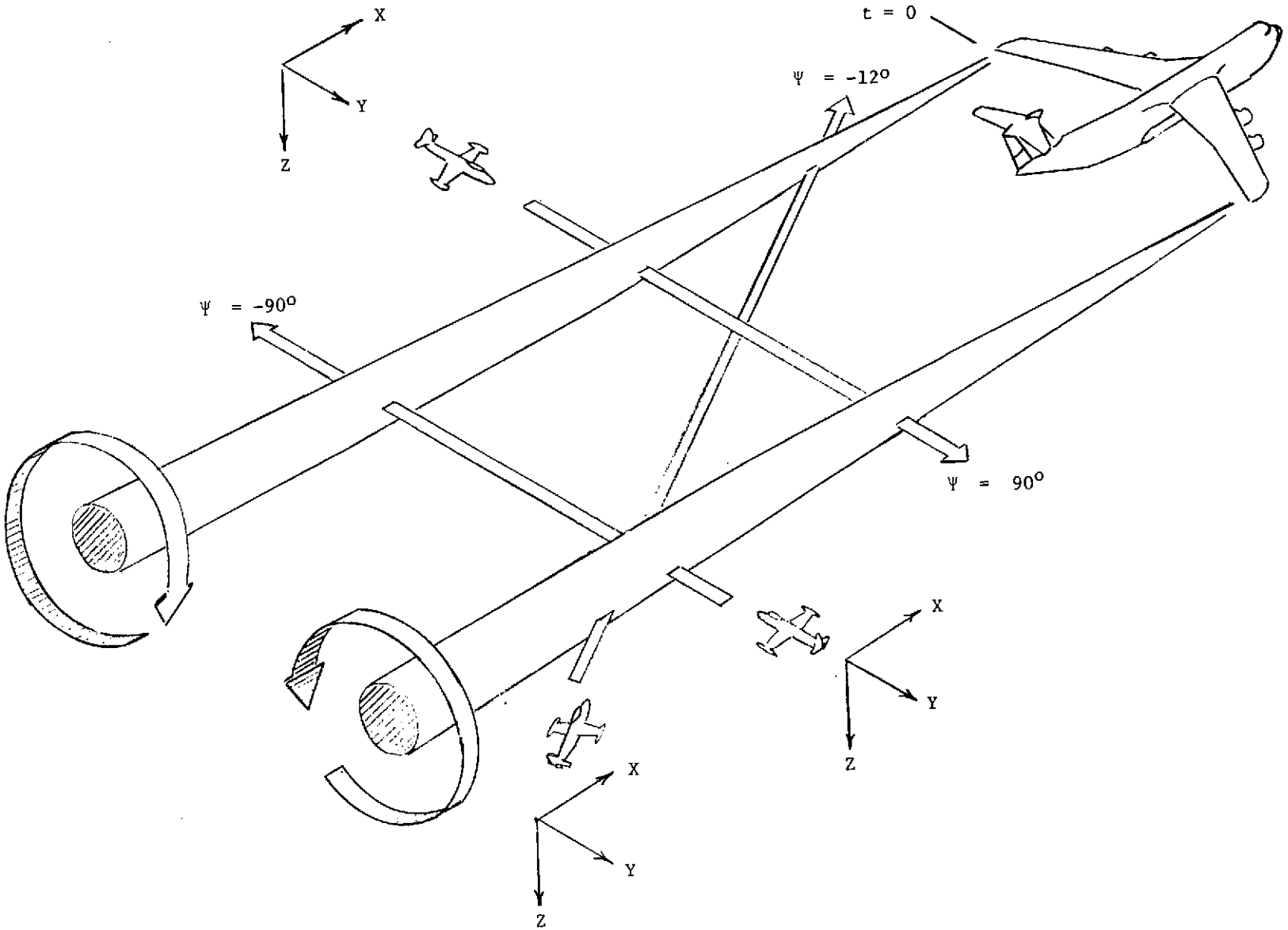

Figure 2.- Paths taken by probing airplane.

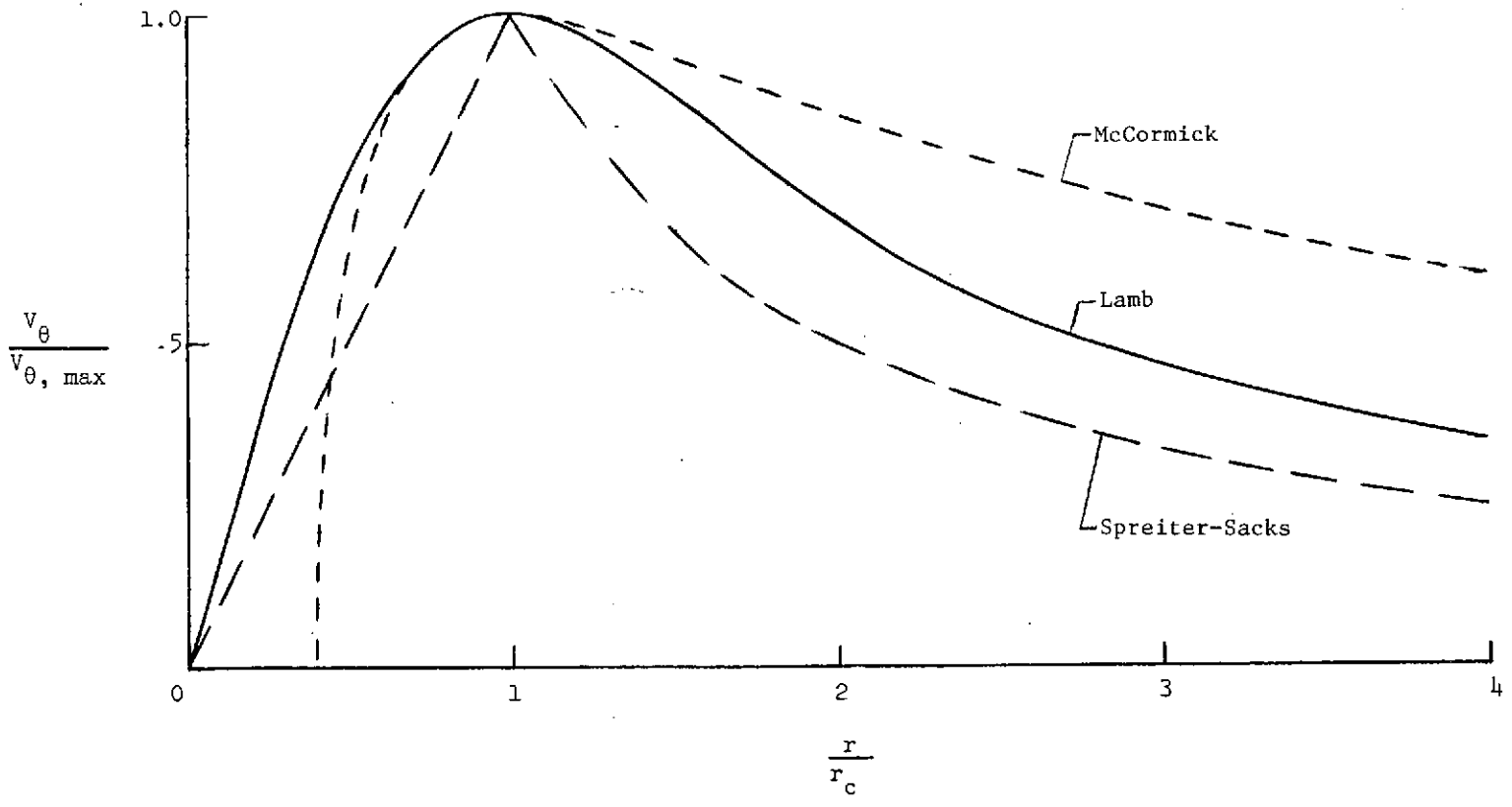

Figure 3.- Comparison of flow equations.

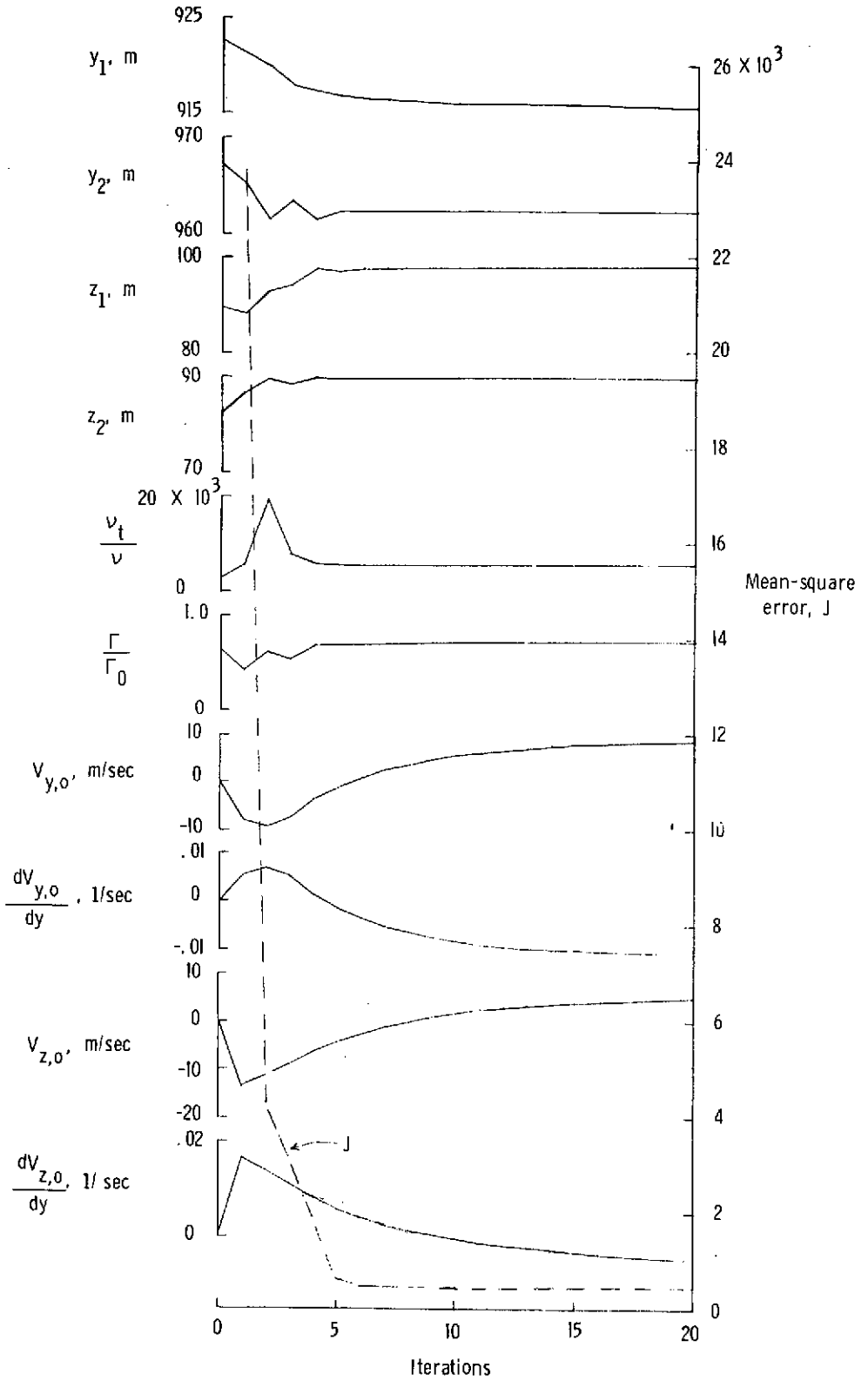

Figure 4.- Convergence properties of modified Newton-Raphson method.

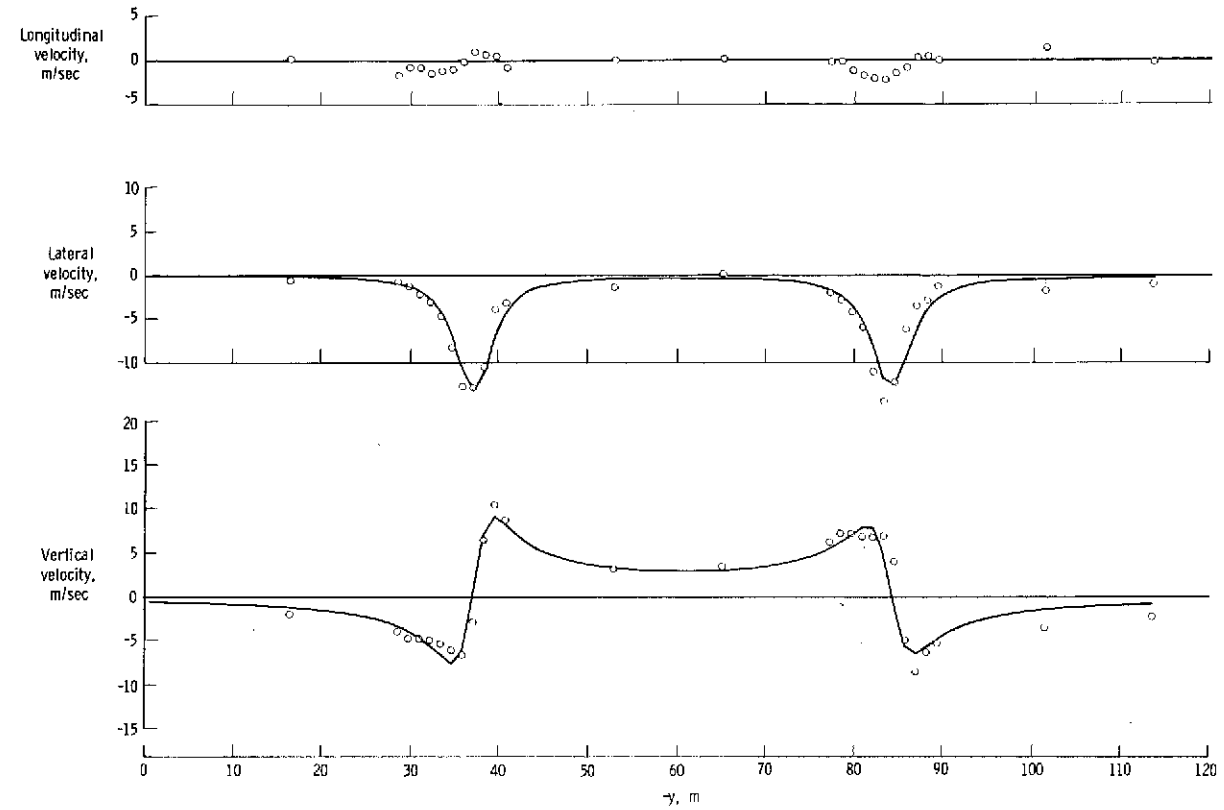

(a) Velocity versus distance.

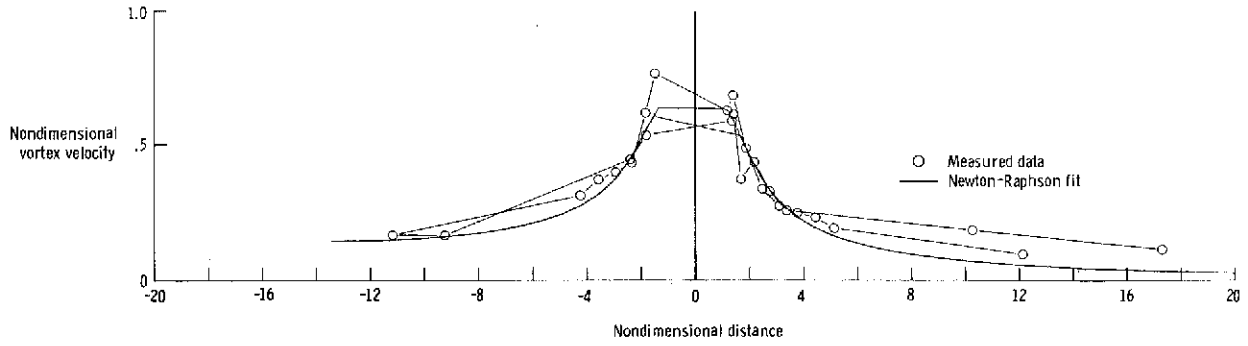

(b) Nondimensional velocity versus nondimensional distance.

Figure 5.- Comparison of measured and theoretical vortex flow.

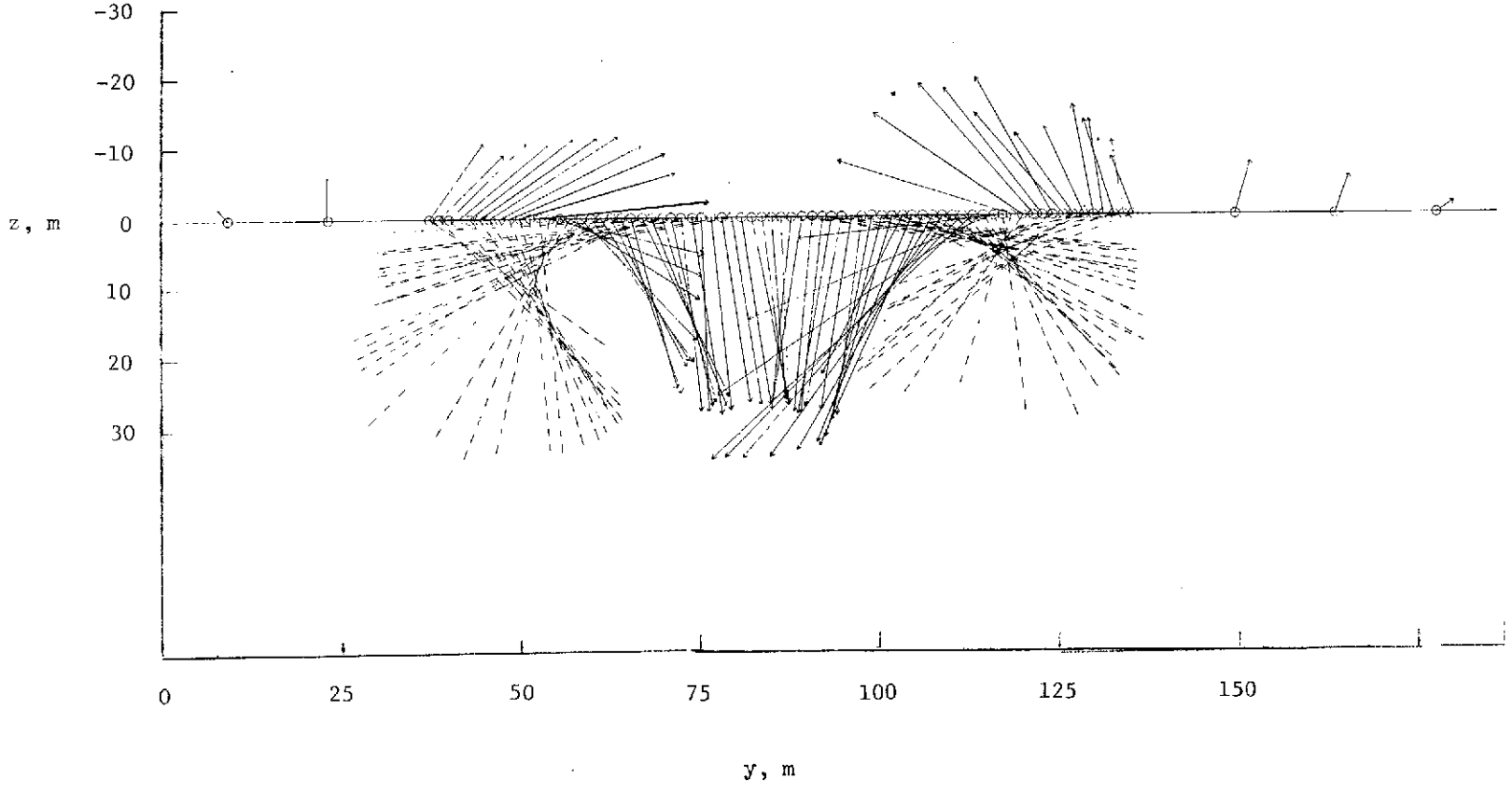

Figure 6.- Graphical method of locating vortex centers.

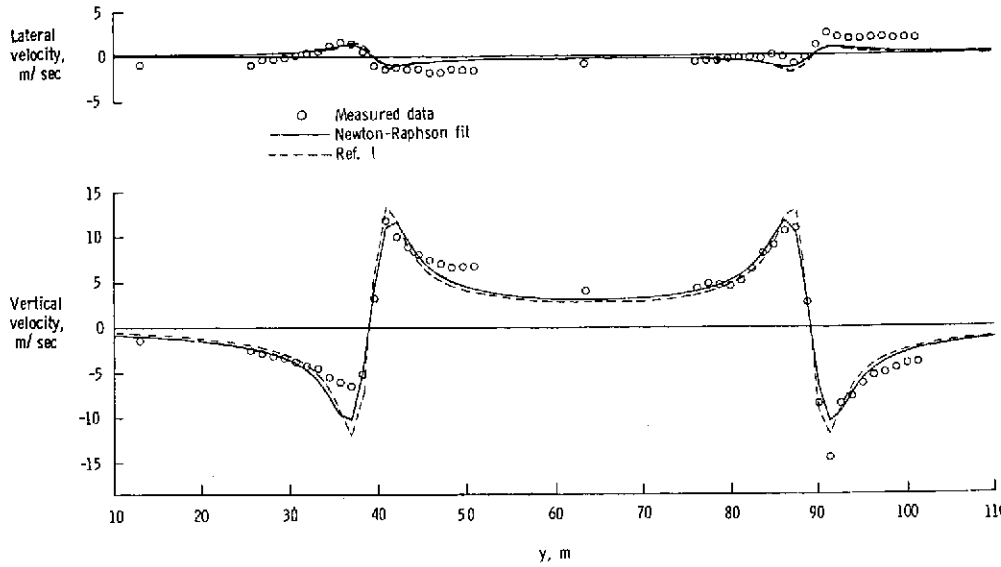

(a) Example 1.

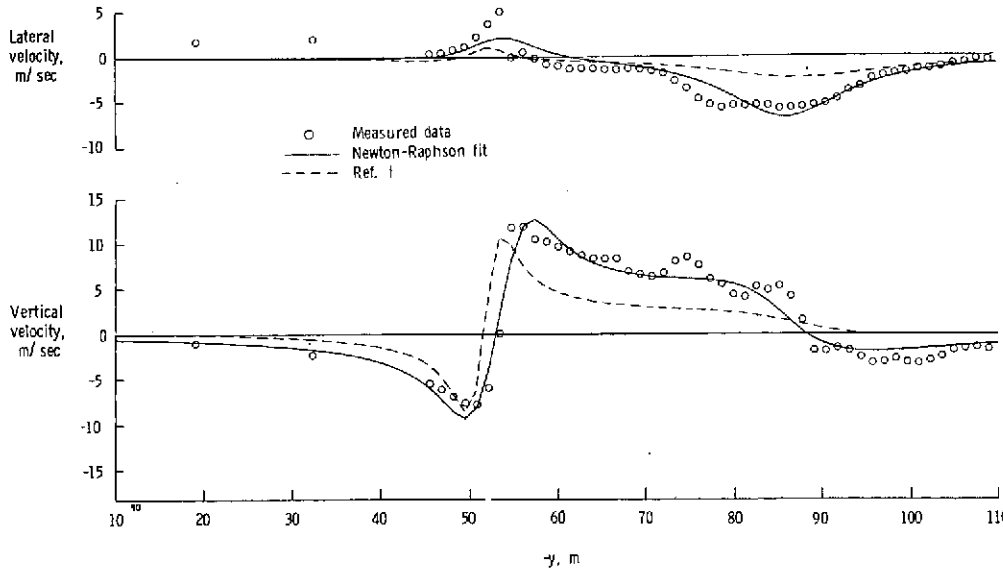

(b) Example 2.

Figure 7.- Comparison of methods used to analyze vortex-flow measurements for two examples.

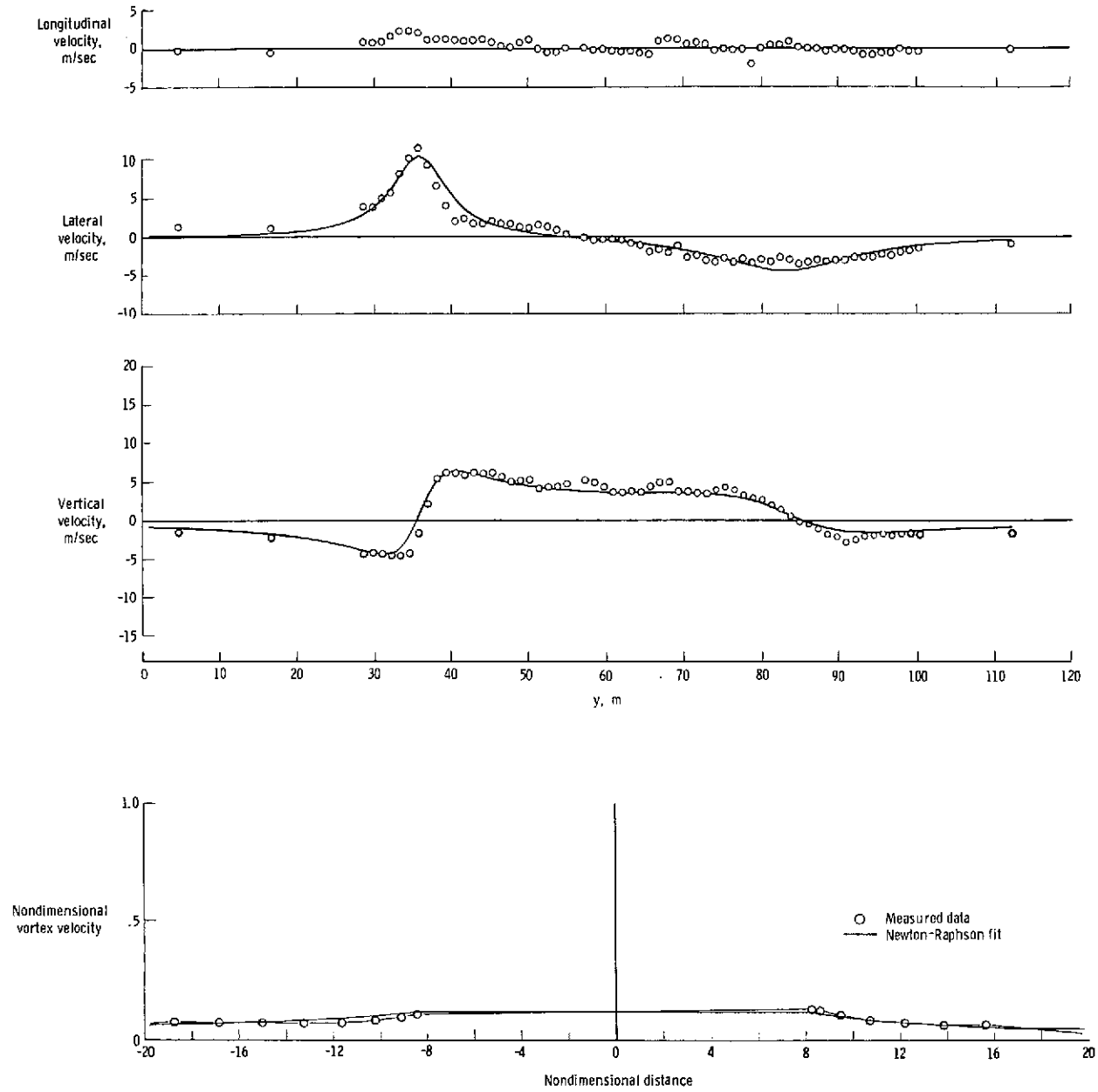

Figure 8.- Comparison of Newton-Raphson fit with measured flow velocities for flaps up and vortex age of 12 seconds.

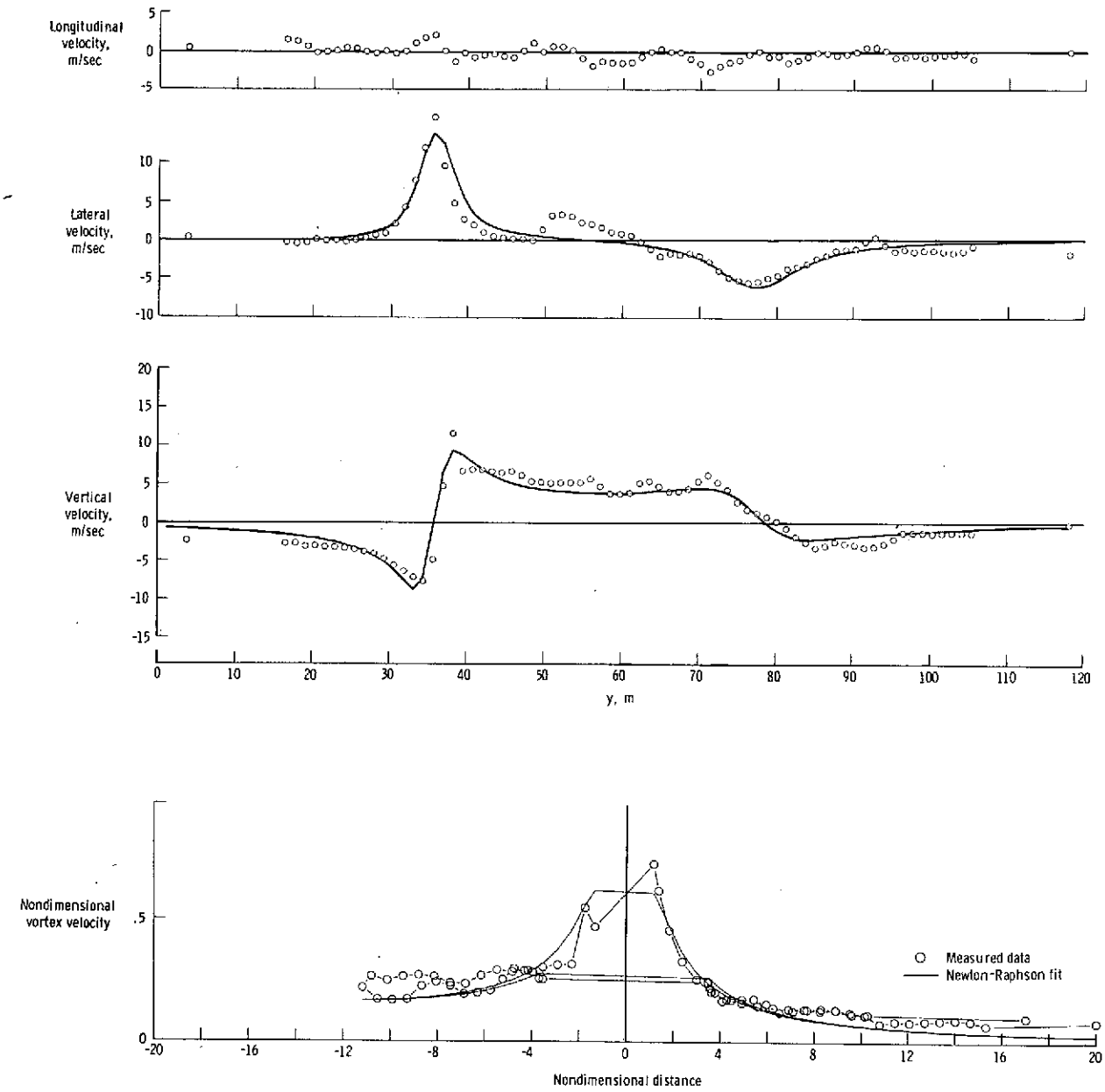

Figure 9.- Comparison of Newton-Raphson fit with measured flow velocities for flaps up and vortex age of 19 seconds.

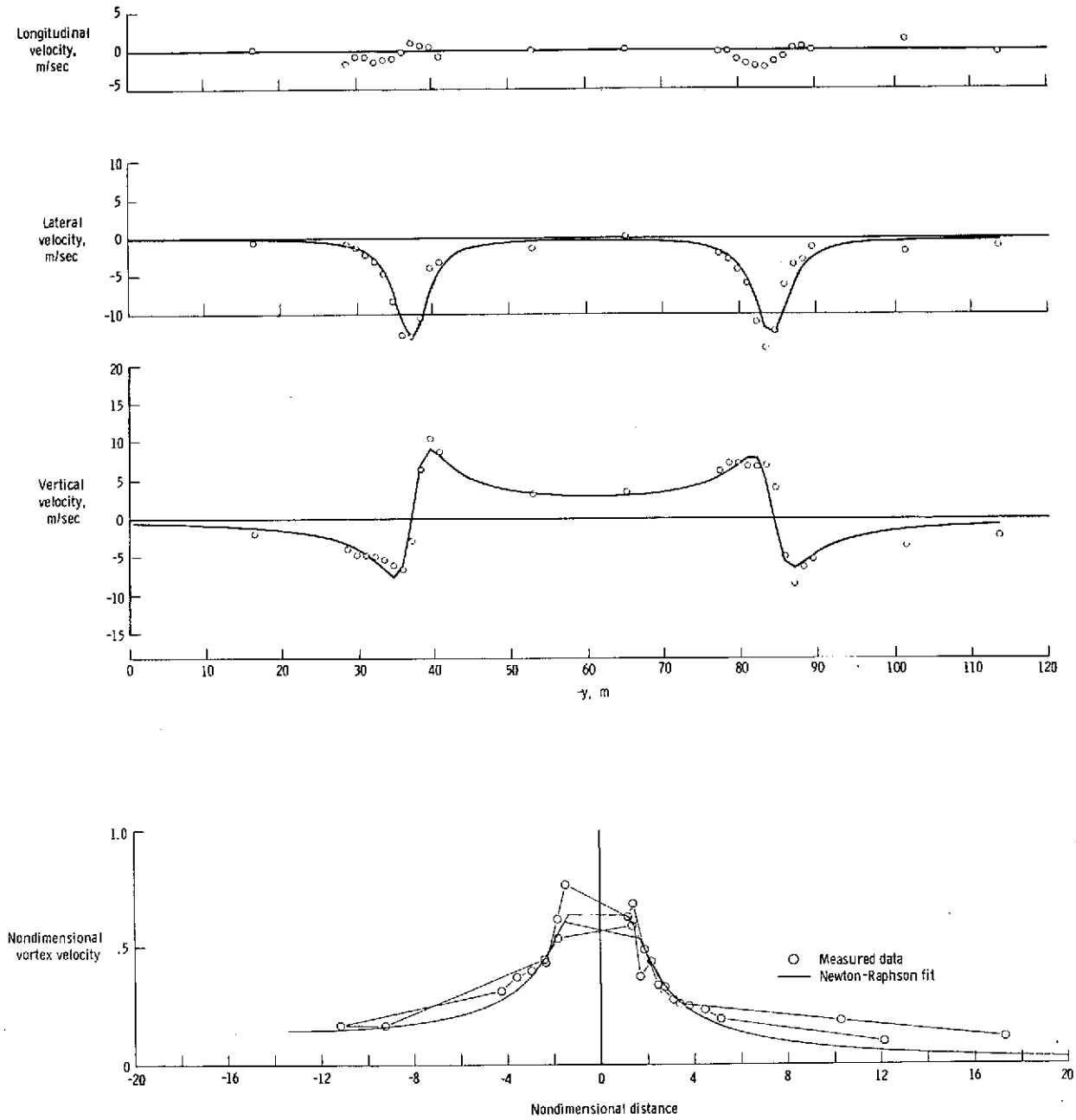

Figure 10.- Fit of measured data using modified Newton-Raphson method for flaps up and vortex age of 24 seconds.

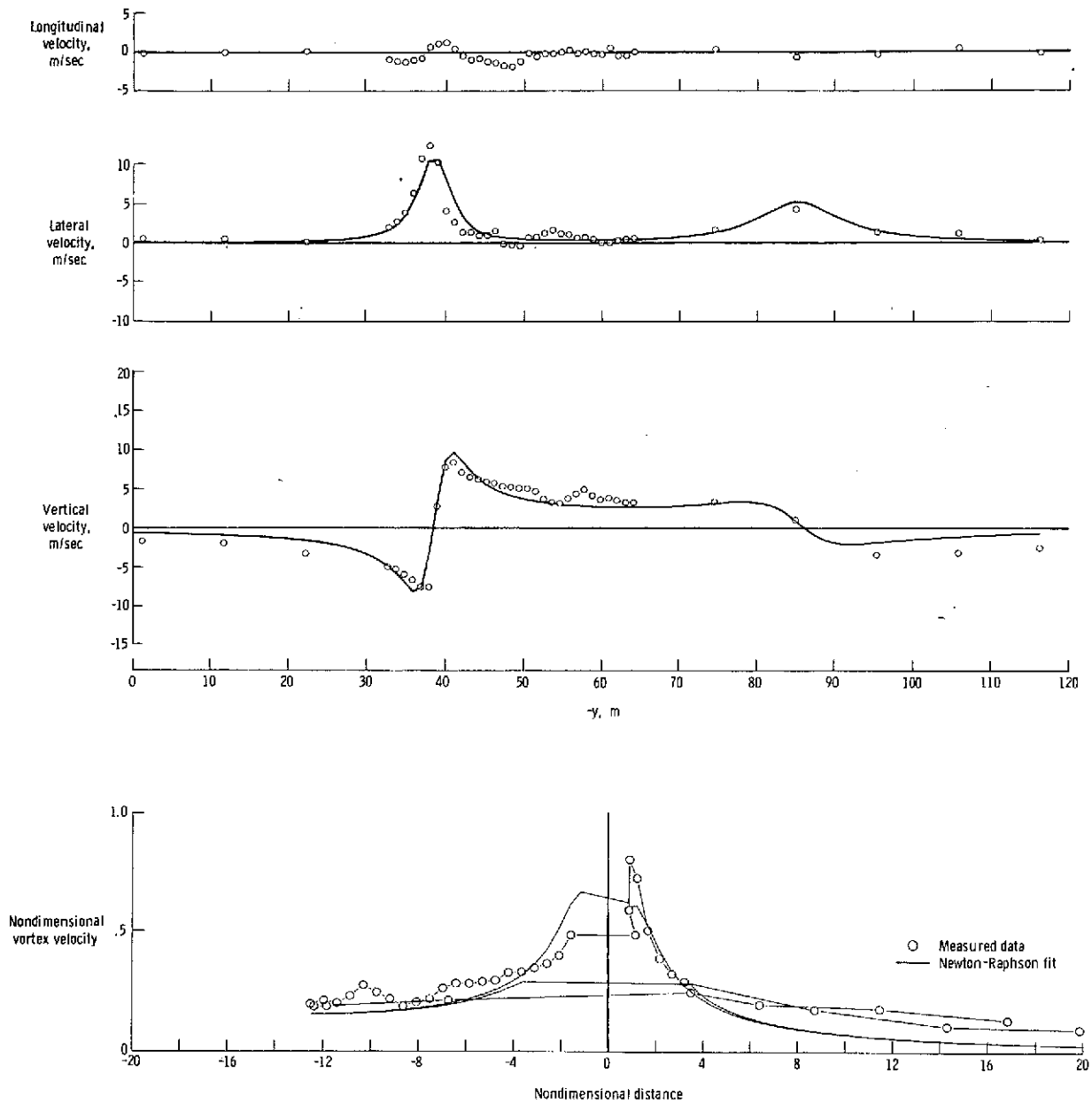

Figure 11.- Comparison of Newton-Raphson fit with measured flow velocities for flaps up and vortex age of 29 seconds.

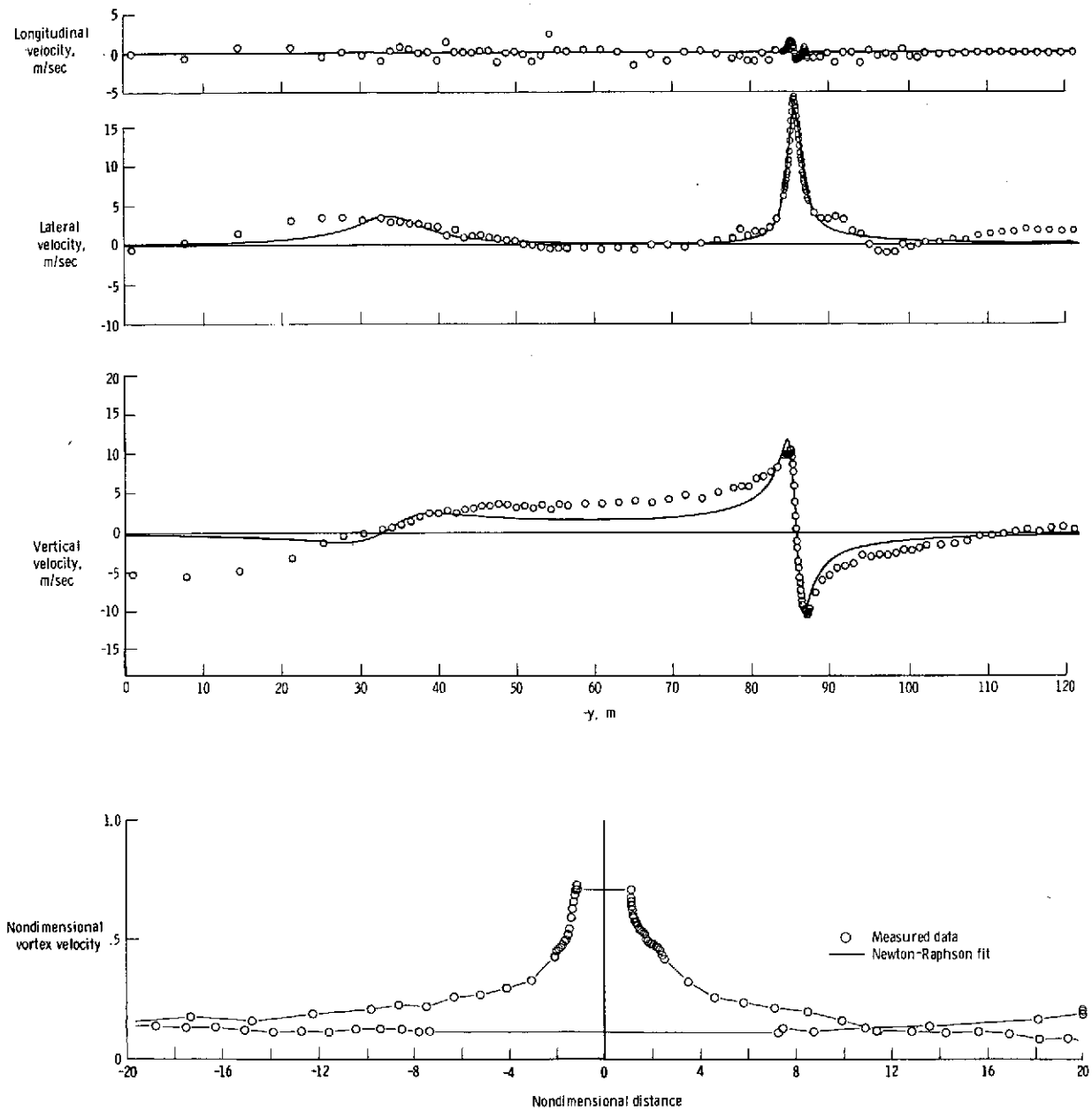

Figure 12.- Comparison of Newton-Raphson fit with measured flow velocities for flaps up (slide through) and vortex age of 32 seconds.

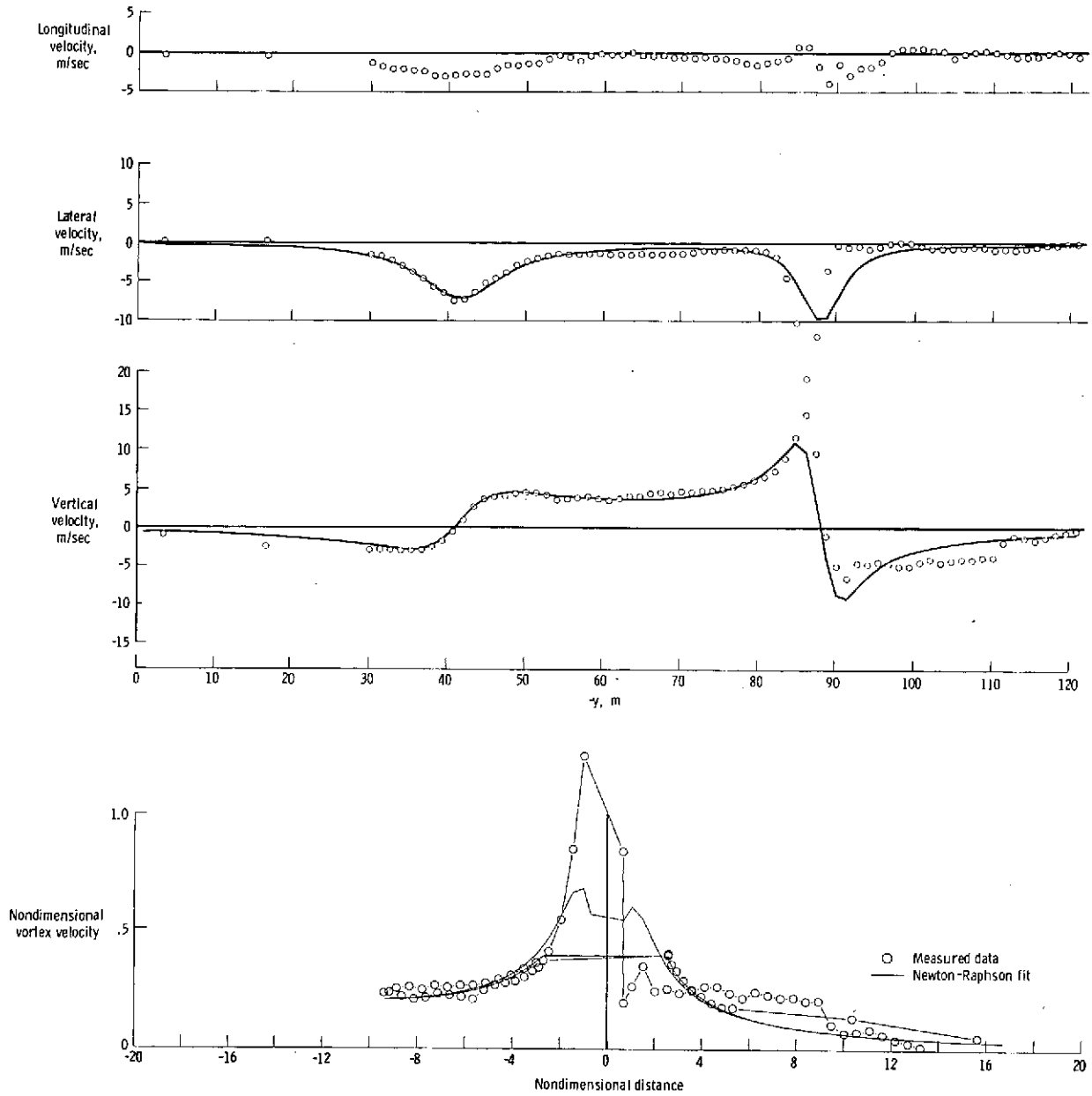

Figure 13.- Comparison of Newton-Raphson fit with measured flow velocities for flaps up and vortex age of 34 seconds.

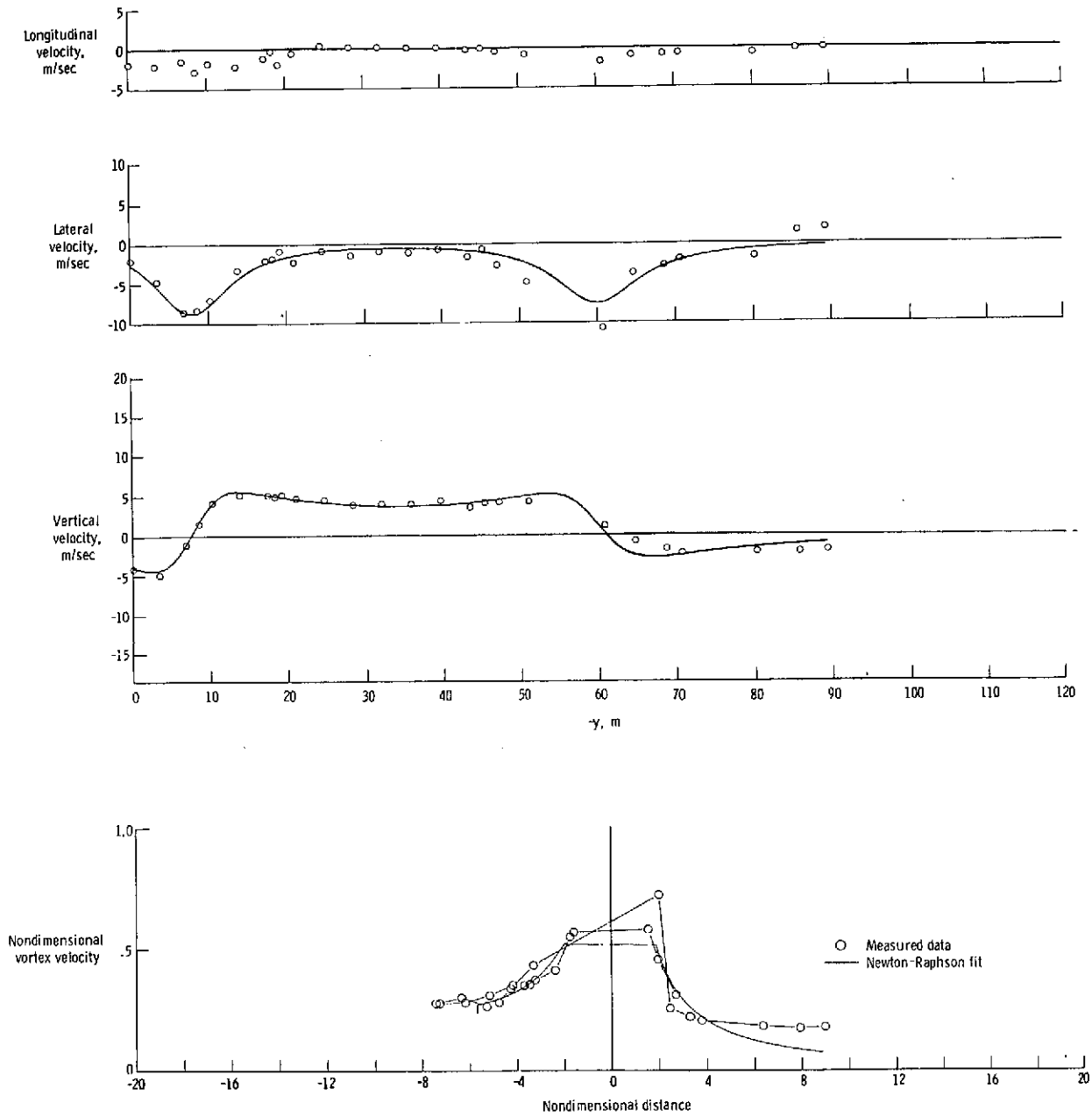

Figure 14.- Comparison of Newton-Raphson fit with measured flow velocities for flaps up (slide through) and vortex age of 42 seconds.

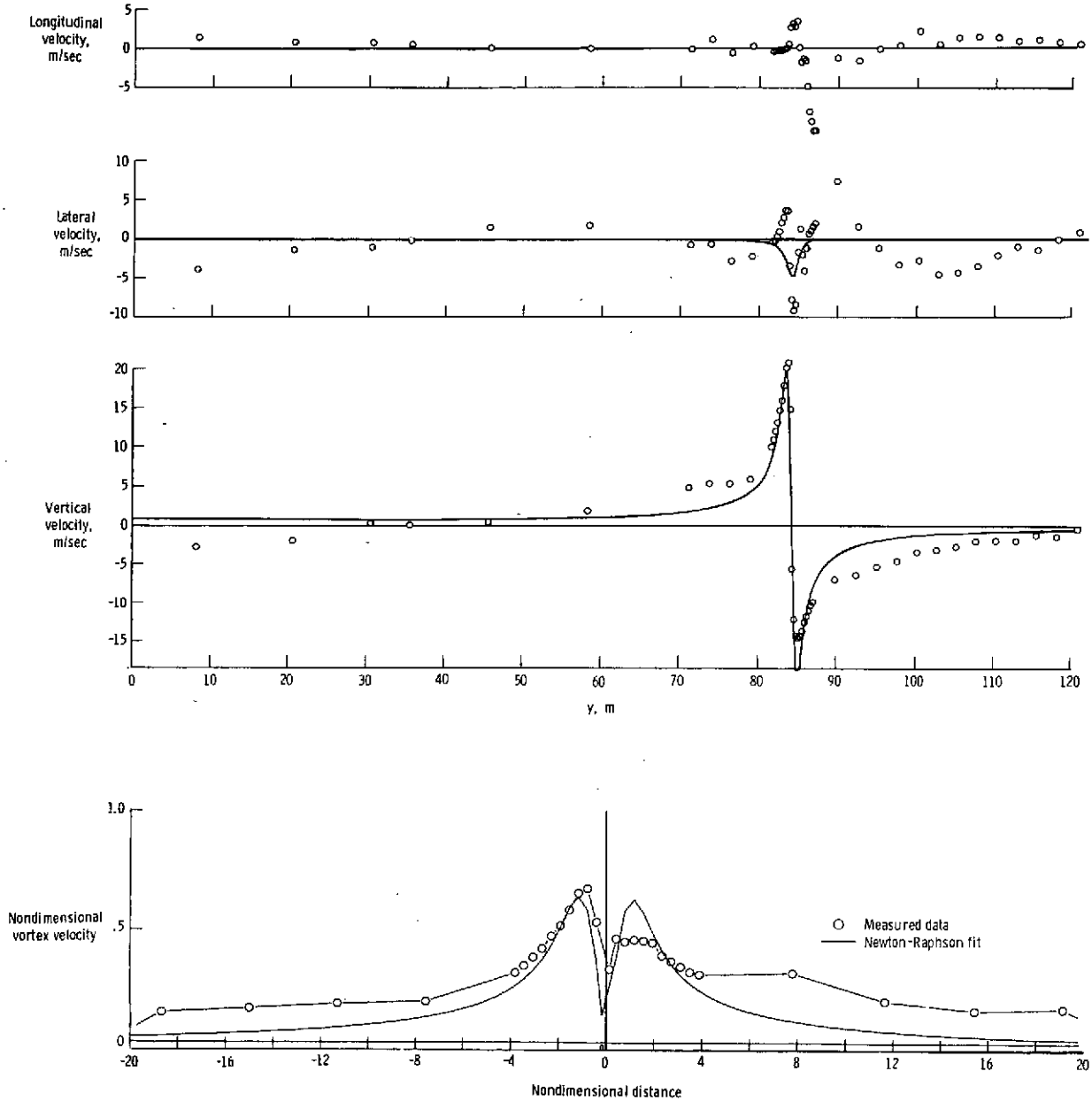

Figure 15.- Comparison of Newton-Raphson fit with measured flow velocities for flaps up (slide through) and vortex age of 46 seconds.

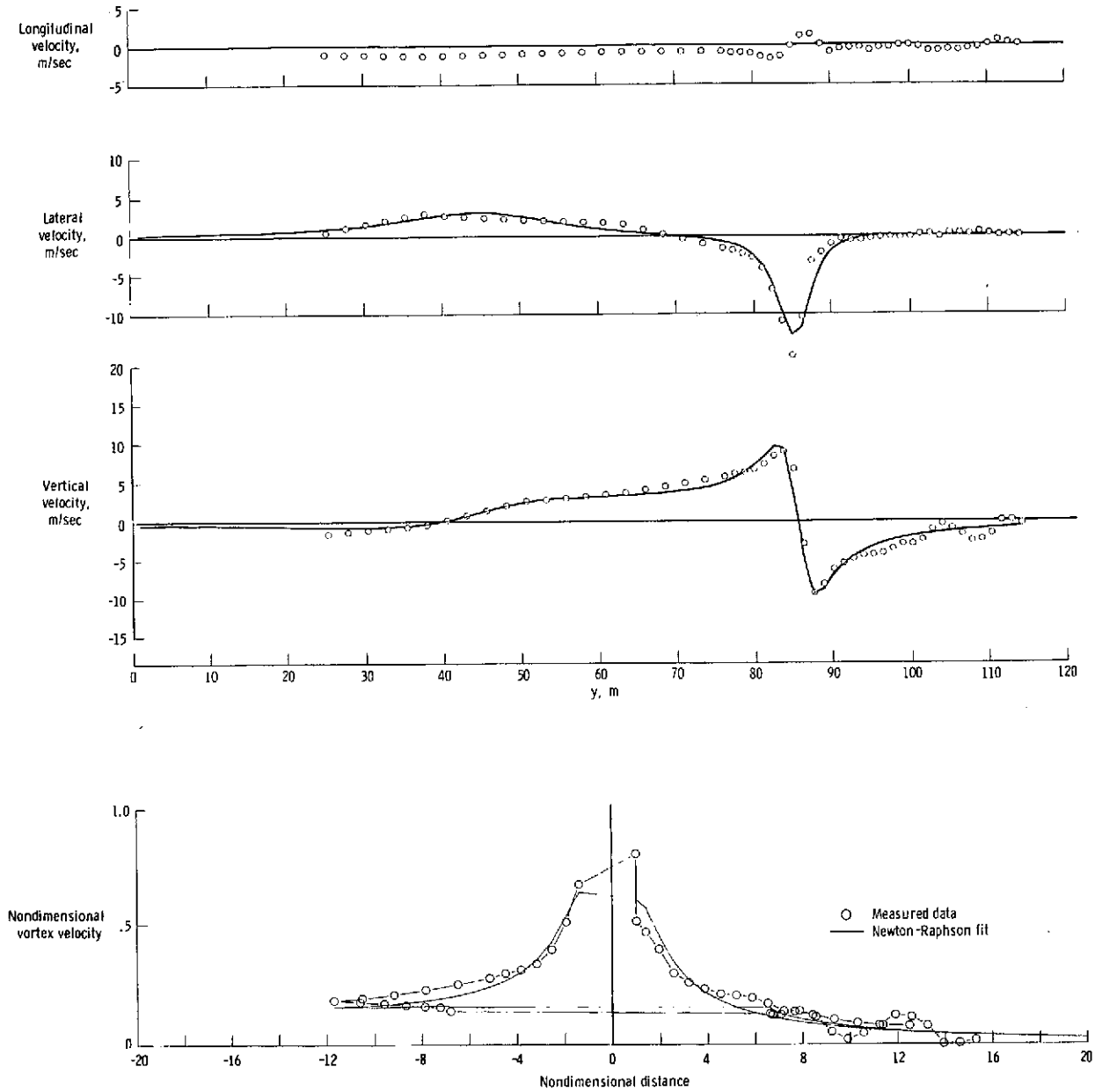

Figure 16.- Comparison of Newton-Raphson fit with measured flow velocities for flaps up and vortex age of 60 seconds.

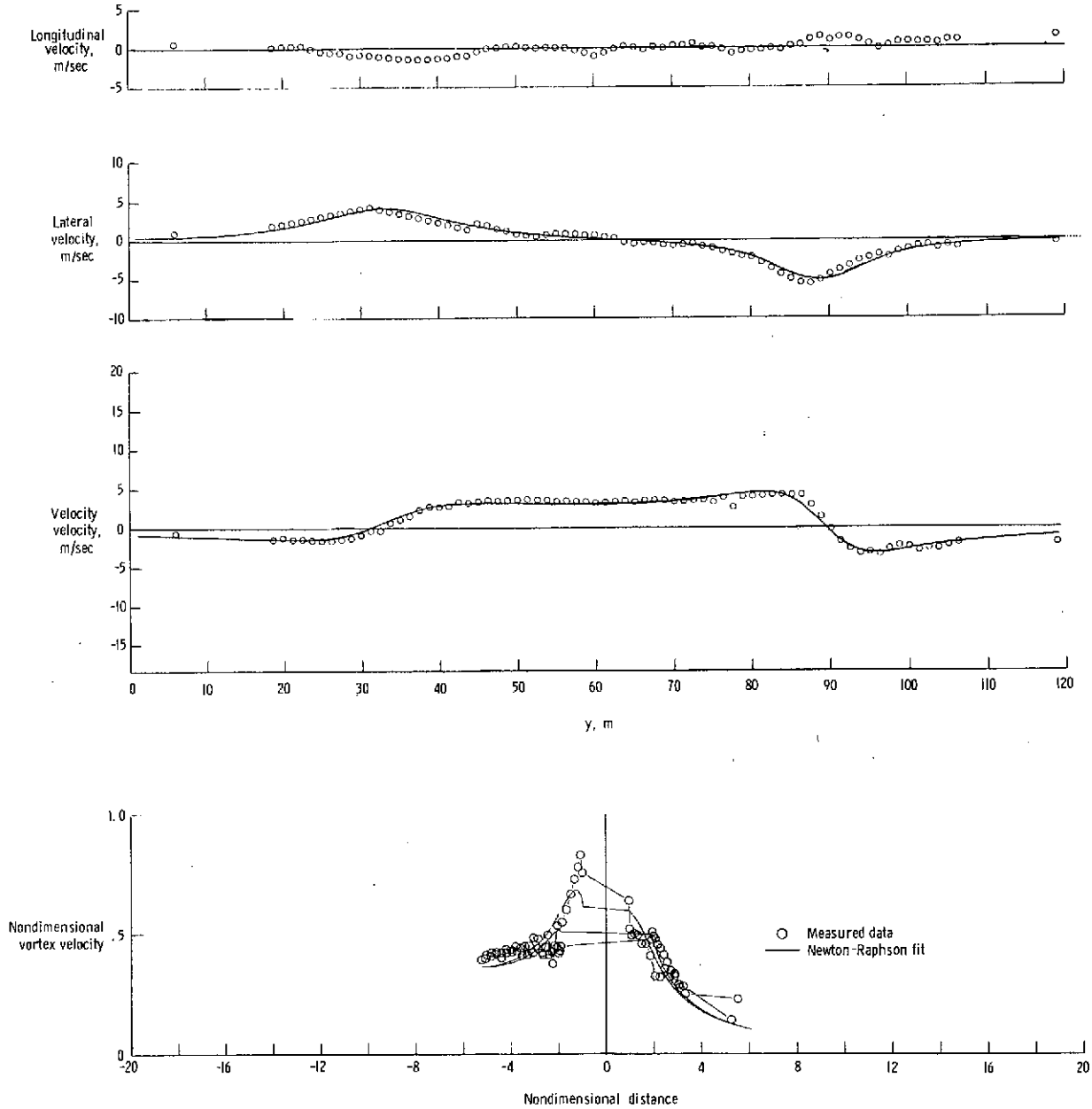

Figure 17.- Comparison of Newton-Raphson fit with measured flow velocities for flaps up and vortex age of 63 seconds.

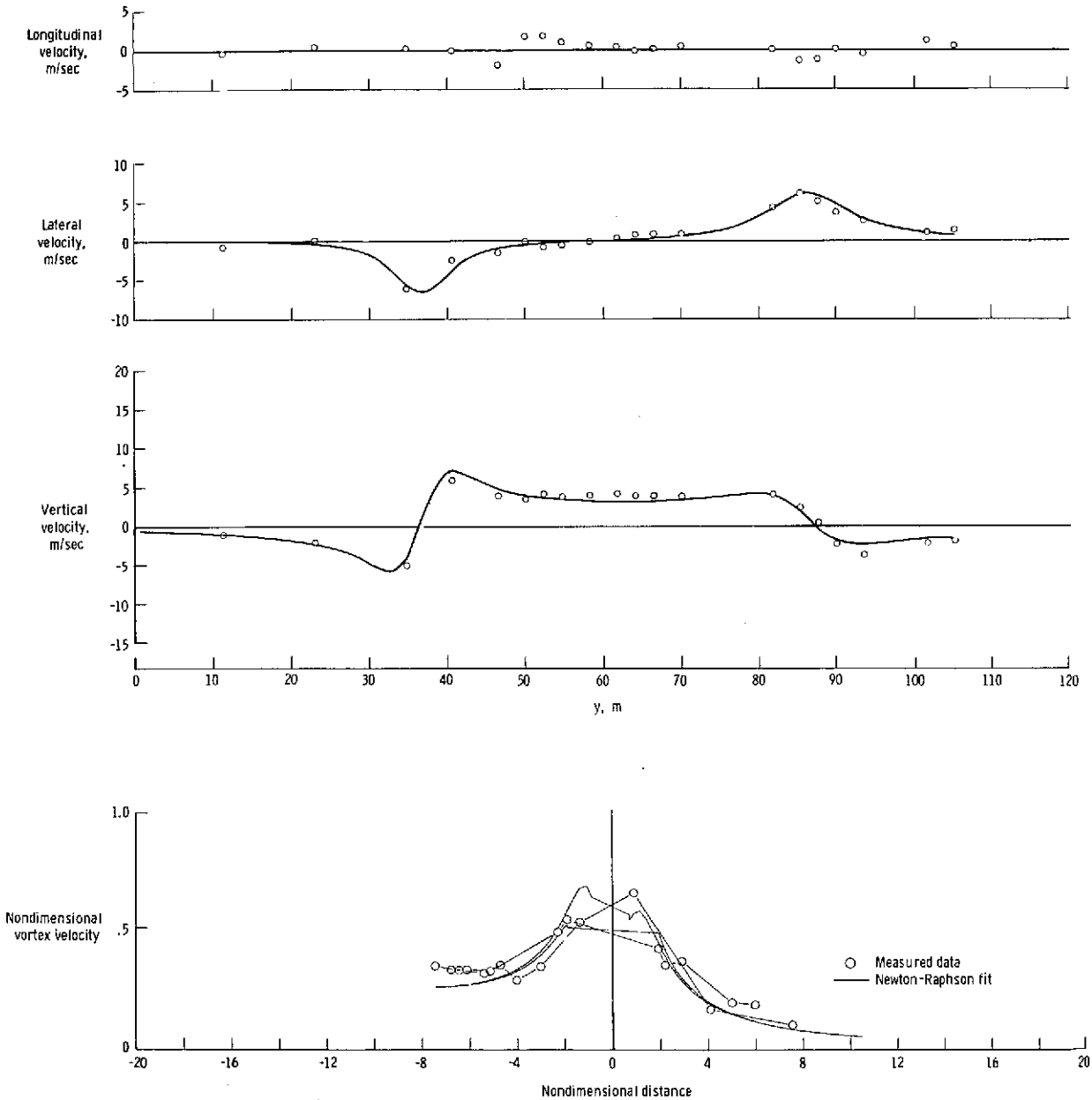

Figure 18.- Comparison of Newton-Raphson fit with measured flow velocities for flaps up and vortex age of 70 seconds.

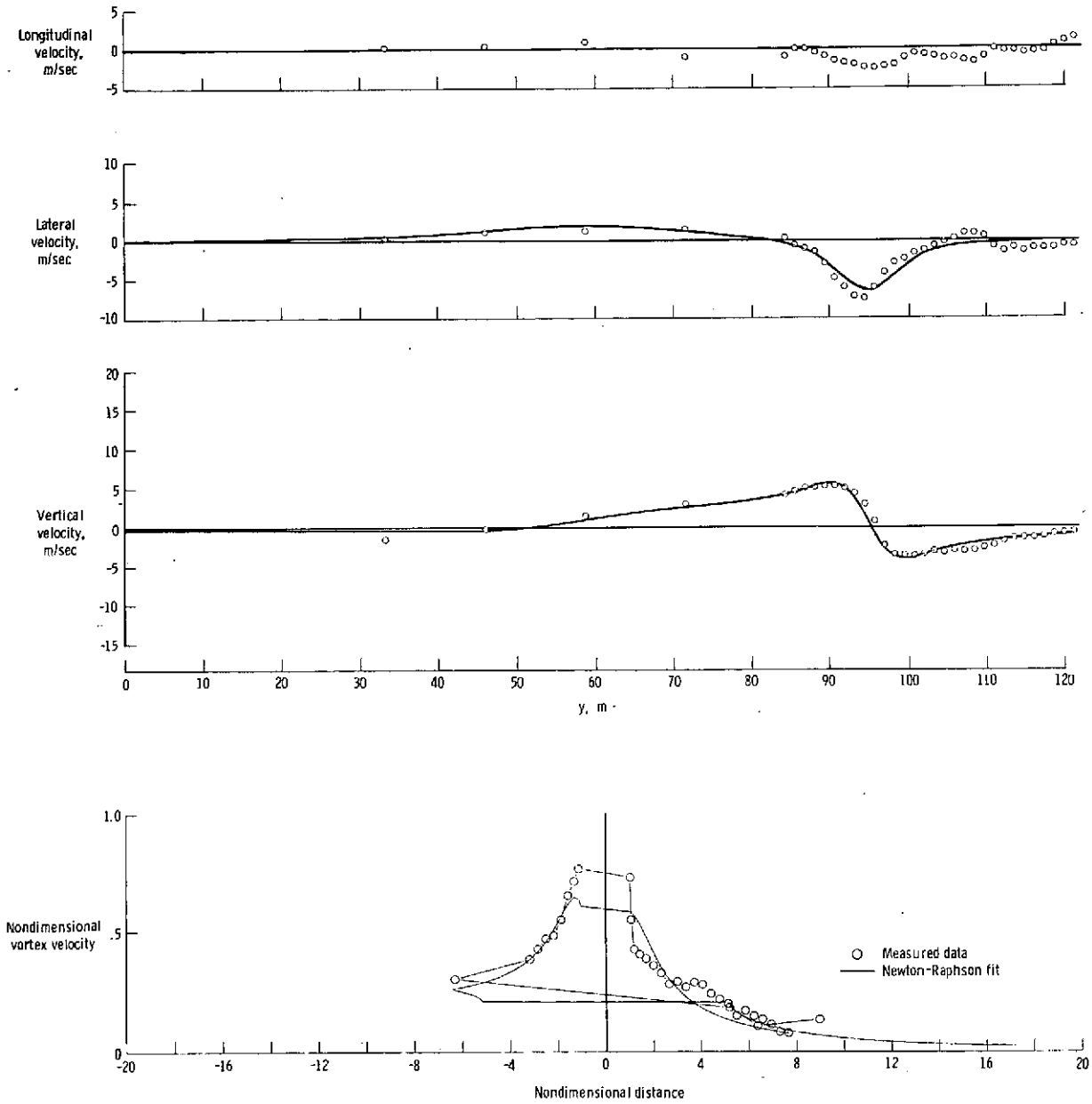

Figure 19.- Comparison of Newton-Raphson fit with measured flow velocities for flaps up and vortex age of 70 seconds.

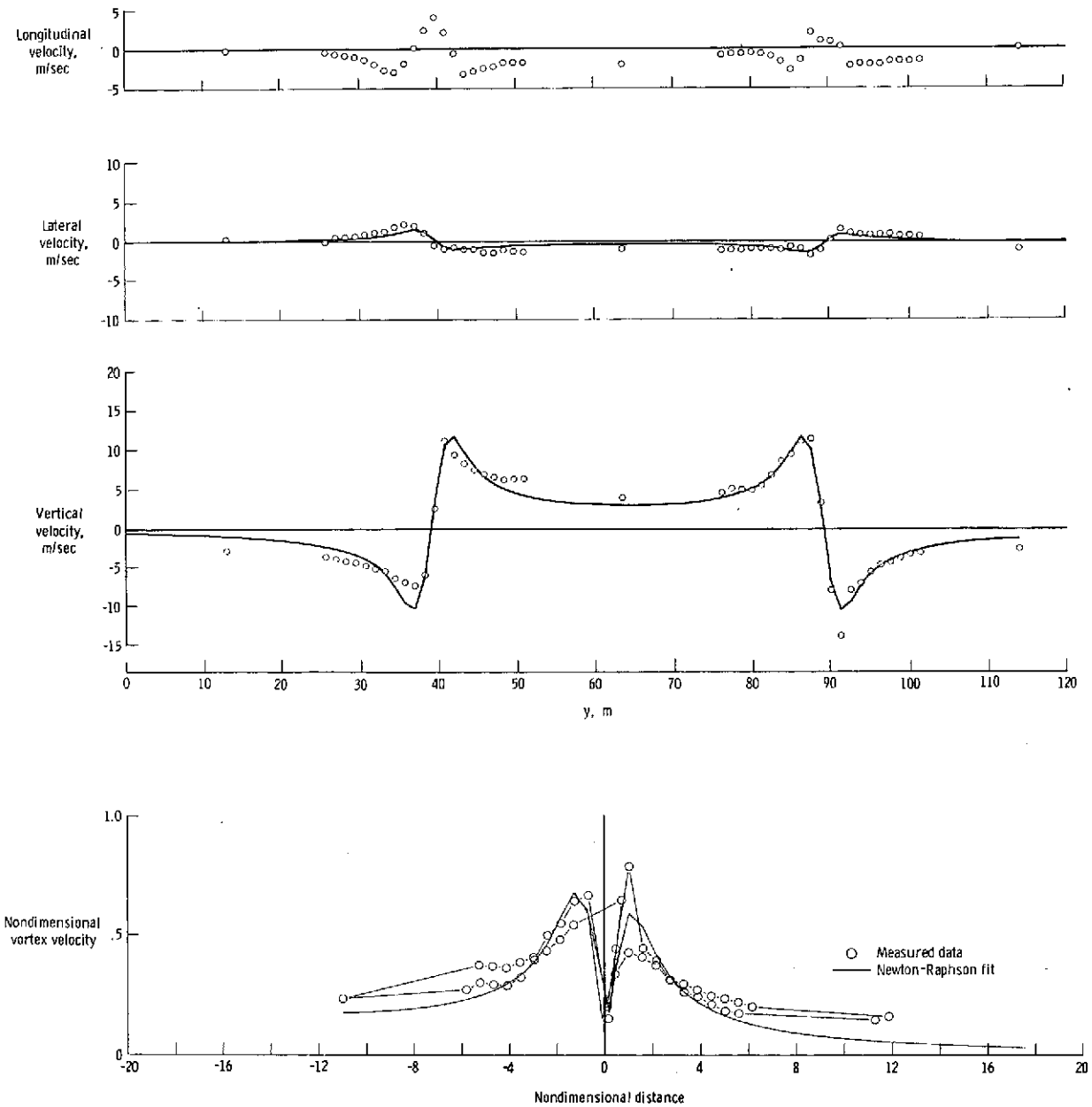

Figure 20.- Comparison of Newton-Raphson fit with measured flow velocities for flaps up and vortex age of 98 seconds.

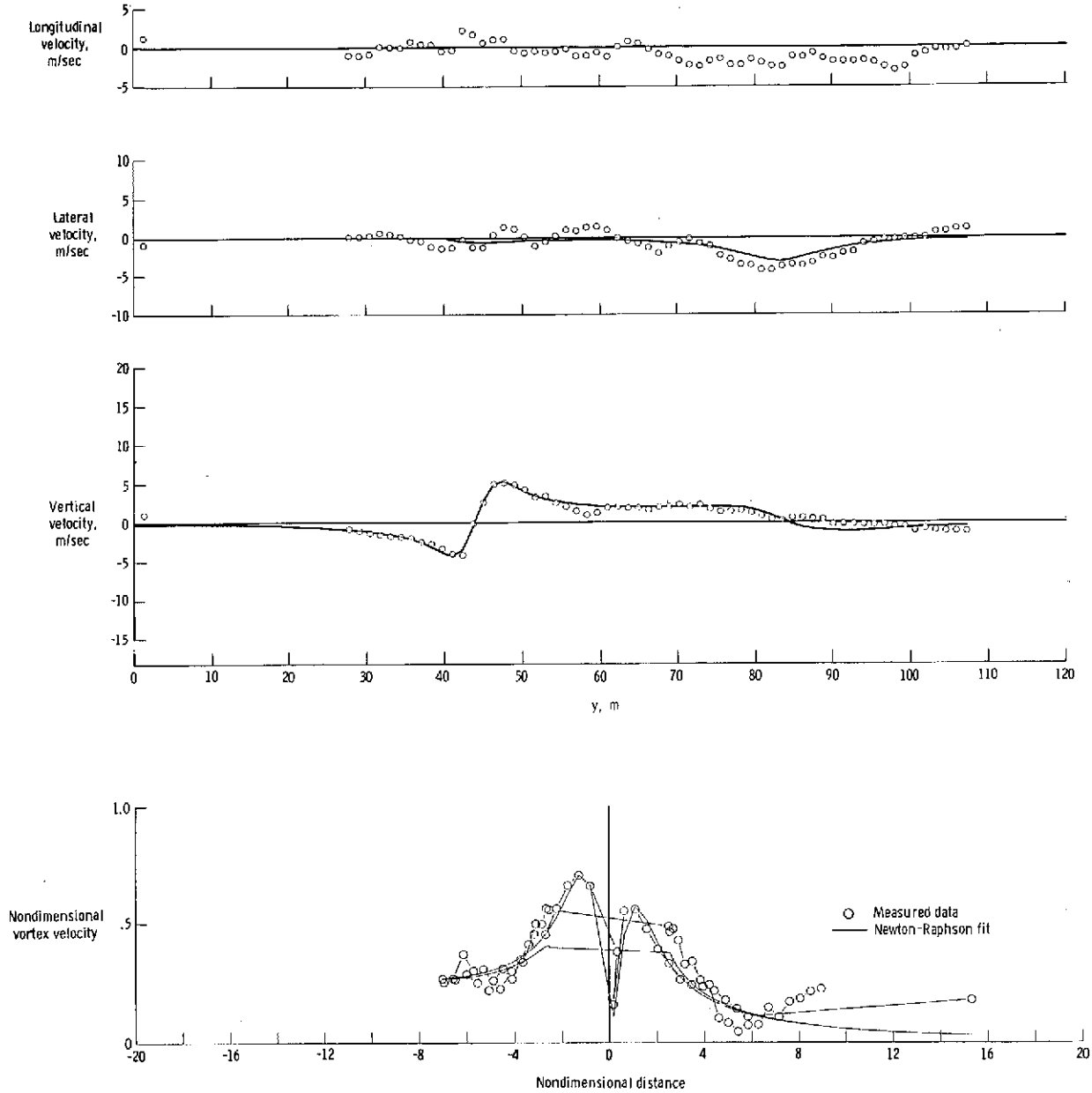

Figure 21.- Comparison of Newton-Raphson fit with measured flow velocities for flaps up and vortex age of 104 seconds.

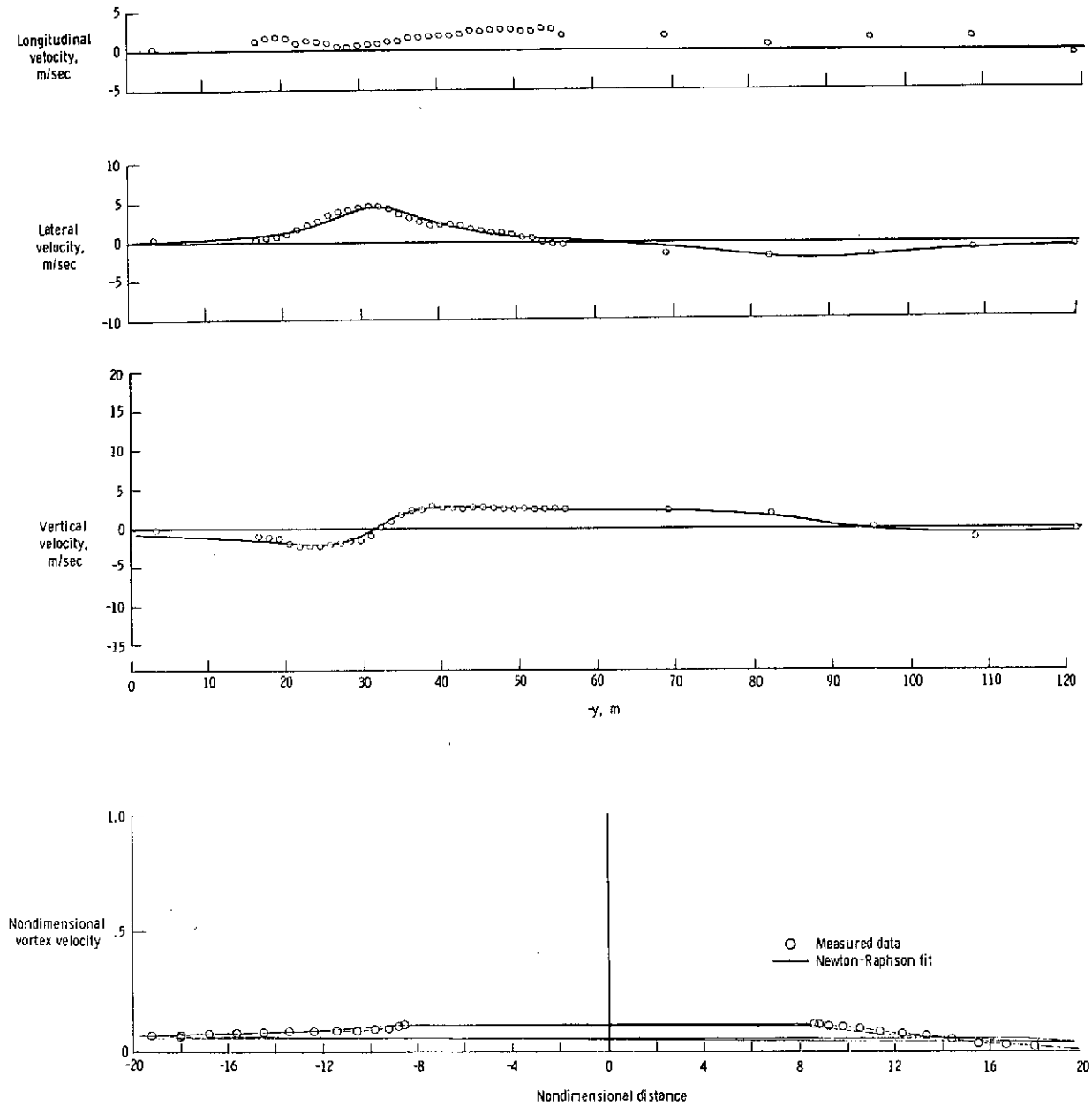

Figure 22.- Comparison of Newton-Raphson fit with measured flow velocities for flaps up and vortex age of 114 seconds.

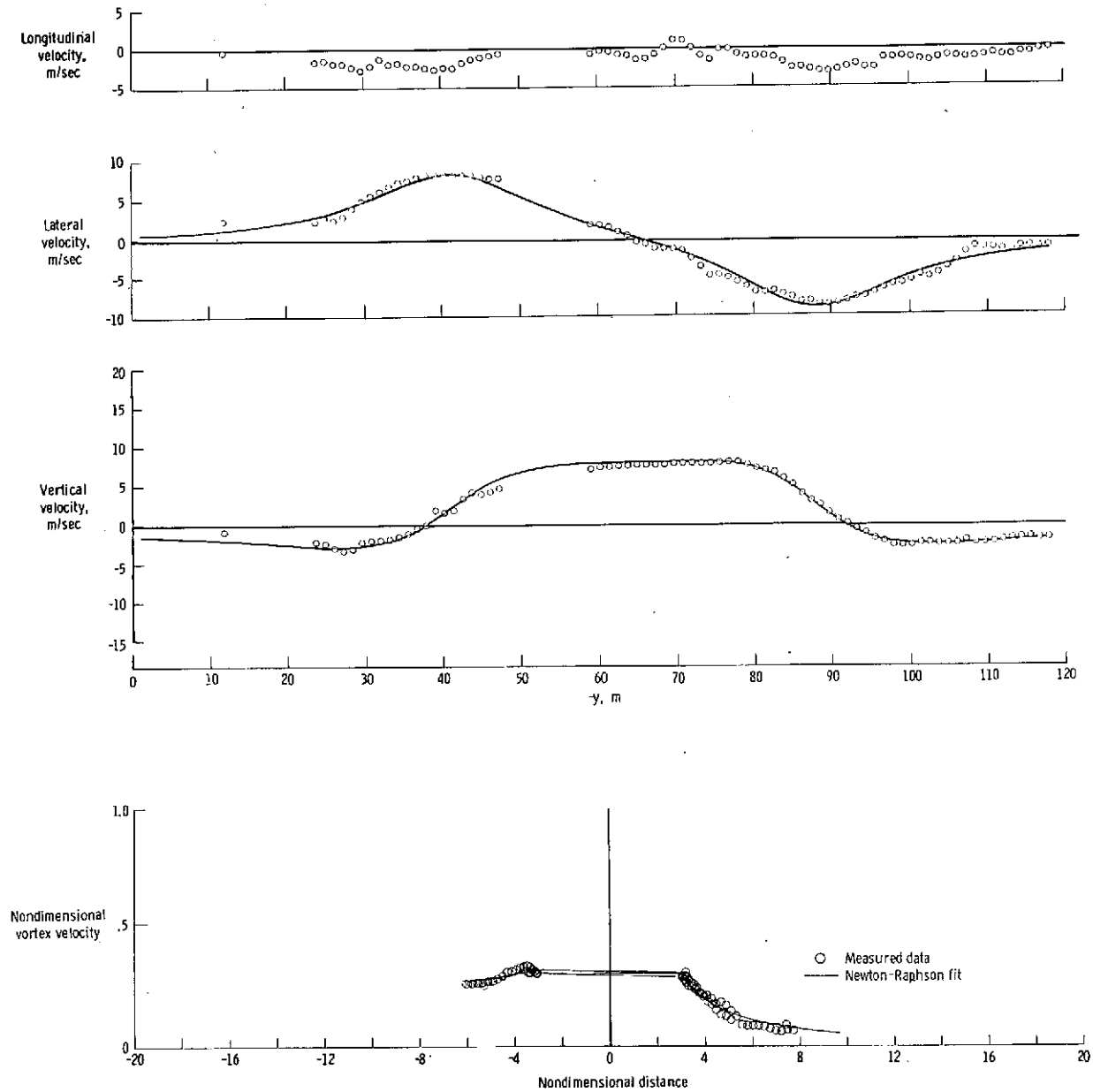

Figure 23.- Comparison of Newton-Raphson fit with measured flow velocities for flaps down and vortex age of 22 seconds.

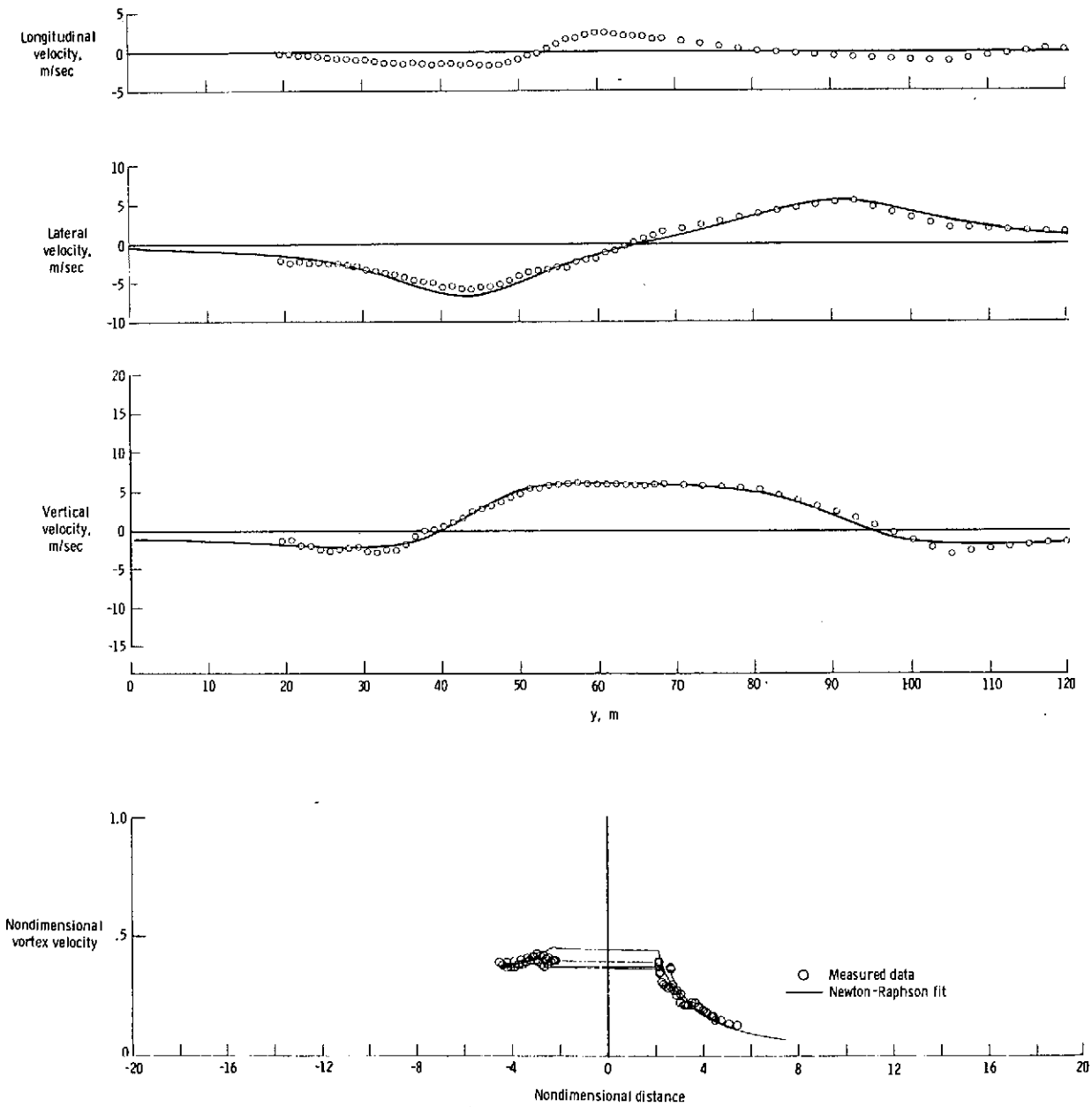

Figure 24.- Comparison of Newton-Raphson fit with measured flow velocities for flaps down and vortex age of 30 seconds.

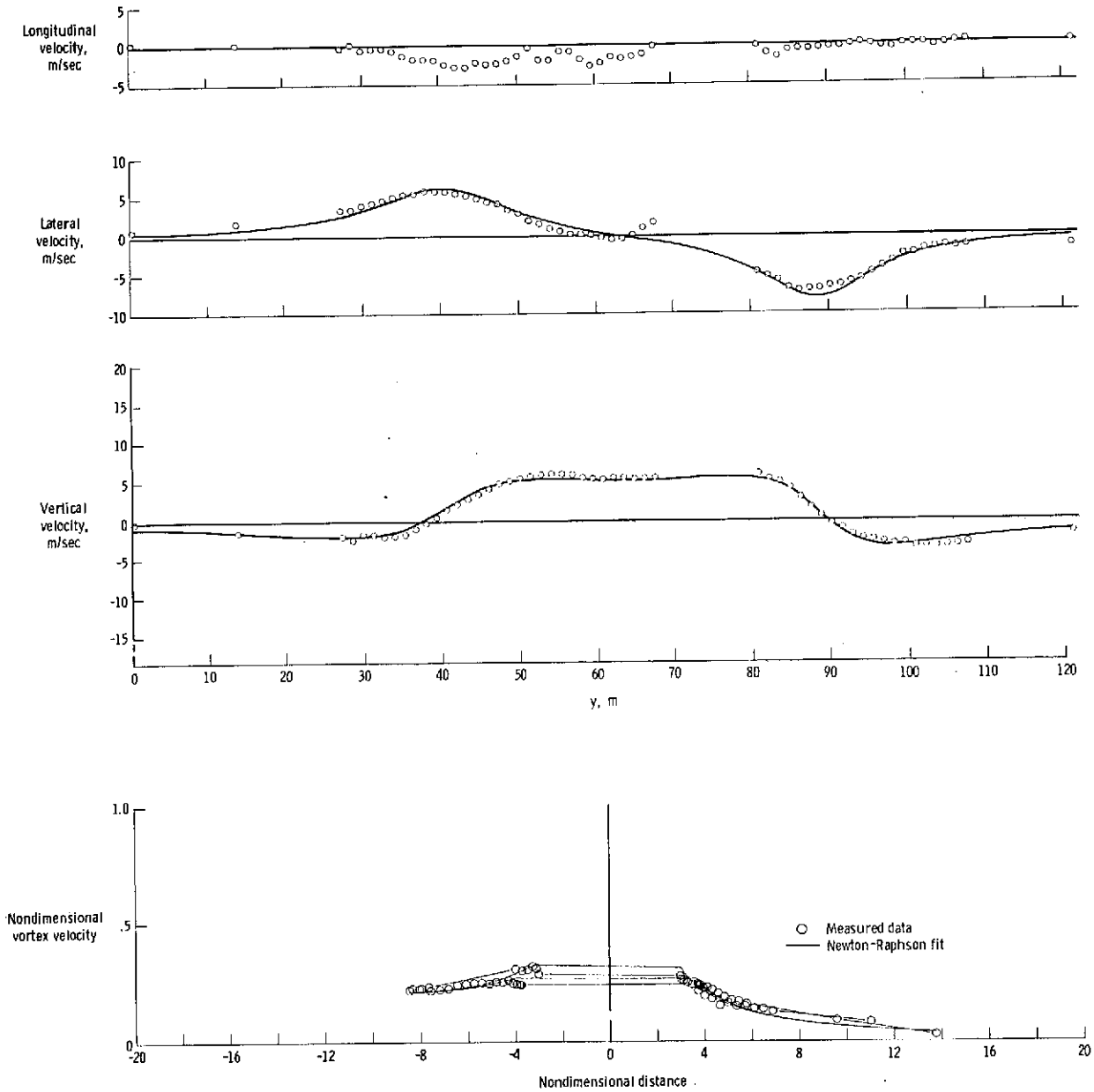

Figure 25.- Comparison of Newton-Raphson fit with measured flow velocities for flaps down and vortex age of 32 seconds.

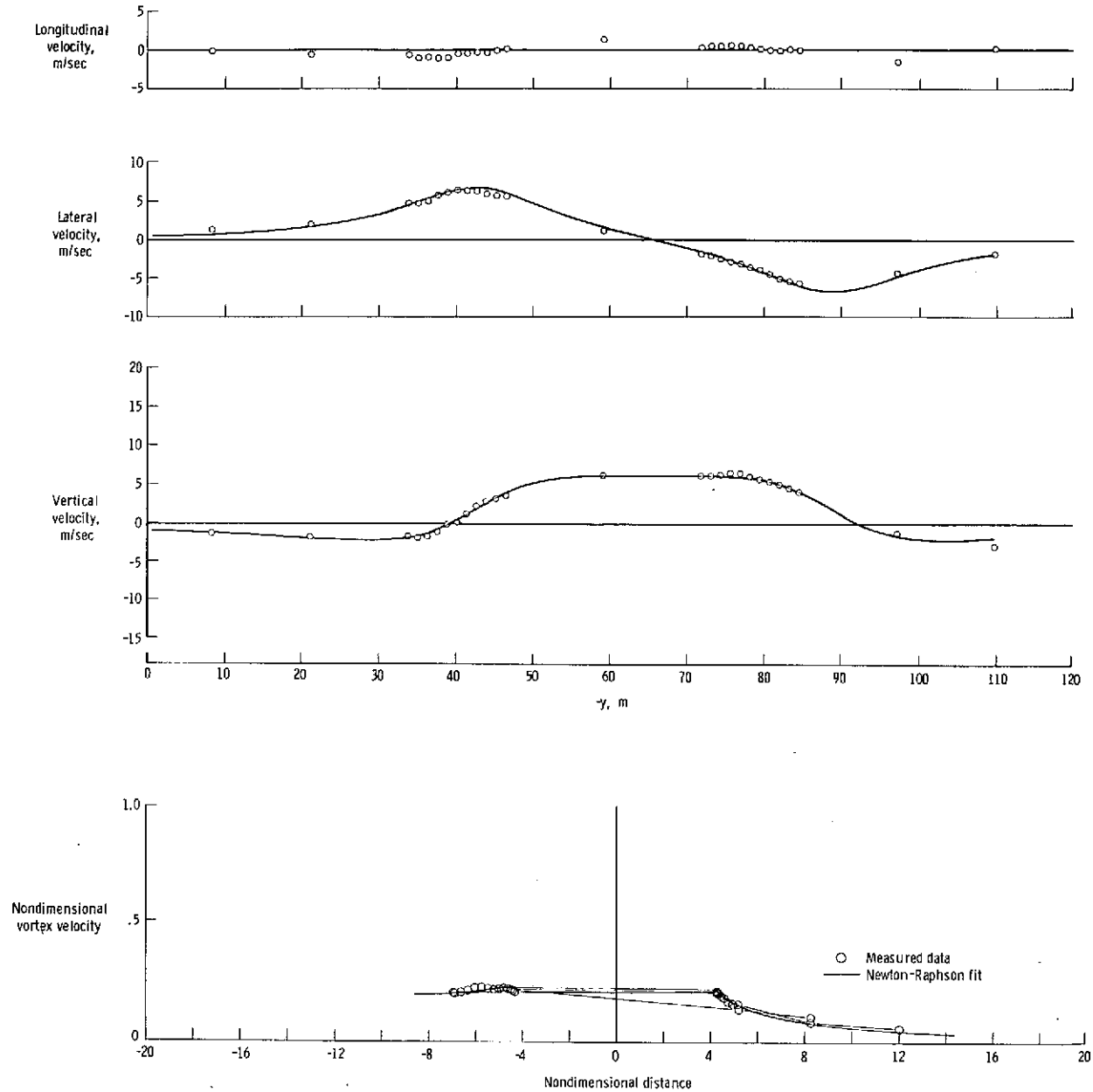

Figure 26.- Comparison of Newton-Raphson fit with measured flow velocities for flaps down and vortex age of 40 seconds.

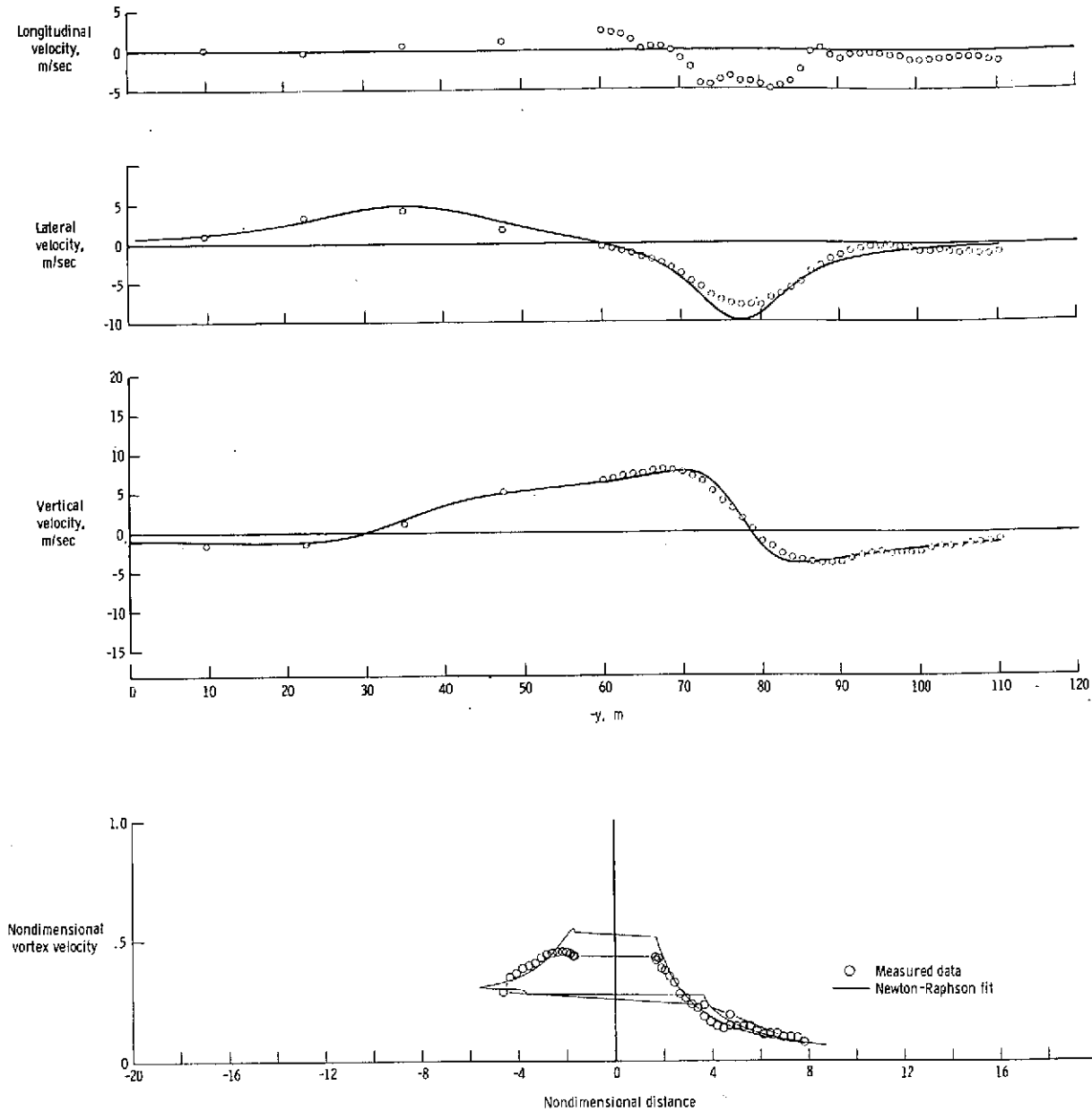

Figure 27.- Comparison of Newton-Raphson fit with measured flow velocities for flaps down and vortex age of 41 seconds. See table I for variable changes.

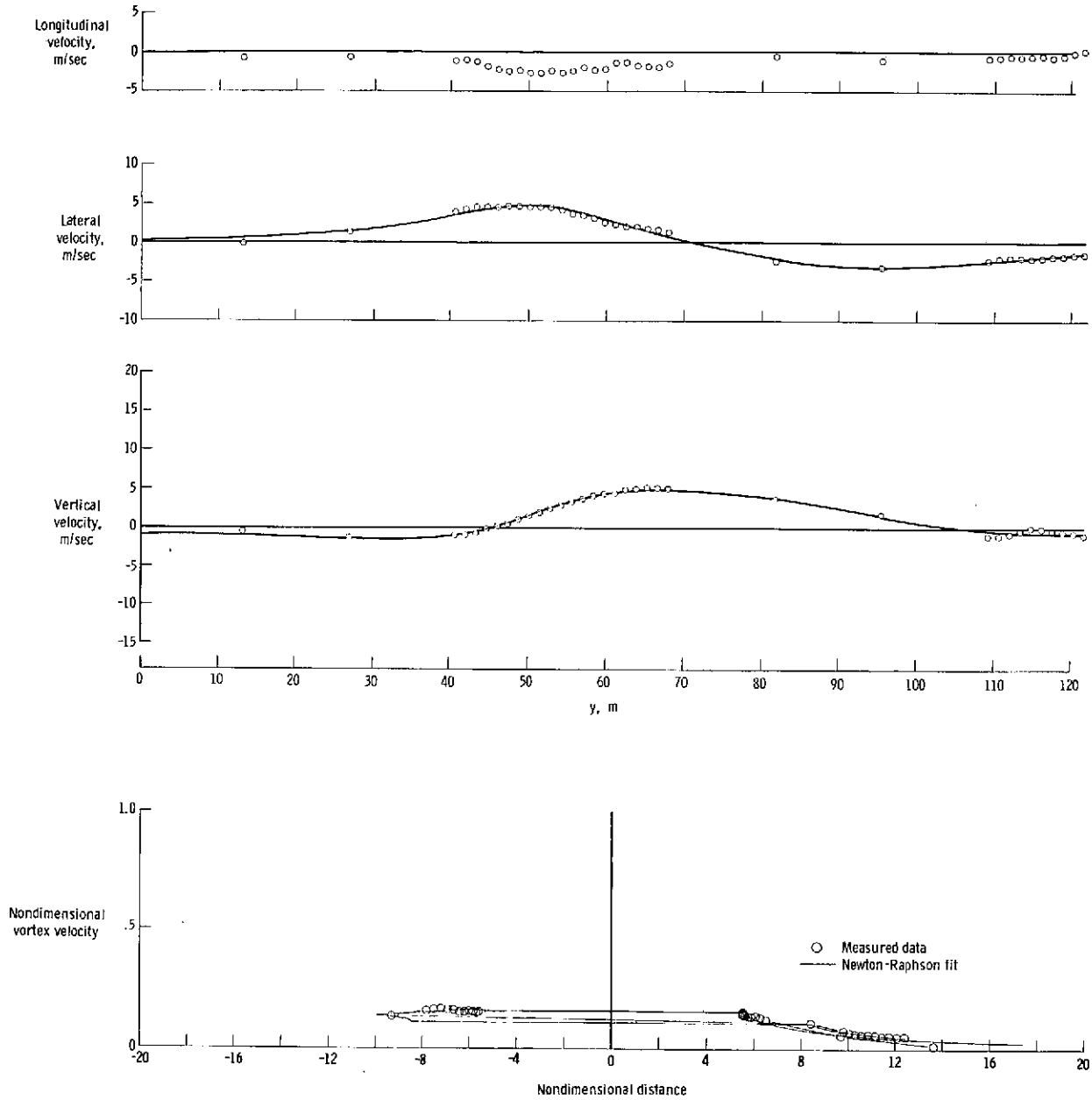

Figure 28.- Comparison of Newton-Raphson fit with measured flow velocities for flaps down and vortex age of 41 seconds. See table I for variable changes.

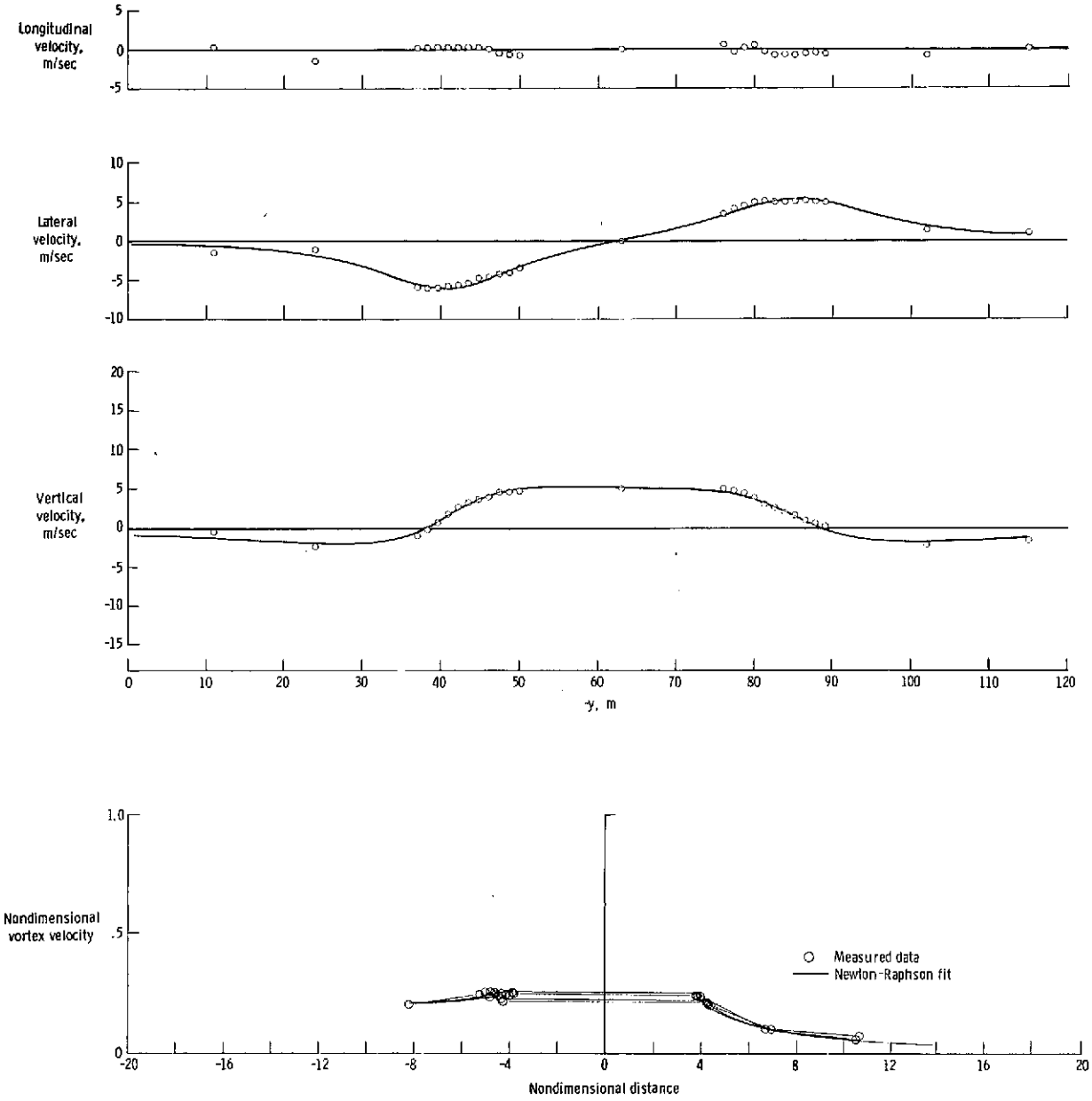

Figure 29.- Comparison of Newton-Raphson fit with measured flow velocities for flaps down and vortex age of 42 seconds.

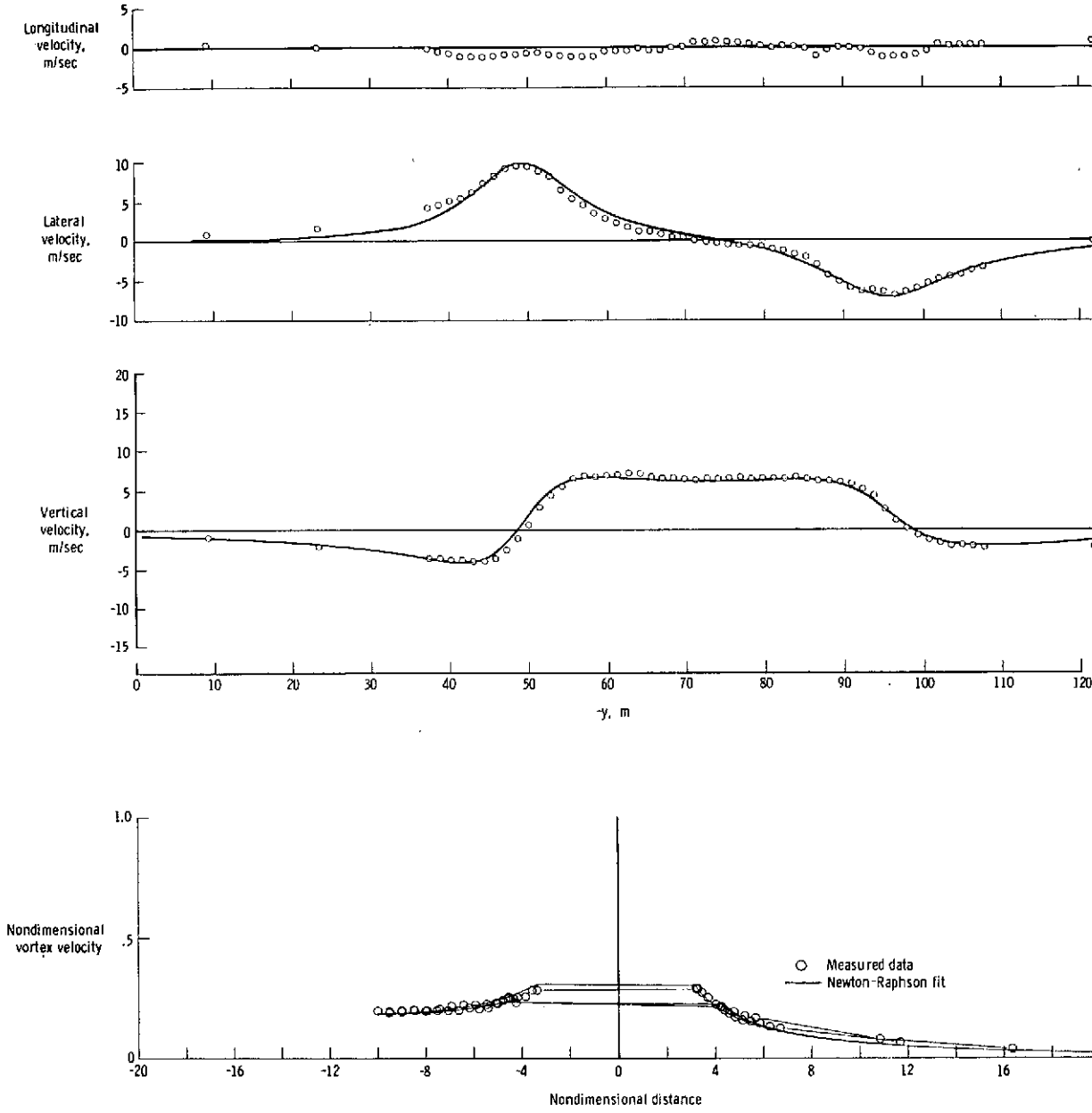

Figure 30.- Comparison of Newton-Raphson fit with measured flow velocities for flaps down and vortex age of 44 seconds.

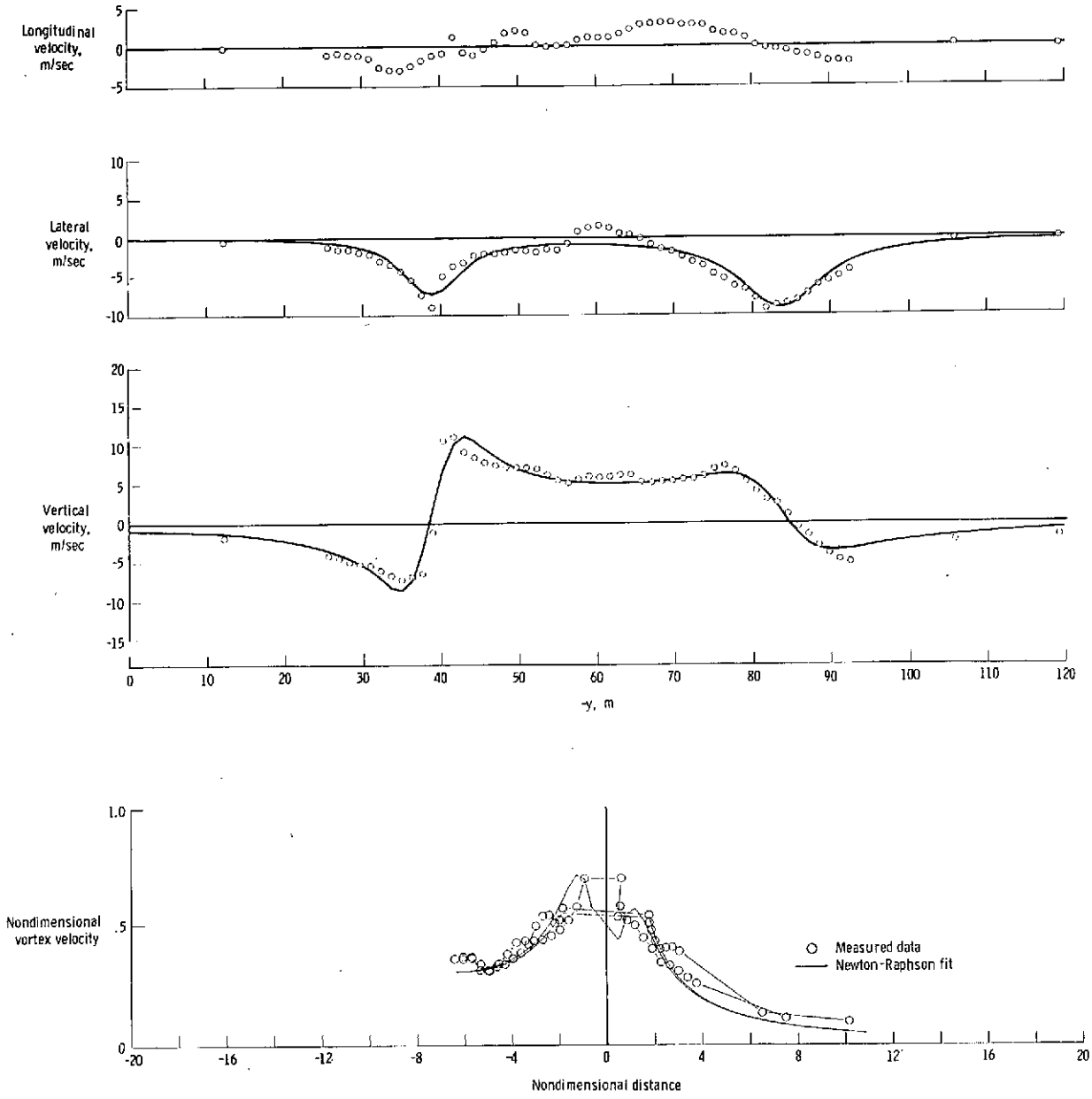

Figure 31.- Comparison of Newton-Raphson fit with measured flow velocities for flaps down and vortex age of 59 seconds.

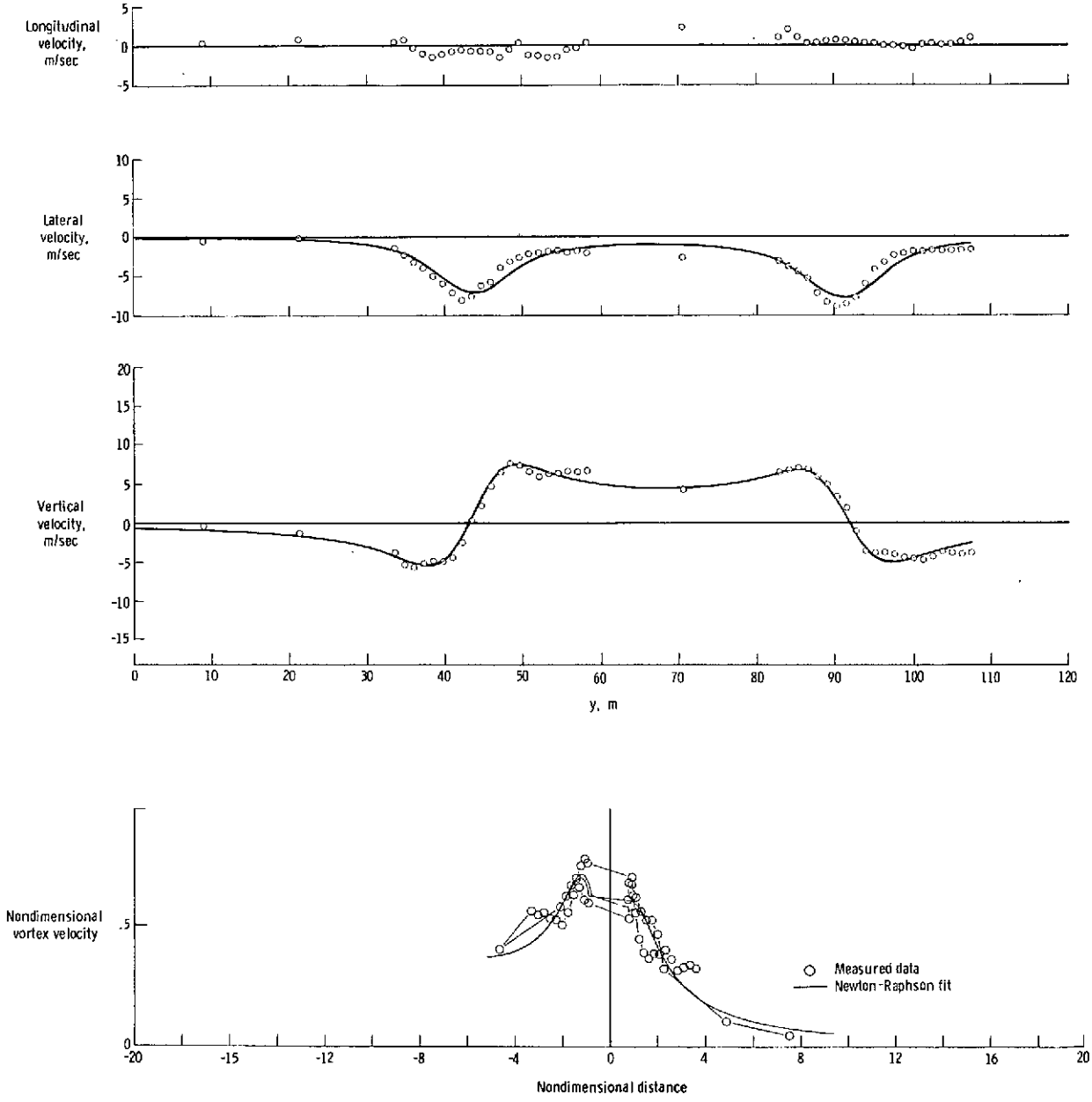

Figure 32.- Comparison of Newton-Raphson fit with measured flow velocities for flaps down and vortex age of 60 seconds. See table I for variable changes.

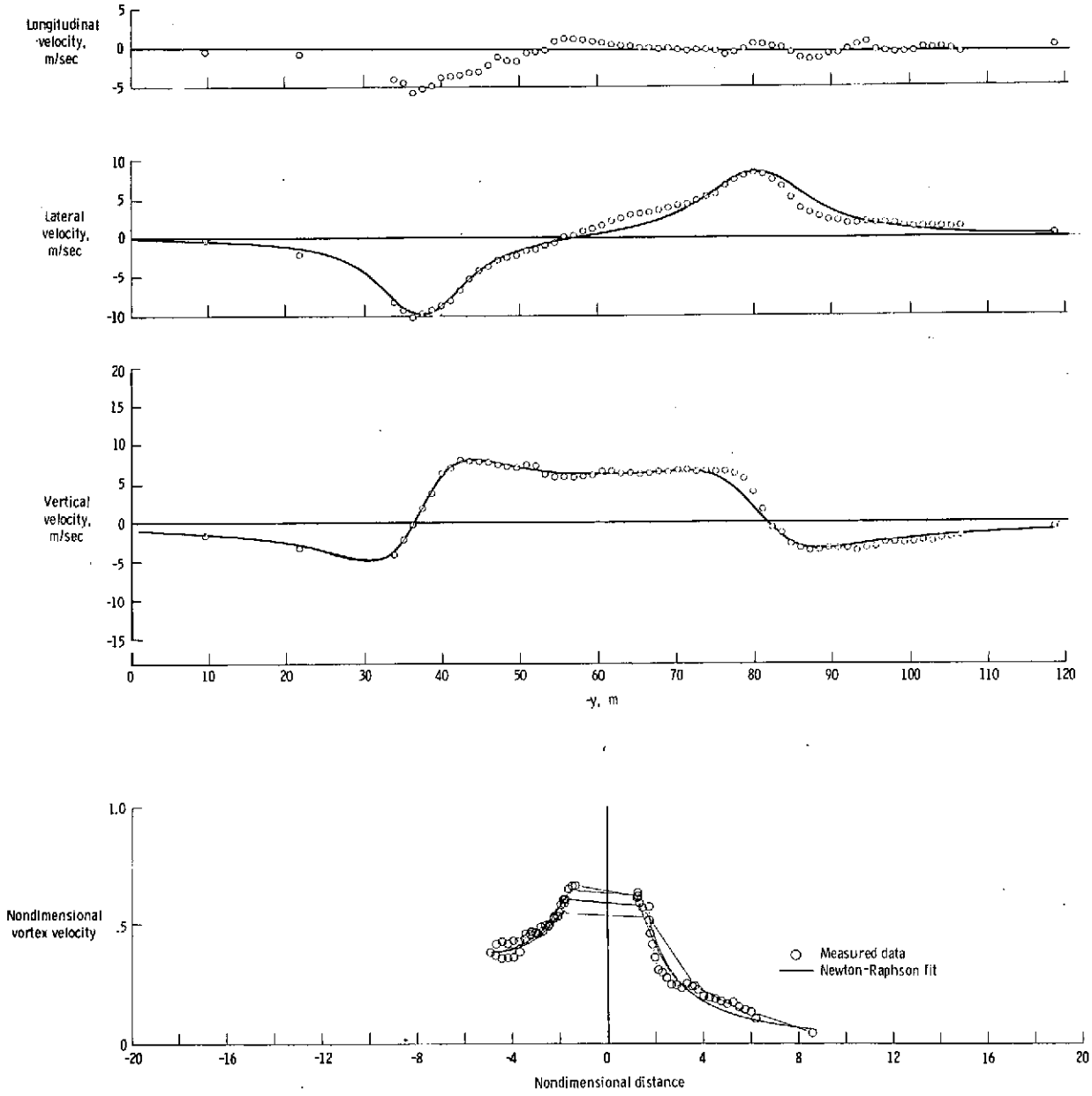

Figure 33.- Comparison of Newton-Raphson fit with measured flow velocities for flaps down and vortex age of 60 seconds. See table I for variable changes.

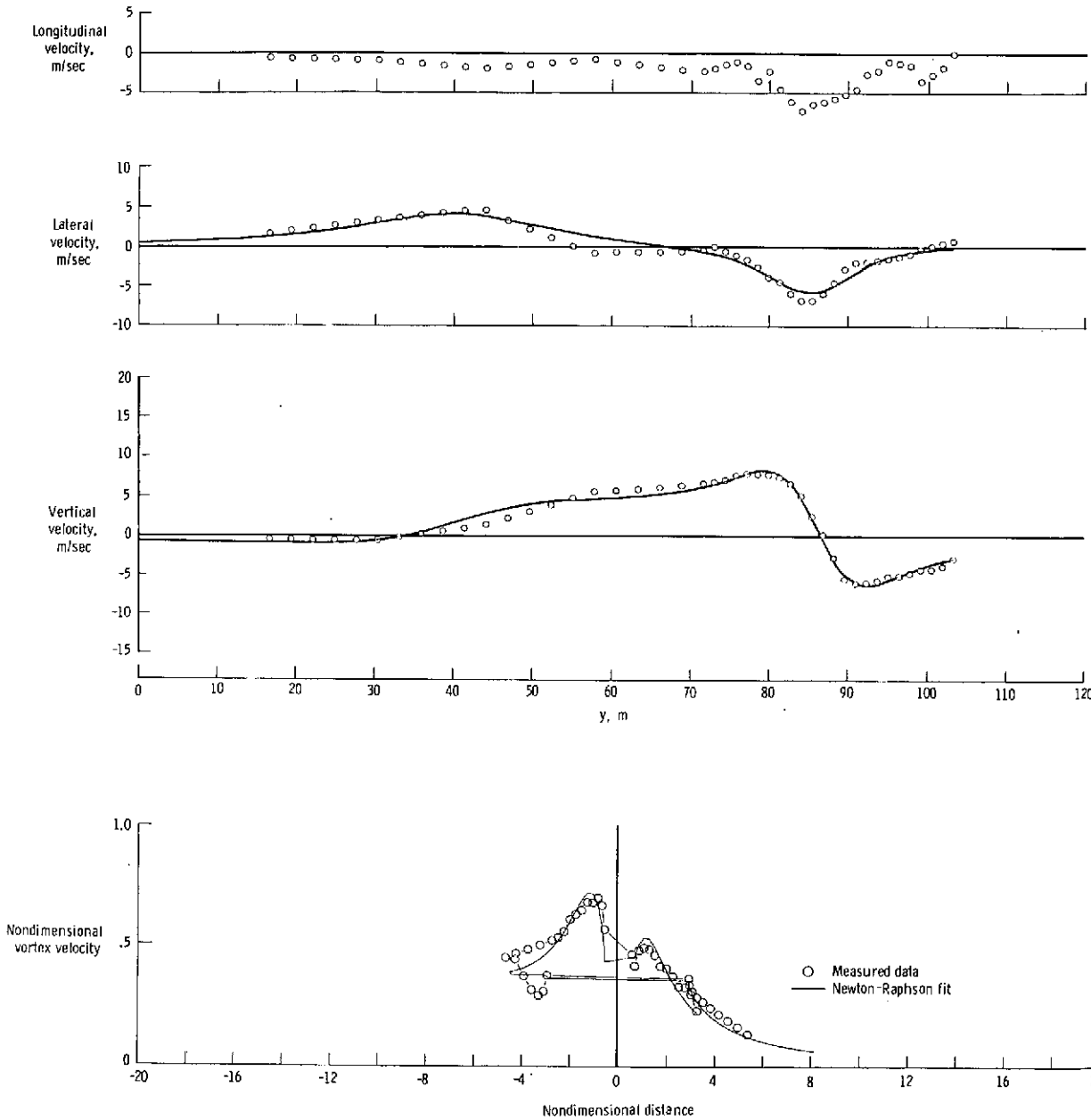

Figure 34.- Comparison of Newton-Raphson fit with measured flow velocities for flaps down and vortex age of 63 seconds.

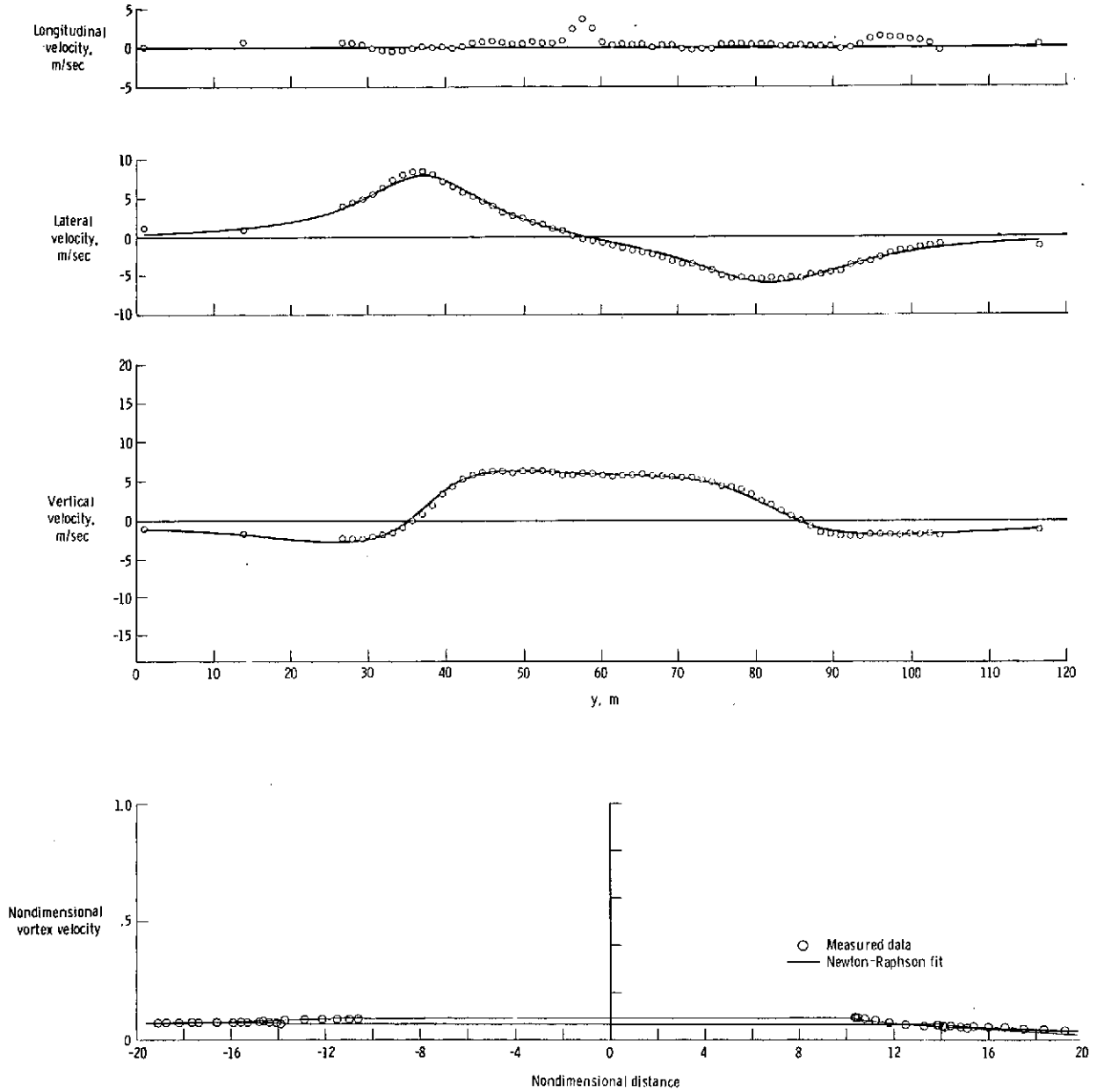

Figure 35.- Comparison of Newton-Raphson fit with measured flow velocities for flaps down and vortex age of 64 seconds.

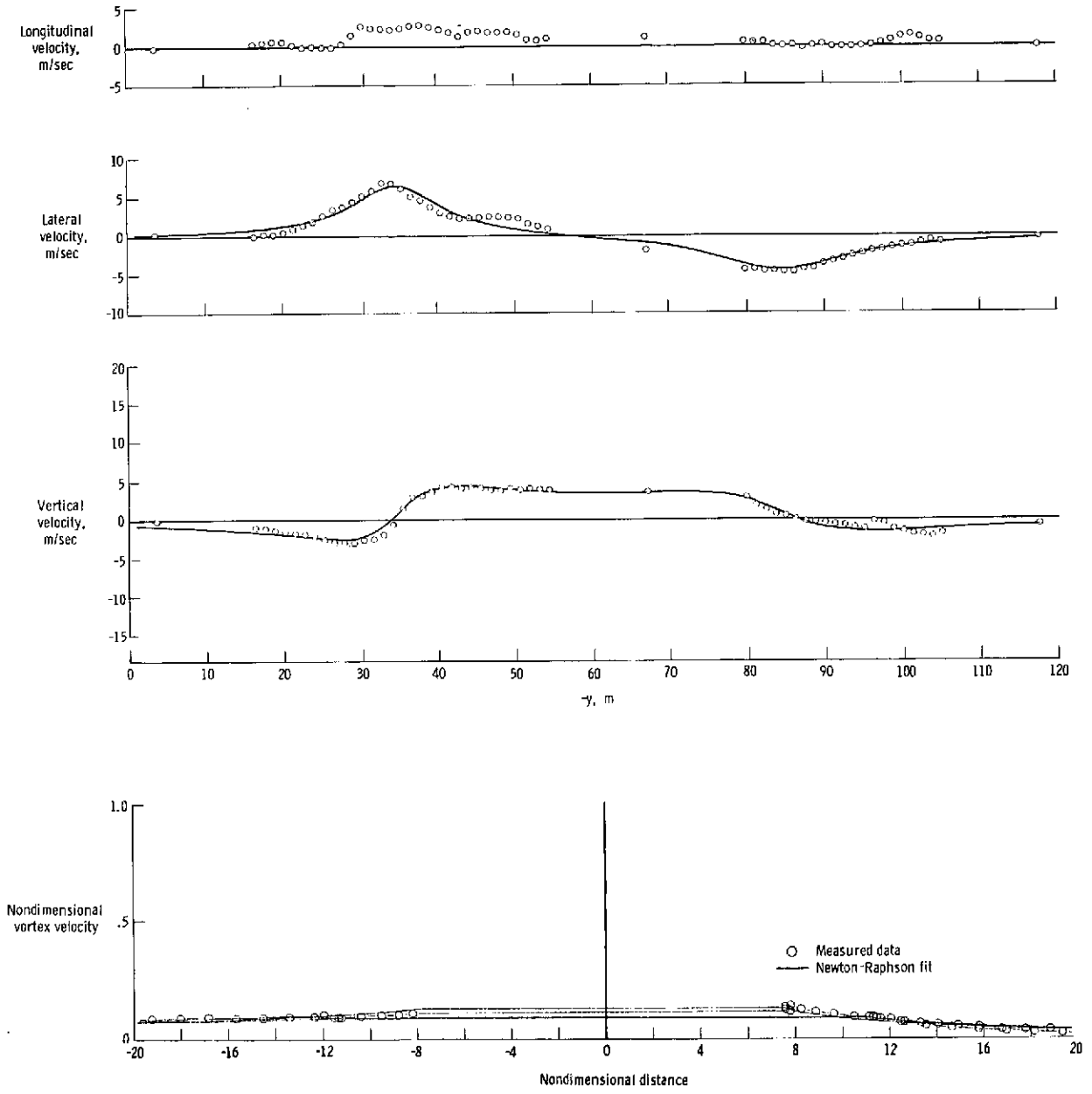

Figure 36.- Comparison of Newton-Raphson fit with measured flow velocities for flaps down and vortex age of 68 seconds.

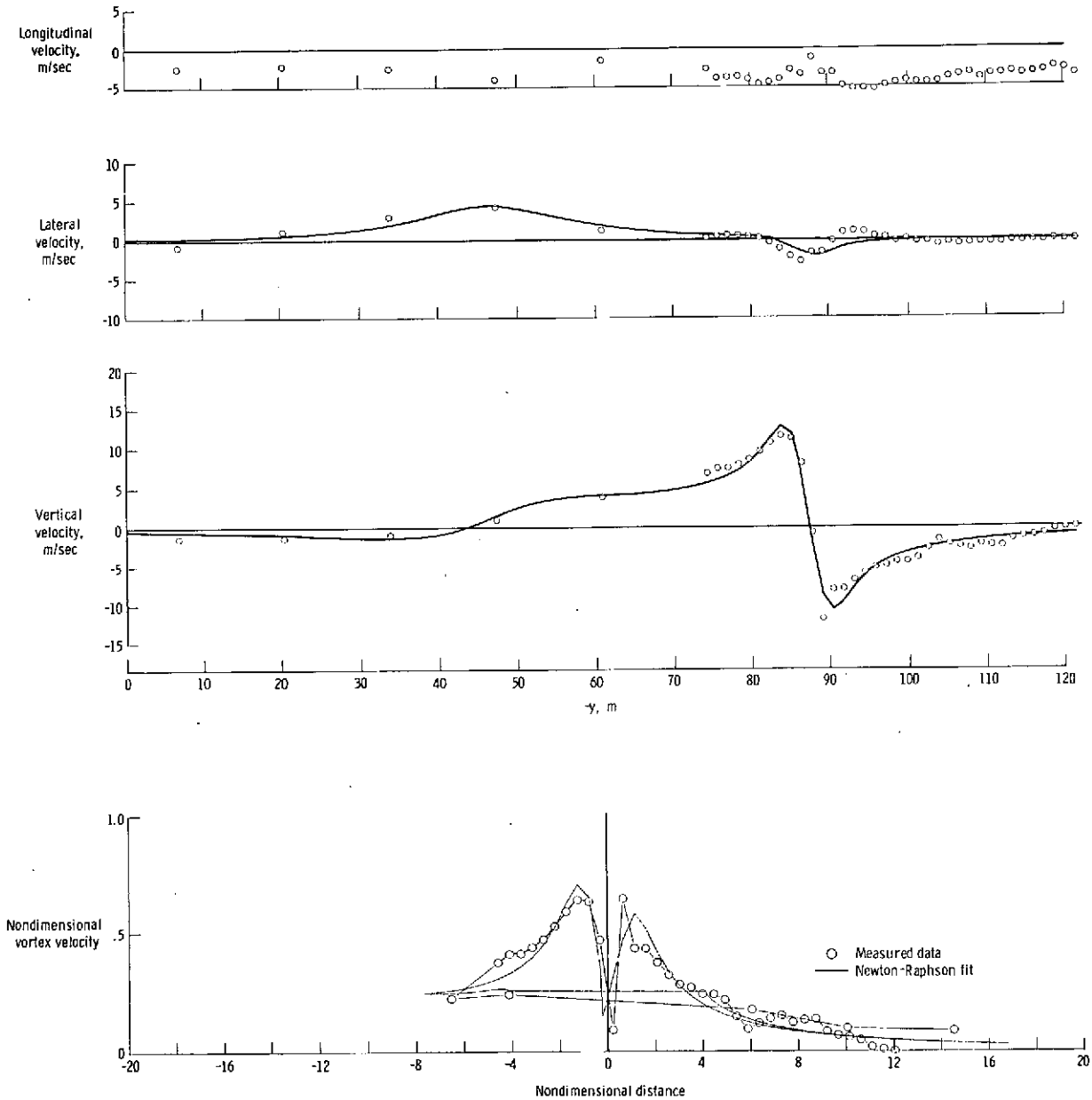

Figure 37.- Comparison of Newton-Raphson fit with measured flow velocities for flaps down and vortex age of 78 seconds.

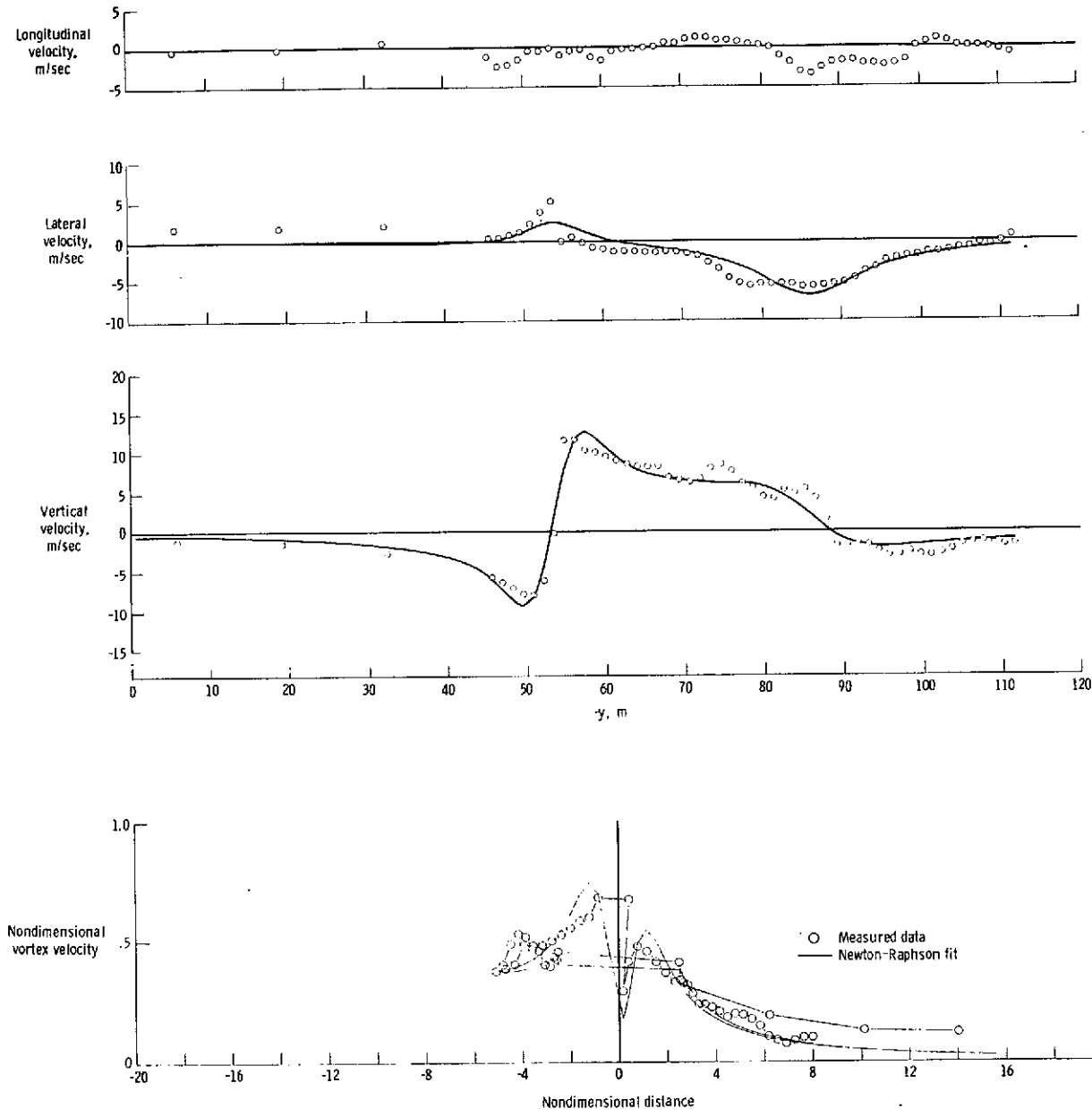

Figure 38.- Comparison of Newton-Raphson fit with measured flow velocities for flaps down and vortex age of 82 seconds.

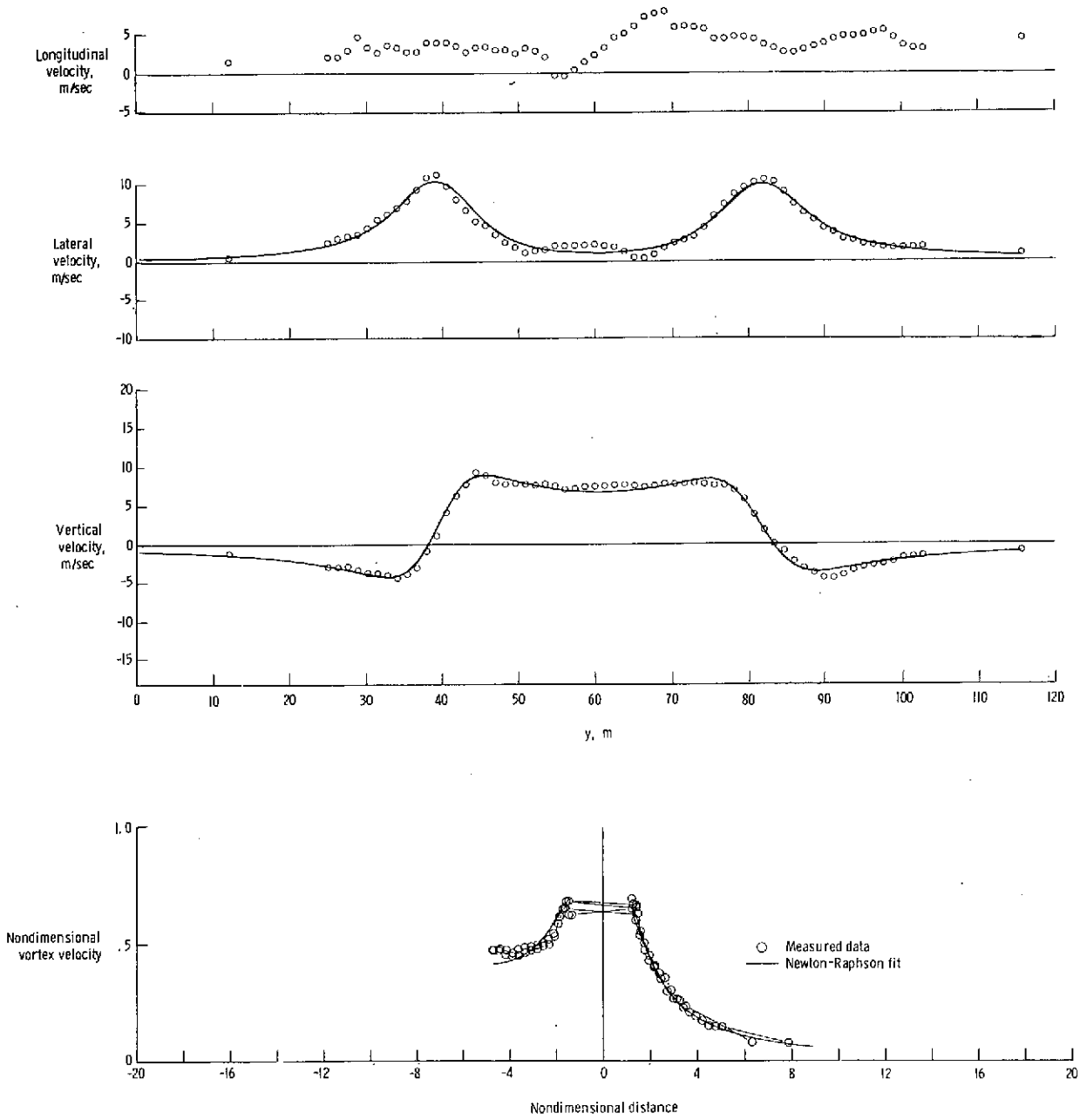

Figure 39.- Comparison of Newton-Raphson fit with measured flow velocities for flaps down and vortex age of 85 seconds.

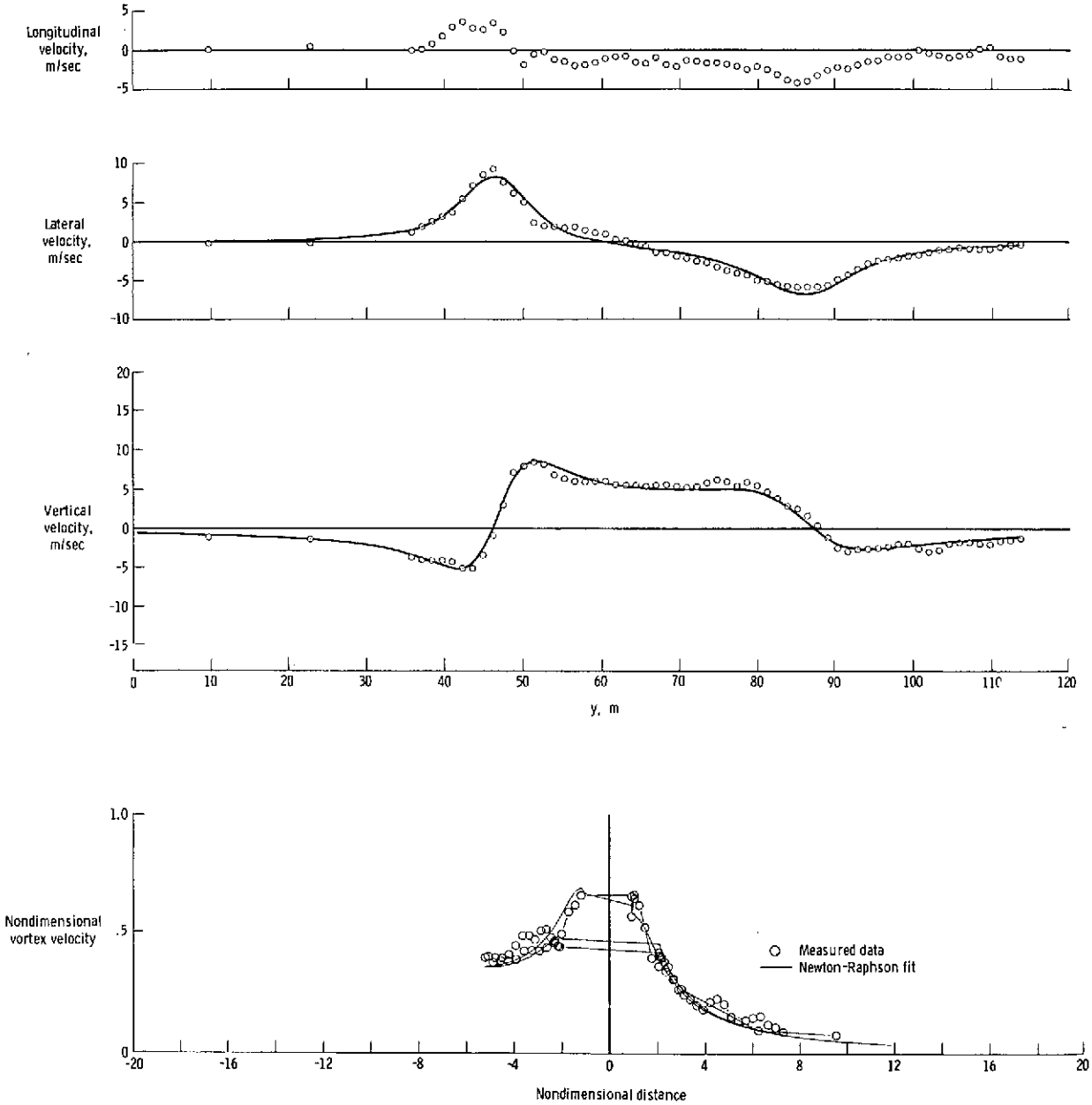

Figure 40.- Comparison of Newton-Raphson fit with measured flow velocities for flaps down and vortex age of 92 seconds.

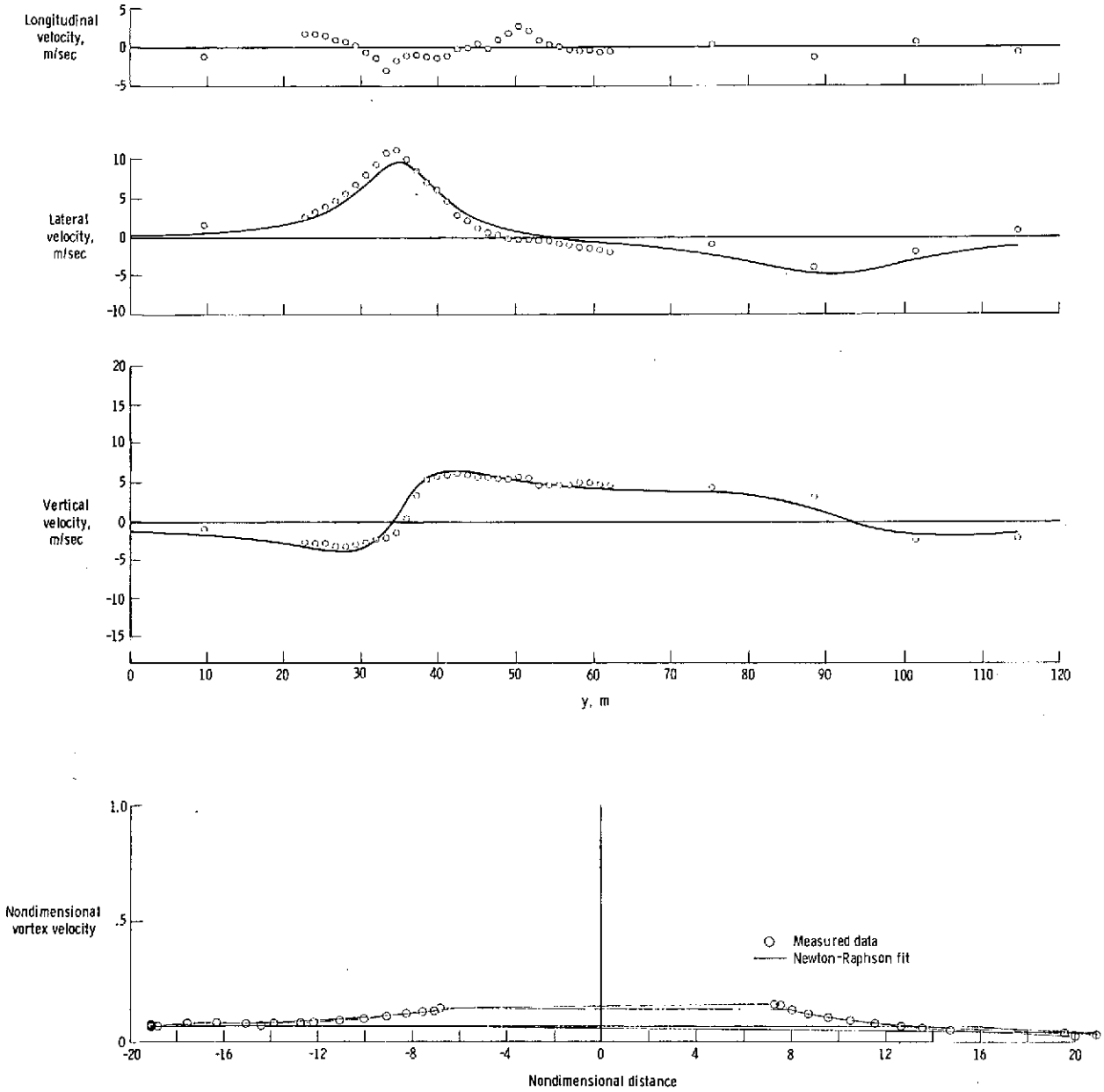

Figure 41.- Comparison of Newton-Raphson fit with measured flow velocities for flaps down and vortex age of 109 seconds.

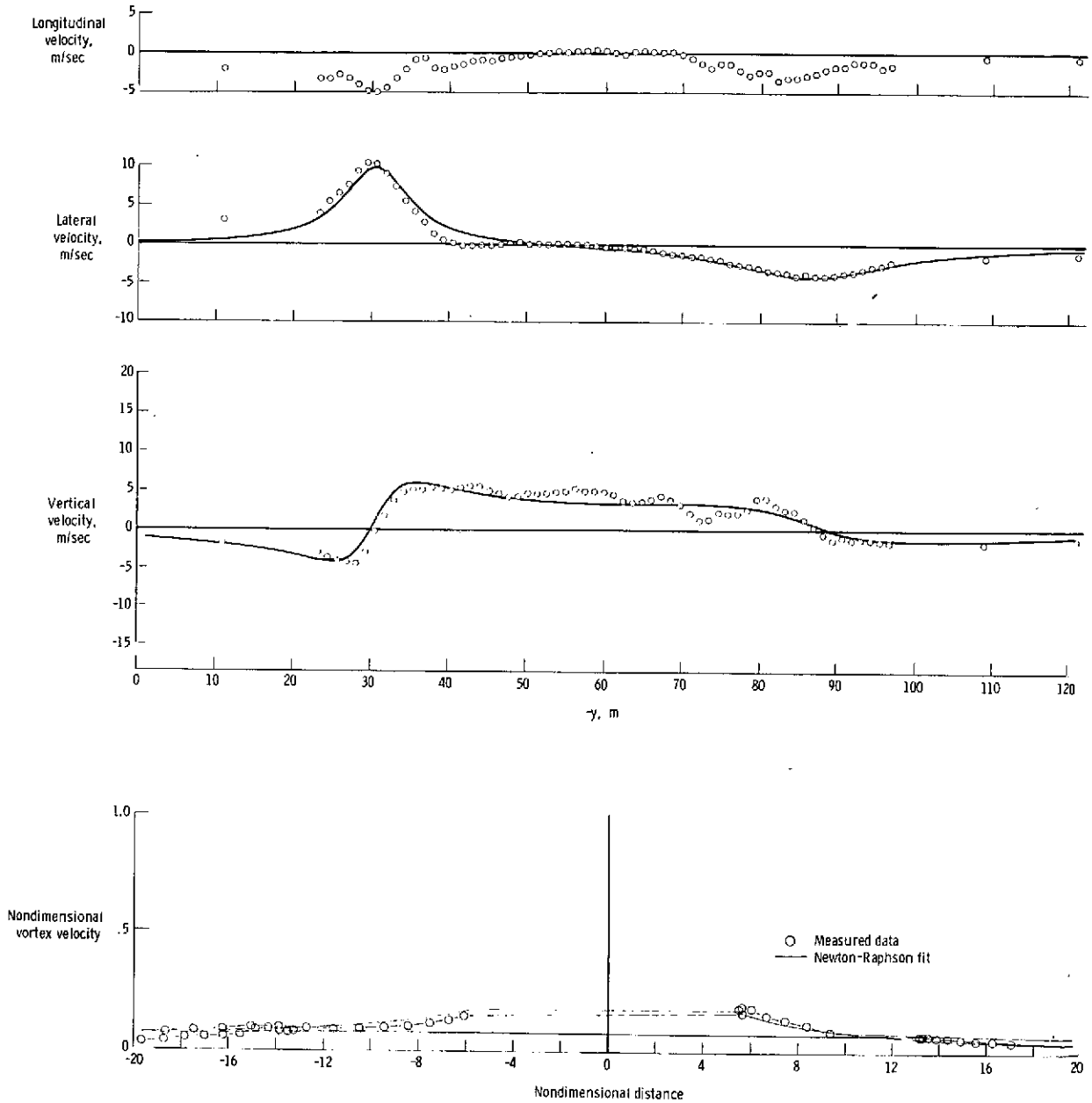

Figure 42.- Comparison of Newton-Raphson fit with measured flow velocities for flaps down and vortex age of 115 seconds.

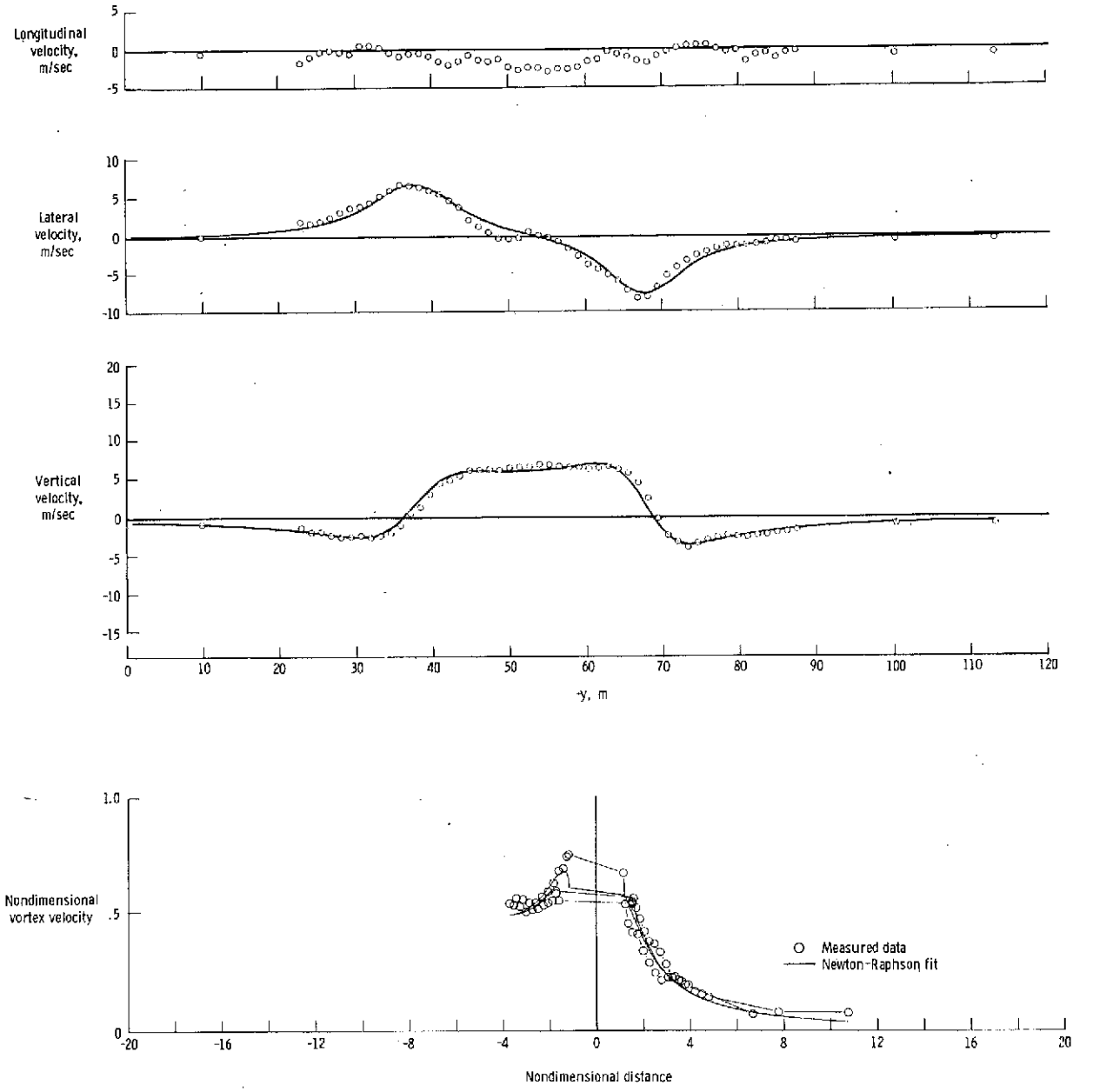

Figure 43.- Comparison of Newton-Raphson fit with measured flow velocities for flaps down and vortex age of 116 seconds.

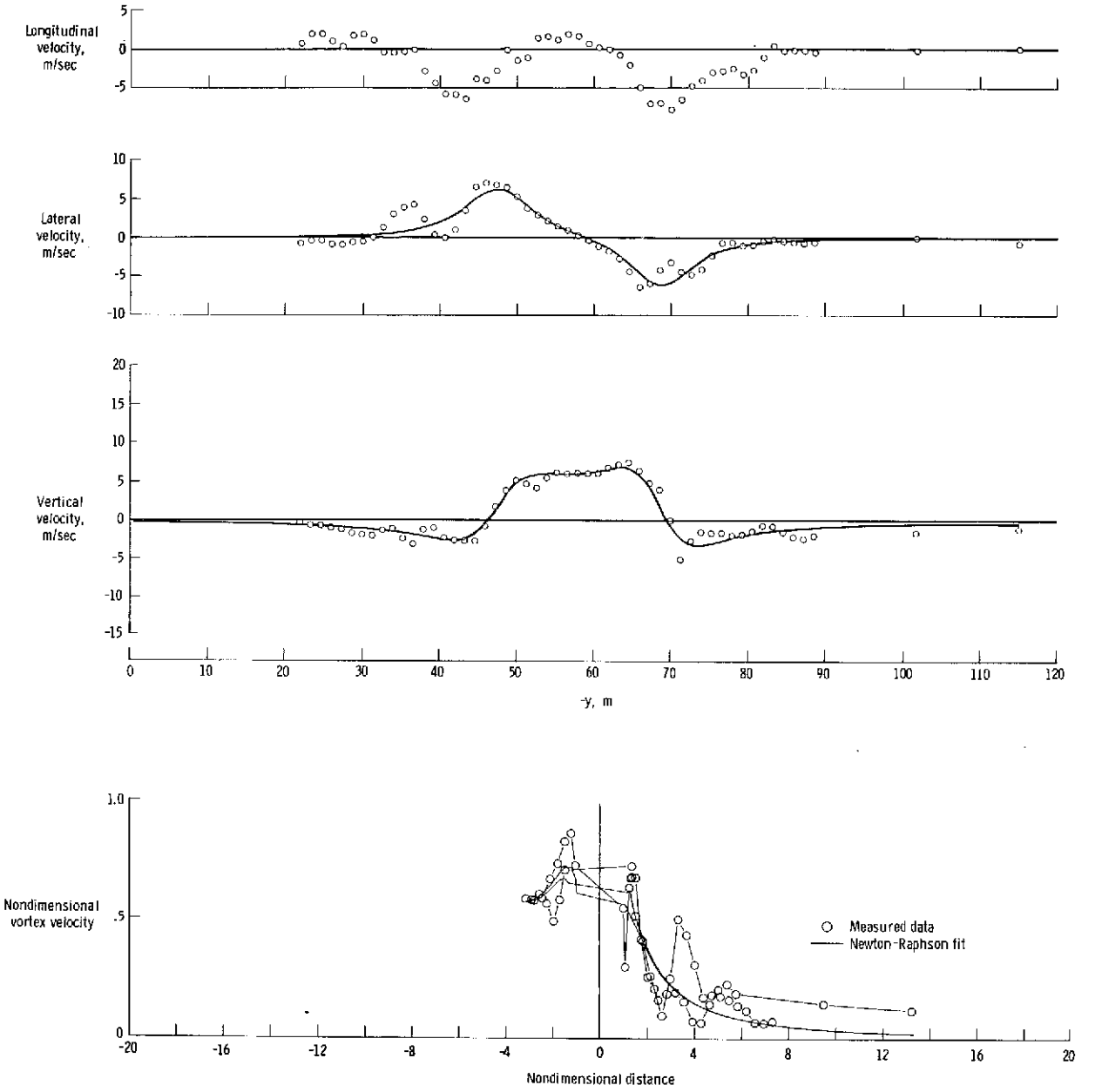

Figure 44.- Comparison of Newton-Raphson fit with measured flow velocities for flaps down and vortex age of 133 seconds.

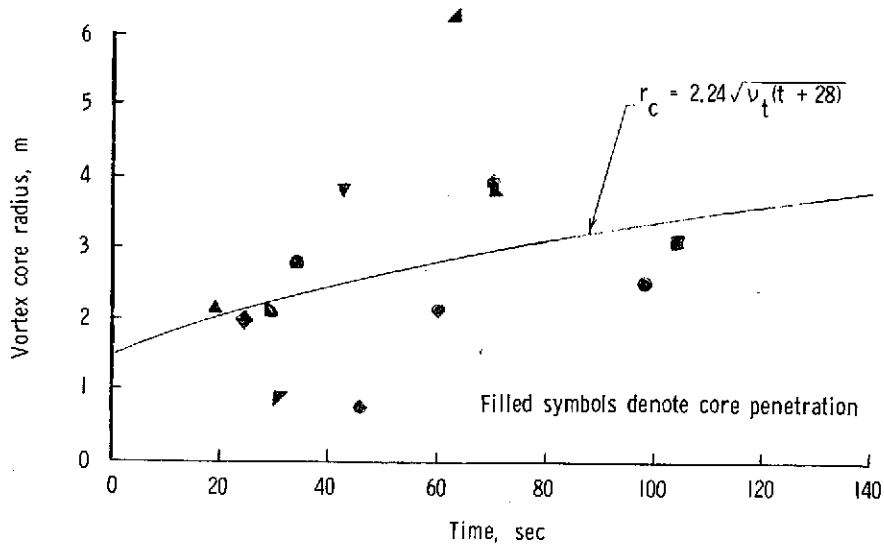

(a) Flaps up.

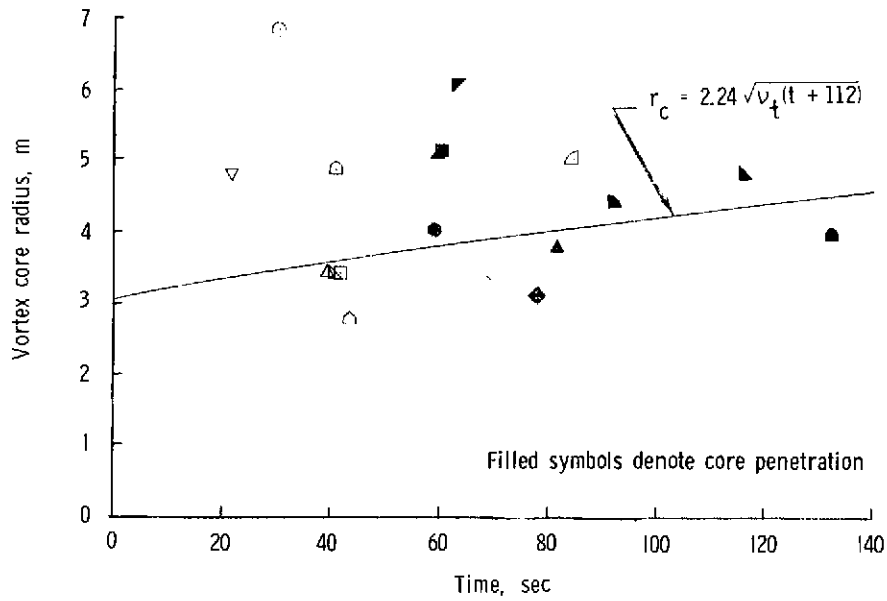

(b) Flaps down.

Figure 45.- Core radius as a function of time. (See table I for symbol notation.)

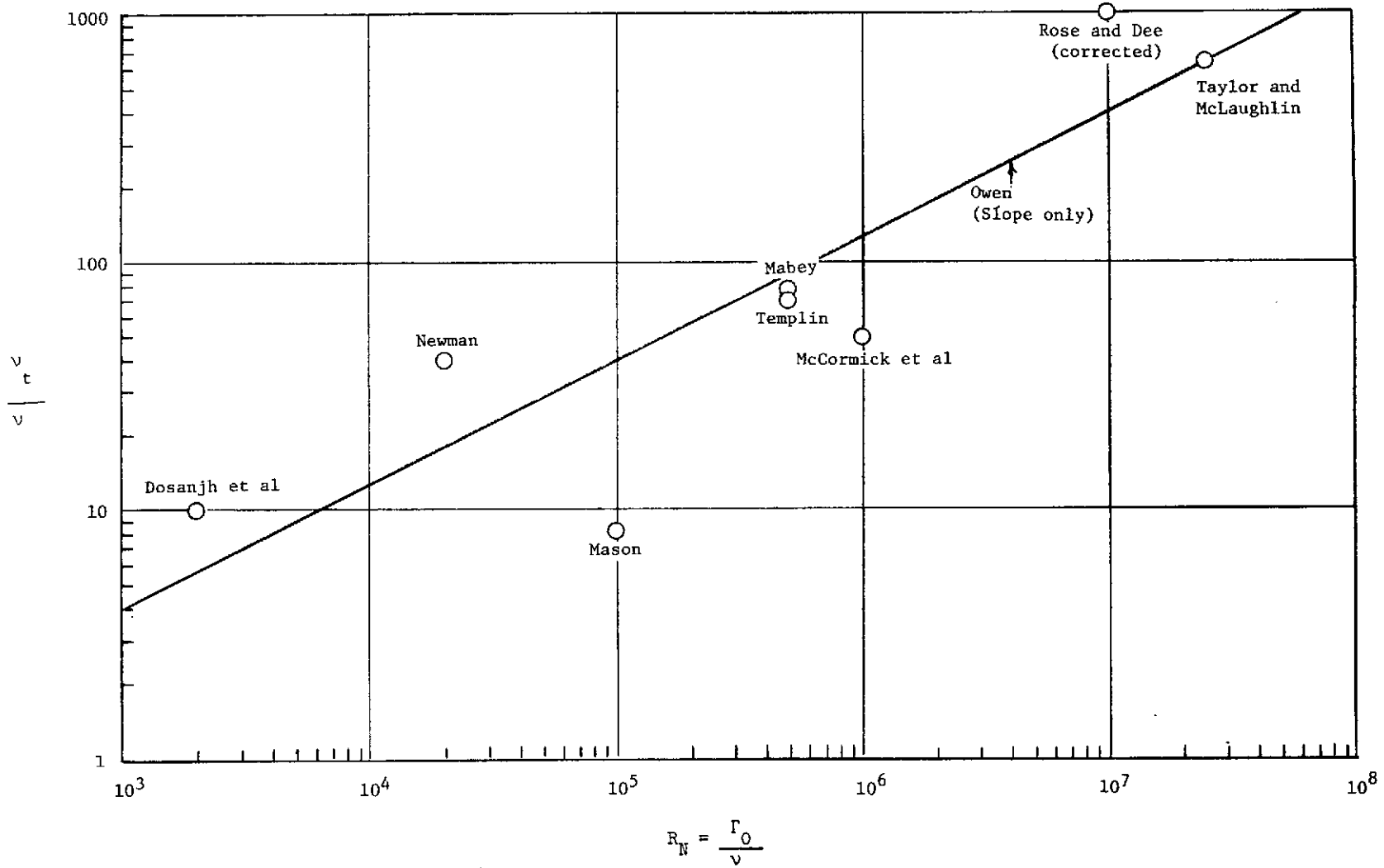

Figure 46.- Normalized effective eddy viscosity versus Reynolds number.

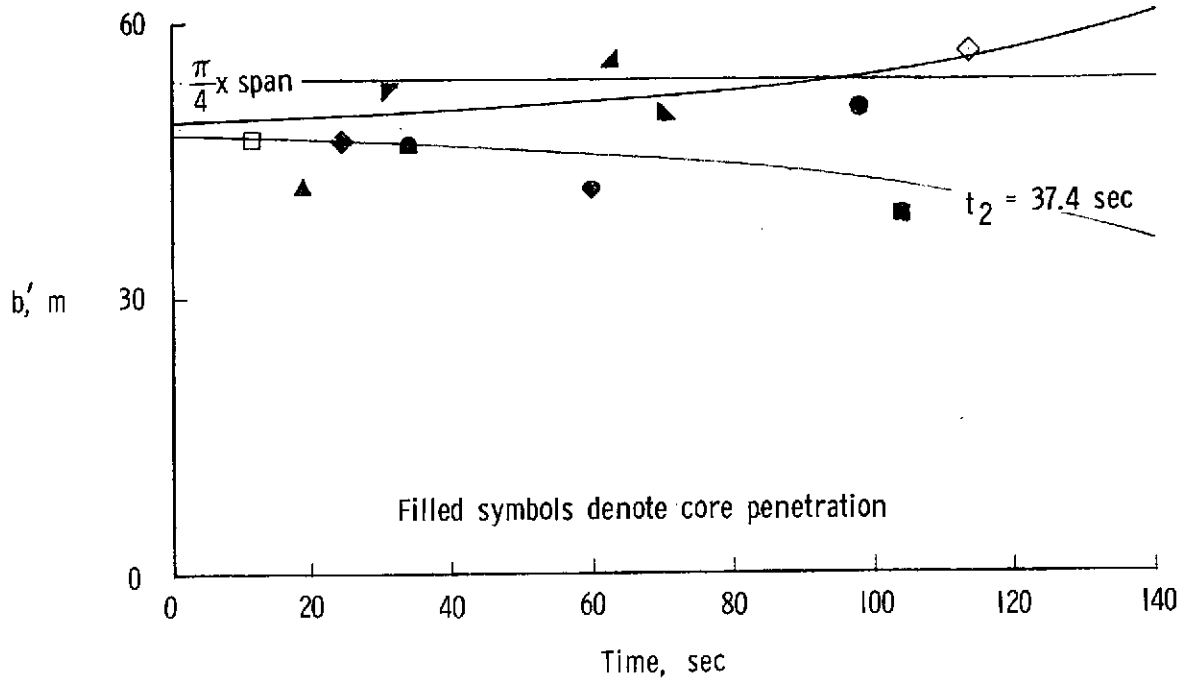

(a) Flaps up.

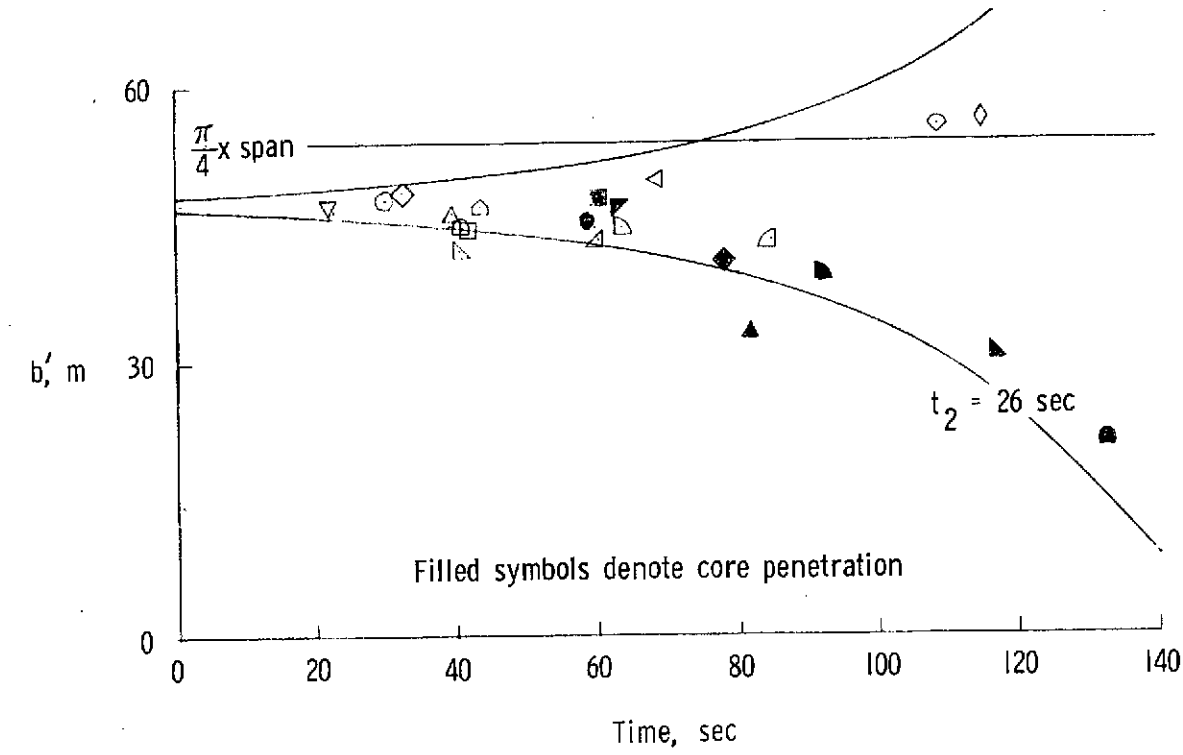

(b) Flaps down.

Figure 47.- Distance separating vortex centers. (See table I for symbol notation.)

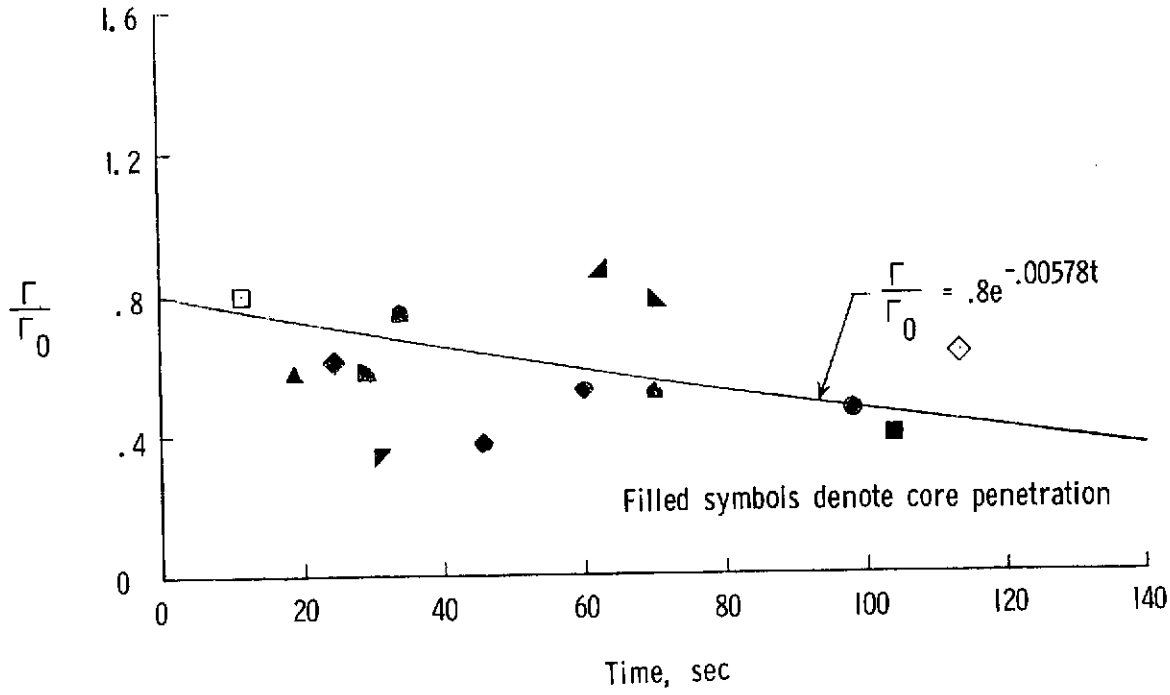

(a) Flaps up.

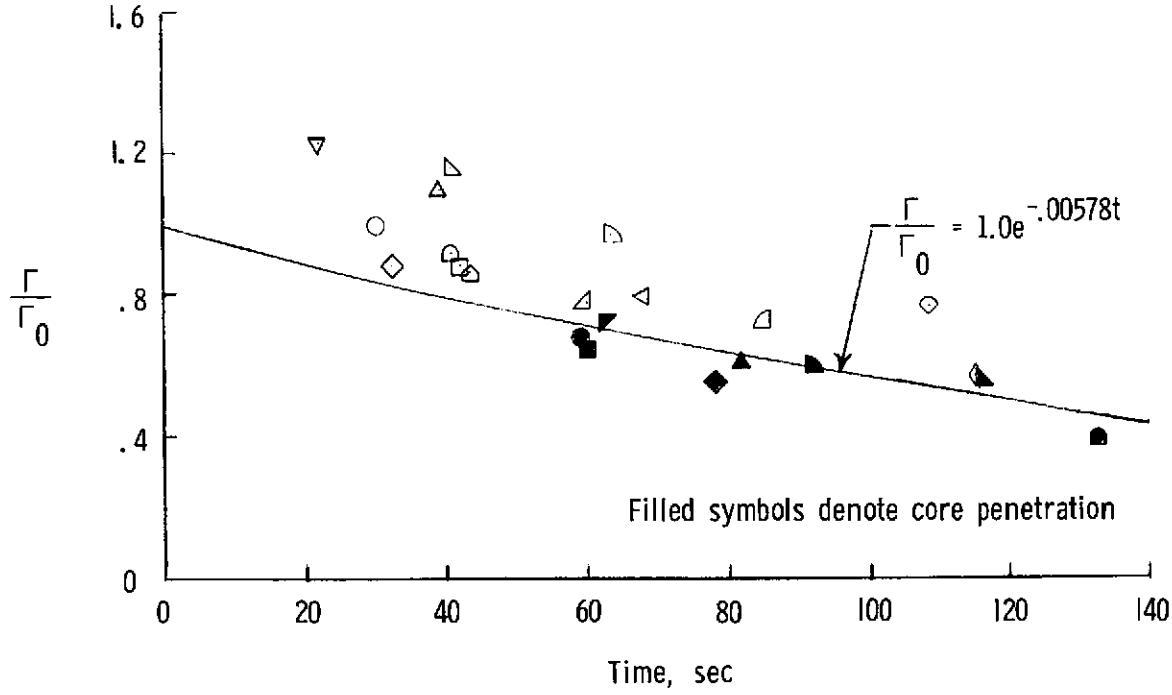

(b) Flaps down.

Figure 48.- Normalized circulation versus time. (See table I for symbol notation.)

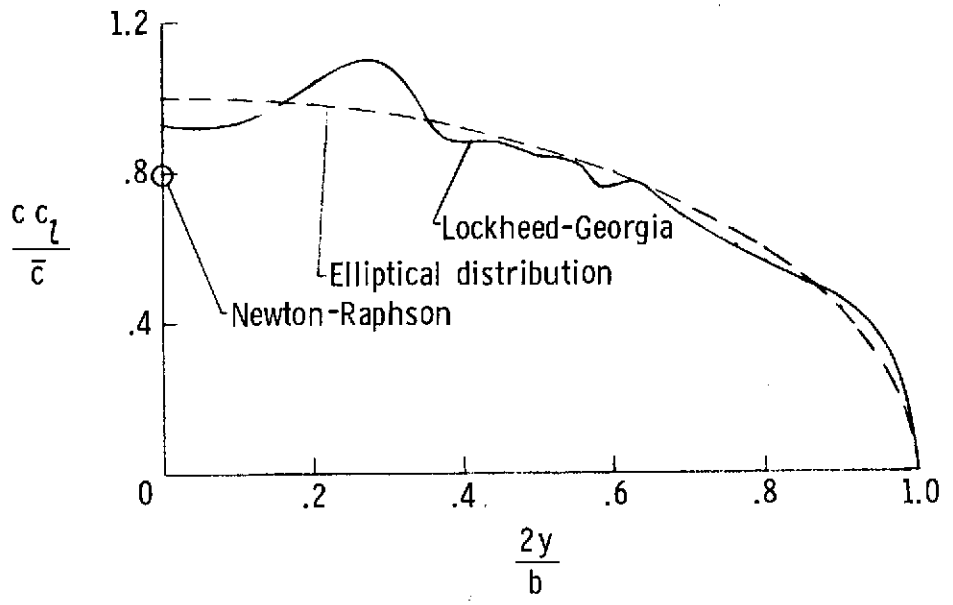

(a) Flaps up.

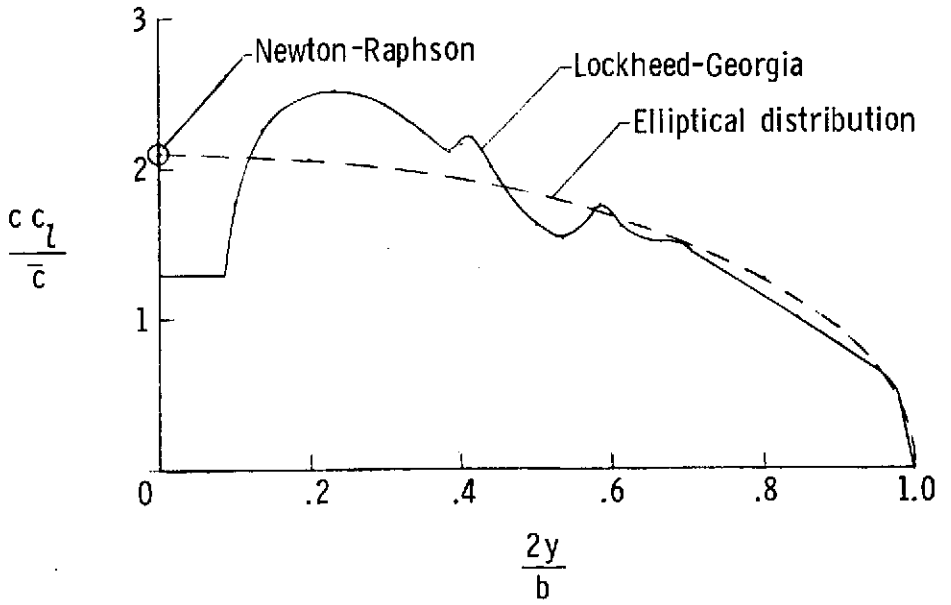

(b) Flaps down.

Figure 49.- Spanwise lift distribution.

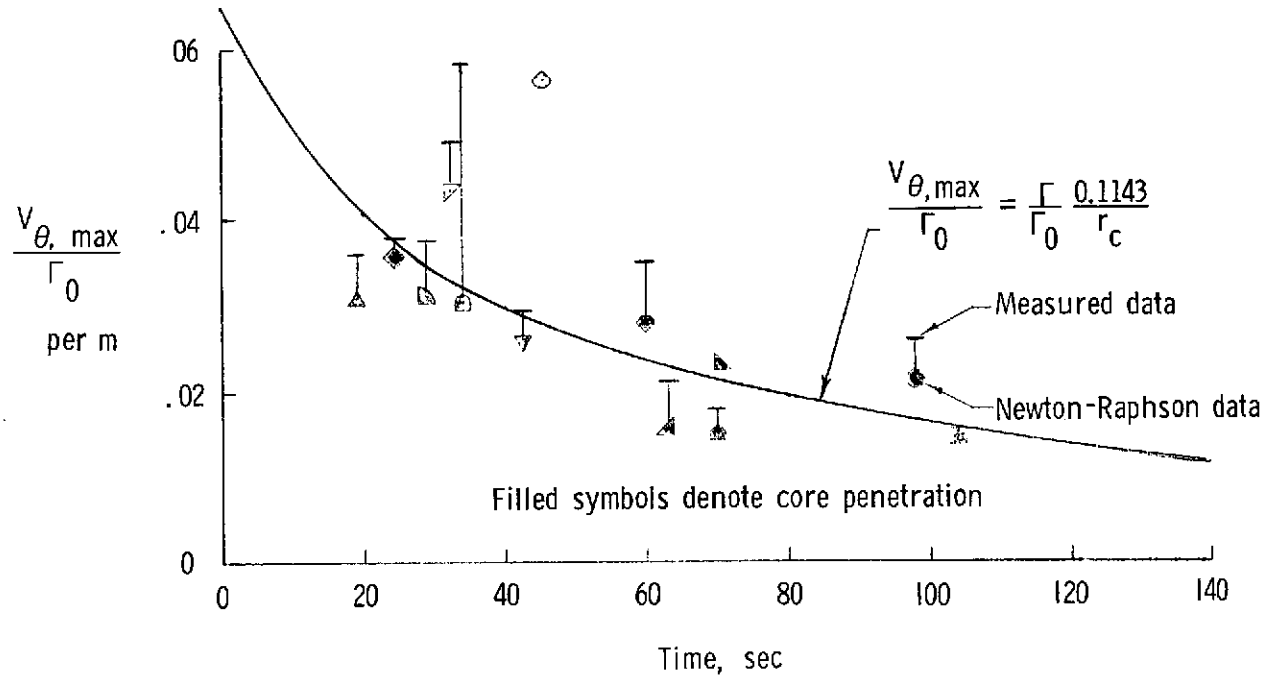

(a) Flaps up.

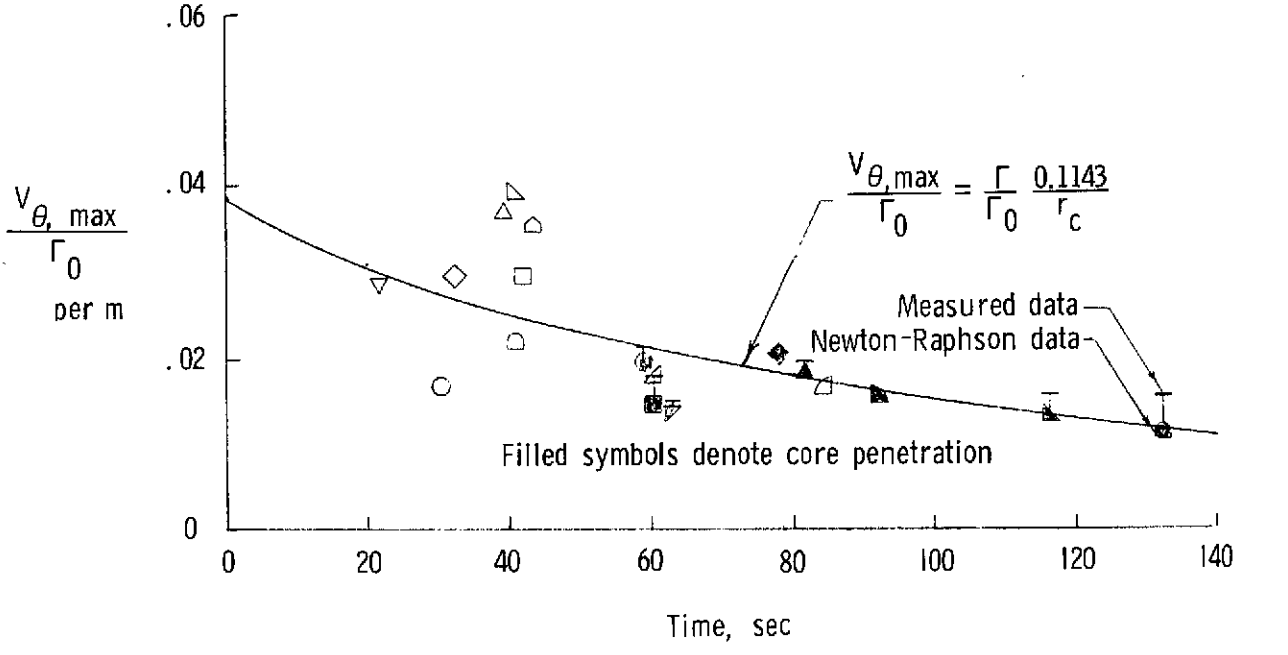

(b) Flaps down.

Figure 50.- Maximum-circumferential-velocity circulation ratio versus time. (See table I for symbol notation.)

NASA-Langley, 1974 L-8838